ORNL/TM-6282

The Thermodynamics of Carbon in Nickel-Based Multicomponent Solid Solutions

Daniel Joseph Bradley

OAK RIDGE NATIONAL LABORATORY
OPERATED BY UNION CARBIDE CORPORATION · FOR THE DEPARTMENT OF ENERGY

DISCLAIMER

Printed in the United States of America. Available from
National Technical Information Service
U.S. Department of Commerce
5285 Port Royal Road, Springfield, Virginia 22161
Price: Printed Copy $11.00; Microfiche $3.00

ORNL/TM-6282

Contract No. W-7405-eng-26

METALS AND CERAMICS DIVISION

THE THERMODYNAMICS OF CARBON IN NICKEL-BASED MULTICOMPONENT SOLID SOLUTIONS

Daniel Joseph Bradley

A thesis submitted to Michigan State University in partial fulfillment of the requirements for the degree of Doctor of Philosophy, Department of Chemistry.

Date Published: April 1978

OAK RIDGE NATIONAL LABORATORY
Oak Ridge, Tennessee 37830
operated by
UNION CARBIDE CORPORATION
for the
DEPARTMENT OF ENERGY

THIS PAGE

WAS INTENTIONALLY

LEFT BLANK

ACKNOWLEDGMENTS

I wish to thank the Oak Ridge Associated Universities and Michigan State University for their financial support in the form of a Graduate Participantship and a teaching assistantship, respectively. I would also like to thank Oak Ridge National Laboratory for the use of its facilities and for its financial support during the final term of this work.

I am very appreciative of the help I received from the staff of Oak Ridge National Laboratory. In particular, I would like to thank: Mr. James Attril, Dr. James Bentley, Mr. David Braski, Mrs. Sharon Buhl, Mr. O. B. Cavin, Mr. Robert Crouse, Dr. J. C. Franklin, Mr. Greggory Gessel, Dr. Gene Goodwin, Dr. William Laing, Mr. John Houston, Dr. Rodney McKee, Mr. Guy Peterson, Mr. Gregory Potter, Mr. Jack Ogle, Mrs. Kay Russell, Dr. James Stiegler, Dr. Robin Williams, Mr. Mark Williams, Mr. Clarence Zachary and Mrs. Joanne Zody.

I am sincerely grateful to Dr. James Leitnaker for his direction and encouragement throughout my time at ORNL. He gave willingly of his time to a sometimes less than thankful pupil.

My genuine thanks to Dr. Frederick Horne for introducing me to the field of thermodynamics and for encouraging my education. Without his counsel and help this work

would never have been started or finished.

I would also like to thank my fellow graduate students, Dr. Robert Cochran and Mr. Richard Rice for their friendship and the many favors they performed for me over the last four years.

Finally I would like to thank my family and my wife for their comfort and understanding throughout the long course of formal education.

ABSTRACT

THE THERMODYNAMICS OF CARBON IN NICKEL-BASED MULTICOMPONENT SOLID SOLUTIONS

By

Daniel Joseph Bradley

The activity coefficient of carbon in nickel, nickel-titanium, nickel-titanium-chromium, nickel-titanium-molybdenum and nickel-titanium-molybdenum-chromium alloys has been measured at 900, 1100 and 1215°C. The results indicate that carbon obeys Henry's Law over the range studied (0-2 at. %). The literature for the nickel-carbon and iron-carbon systems are reviewed and corrected. For the activity of carbon in iron as a function of composition, a new relationship based on re-evaluation of the thermodynamics of the CO/CO_2 equilibrium is proposed. Calculations using this relationship reproduce the data to within 2.5%, but the accuracy of the calibrating standards used by many investigators to analyze for carbon is at best 5%. This explains the lack of agreement between the many precise sets of data.

The values of the activity coefficient of carbon in the various solid solutions are used to calculate a set

of parameters for the Kohler-Kaufman equation. The calculations indicate that binary interaction energies are not sufficient to describe the thermodynamics of carbon in some of the nickel-based solid solutions. The results of previous workers for carbon in nickel-iron alloys are completely described by inclusion of ternary terms in the Kohler-Kaufman equation.

Most of the carbon in solid solution at high temperatures in nickel and nickel-titanium alloys precipitates from solution on quenching in water. The precipitate is composed of very small particles (>2.5 nm) of elemental carbon.

The results of some preliminary thermomigration experiments are discussed and recommendations for further work are presented.

TABLE OF CONTENTS

Chapter Page

LIST OF FIGURES

Figure Page

THIS PAGE

WAS INTENTIONALLY

LEFT BLANK

LIST OF TABLES

CHAPTER I

INTRODUCTION

A. Purpose

Solid solutions are of great technological importance, in particular in alloy metallurgy and semi-conductor manufacture. Solid solutions are also of considerable theoretical interest. According to Darken (1967), no general theory for the solution thermodynamics of strongly interacting components has been developed. The best theories to date are the regular solution theory of Hildebrand (1927) and the quasi-chemical theory of Herzfeld and Heitler (1925) and Scatchard (1931). Regular solution theory does not account for experimentally-observed negative heats of mixing, and neither theory accounts for experimentally-observed asymmetries in the relative excess Gibbs free energy.

A primary purpose of the work reported here was to check the validity of extending to multicomponent solutions the equation proposed by Kohler (1960) for the relative excess Gibbs free energy of mixing for binary solutions

$$\overline{G}^{E}(\text{rel}) = x_1 x_2 (x_1 \psi_{12} + x_2 \psi_{21}) \qquad (1)$$

where x_i is mole fraction and ψ_{ij} is an interaction energy dependent on temperature.

Sigworth and Elliott (1974,1976) and Chipman and Brushy (1968) provide extensive lists of references on thermodynamic investigations of multicomponent alloys. However, no attempt has previously been made to use an analytical expression for the integral relative excess Gibbs free energy of the alloys.

The experiments reported here provide data that can be used to determine whether interactions of elements in metallic solutions can be described in terms of binary interactions alone. The Kohler equation as modified by Kaufman (1975) requires that the ψ_{ij} depend only on components i and j. If this binary model can be verified, then the number of experiments needed to describe most systems can be reduced dramatically. There are 4.4×10^6 possible elemental quaternary mixtures but only 5.2×10^3 binary mixtures.

A second purpose for the work reported here was to obtain quantitative results for the thermodynamics of multicomponent solutions by a multi-pronged attack which includes gas phase carburization coupled with electrolytic extraction and analysis of the carbide phases. Such results are essential in attempting to understand the complicated precipitation processes that occur in multicomponent solid solutions.

B. Experimental Paths

Because diffusion in solids is both minuscule and slow, experiments to determine the thermodynamic properties of solid solutions have been both difficult and time consuming. In the study of interstitial elements such as carbon, oxygen, and nitrogen in metal matrices, the problem of slow diffusion rates is alleviated by performing experiments at relatively high temperatures. All of the techniques developed to take advantage of the relatively large mobilities of the interstitial elements rely on equilibrating the system of interest with a system of known properties.

The earliest investigations of the solution thermodynamics of interstitial elements involved long term annealing. A mixture of known composition is annealed at a fixed temperature until equilibrium is achieved. The sample is then quenched. The microstructure of the quenched material is studied with an optical microscope or other surface analytical techniques. This method is still used in many phase diagram studies (Stover and Wulff, 1959). Although useful information is obtained from this type of experiment, quantitative values for thermodynamic functions are not available from it.

The method of welded samples employed by Darken (1949) and Golovanenko, et al. (1973) involves welding two

samples of different composition. The concentration dependence of the activity for the element of interest is known for one of the samples. After equilibrium is achieved, the composition of each half is determined. The activity of the element of interest in the experimental half is set equal to that in the reference half. The method is limited due to the difficulty in obtaining good bonding between dissimilar materials.

A third method, used here, involves annealing specimens in an atmosphere in which the element of interest has a constant activity (Dunn and McLellan, 1968; Ban-Ya, et al., 1969 and 1970). The specimens thus equilibrate with a bathing medium. Knowledge of the thermodynamics of the bath allows calculation of the equilibrium activity of the element of interest.

C. Results

The relative partial molar excess Gibbs free energy of carbon in nickel solid solutions have been determined via a gas phase carburization technique, and quantitative methods for the determination of carbon and metal element concentrations in dilute solutions and in the carbide phase have been developed. The data are used to test the ability of the multi-component Kohler equation to describe the solution thermodynamics of nickel alloys. We show that

the equation is adequate for our systems, but that a ternary interaction term must be added to describe the Ni-Mo-C and the Ni-Cr-C systems. A ternary term is also necessary to describe completely the Fe-Ni-C system. The application of the parameters determined in nickel solid solutions to other solvent systems are checked by comparing literature values for iron-based systems with those determined here. The results obtained for nickel solution are not always applicable to iron solutions. Thermomigration of carbon in nickel-based alloys is discussed in Chapter 11.

Appendix A includes all of the data obtained from the carburization experiments.

CHAPTER II

SOLUTION THERMODYNAMICS

A. Chemical Potentials and Activity Coefficients

For every component i in any mixture of n components, the general formula for the chemical potential is

$$\mu_i = \mu_i^{\theta} + RT \ln a_i, \quad i = 1,\ldots,n, \tag{2.1}$$

where μ_i^{θ} is independent of composition and a_i is the activity. The values of a_i and μ_i^{θ} depend upon each other through the reference state and composition variable chosen.

For the pure component reference state and mole fraction x_i as composition variable,

$$\mu_i = \mu_i^{o} + RT \ln x_i \hat{\gamma}_i, \quad i = 1,\ldots n, \tag{2.2}$$

where μ_i^{o} is the chemical potential of pure component i at the temperature and pressure of interest and where the activity coefficient $\hat{\gamma}_i$ referred to the pure component has the property

$$\lim_{x_i \to 1} \hat{\gamma}_i = 1, \quad i = 1,\ldots,n. \tag{2.3}$$

Another useful reference state is the infinite dilution state. For component 1 as solvent,

$$\mu_i = \mu_i^{\infty} + RT \ln x_{i\,i}, \quad i = 2,\ldots,n, \tag{2.4}$$

with

$$\mu_i^{\infty} = \lim_{x_1 \to 1}(\mu_i - RT \ln x_i),$$

$$\lim_{x_1 \to 1} \gamma_i = 1, \quad i = 2,\ldots,n \tag{2.5}$$

For the solvent itself,

$$\hat{\gamma}_1 = \gamma_1, \quad \mu_1^{o} = \mu_1^{\infty}. \tag{2.6}$$

For the solutes, the chemical potential constants μ_i^{o} and μ_i^{∞} are related to each other by

$$\mu_i^{\infty} = \mu_i^{o} + RT \ln \hat{\gamma}_i^{\infty},$$

$$\mu_i^{o} = \mu_i^{\infty} + RT \ln \gamma_i^{o}, \tag{2.7}$$

where

$$\hat{\gamma}_i^{\infty} = \lim_{x_1 \to 1} \hat{\gamma}_i, \quad \gamma_i^{o} = \lim_{x_i \to 1} \gamma_i. \tag{2.8}$$

Moreover, the two types of activity coefficients are related to each other by

$$\gamma_i = \hat{\gamma}_i/\hat{\gamma}_i^{\infty}, \quad \hat{\gamma}_i = \gamma_i/\gamma_i^{o}, \tag{2.9}$$

with

$$\gamma_i^{o}\ \hat{\gamma}_i^{\infty} = 1. \tag{2.10}$$

an <u>ideal mixture</u> would have

$$\mu_i = \mu_i^{\theta} + RT\ \ell n\ x_i,\ i=1,\ldots,n, \tag{2.11}$$

which is valid for all compositions if and only if $\mu_i^{o} = \mu_i^{\infty}$ for all components. Ideality is approached closely in dilute solutions. The <u>ideal dilute solution</u> is defined by

$$\mu_i = \mu_i^{\infty} + RT\ \ell n\ x_i,\ i = 2,\ldots,n,$$

$$\mu_1 = \mu_1^{o} + RT\ \ell n\ x_1. \tag{2.12}$$

Thus, $\gamma_i = 1$ for all the components in the ideal dilute solute. In many cases of practical importance, including most studies of interstitial elements in alloys, the concentrations of some solutes are so low that $\gamma_i = 1$. Then the

first of Eqs. (2-12) holds for those solutes in the composition range studied. This does not imply, however, that γ_i would be unity over the entire composition range. In particular, effective ideality at high dilution does not imply $\gamma_i^o = 1$. Thus, $\hat{\gamma}_i^\infty \neq 1$, and Eqs. (2.7) and (2.12) yield

$$\mu_i = \mu_i^o + RT \ln x_i + RT \ln \hat{\gamma}_i^\infty. \qquad (2.13)$$

Thus, $\hat{\gamma}_i$ is a constant (namely, $\hat{\gamma}_i^\infty$), for compositions such that $\gamma_i = 1$. Note that Eq. (2.13) is a form of Henry's Law since all the composition dependence of μ_i resides in the $\ln x_i$ term; stated otherwise, the activity of component i is directly proportional to its mole fraction for highly dilute solutions.

The formulas displayed so far in this section are valid for any homogeneous phase. When two or more phases are in equilibrium, or when two or more crystalline modifications are stable, we designate the phase by a superscript. For example, for a phase α, Eq. (2.2) becomes

$$\mu_i^\alpha = \mu_i^{o\alpha} + RT \ln x_i + RT \ln \hat{\gamma}_i^\alpha. \qquad (2.14)$$

B. Excess Functions

For any intensive property y in a mixture, the excess property y^E is defined (Scatchard, 1949; Haase, 1971) by

$$y^E \equiv y - y^{id}, \tag{2.15}$$

where y^{id} is the value of the same property in an ideal mixture formed from the same pure components. Thus, by Eqs. (2.2), (2.11) and (2.15)

$$\mu_i^E = RT \ln \hat{\gamma}_i, \quad i = 1,\ldots,n. \tag{2.16}$$

Any total molar property $\overline{Z}$ is related to the partial molar properties $\overline{Z}_i \equiv (\partial Z/\partial n_i)_{T,P,n_{j\neq i}}$ by

$$\overline{Z} = \sum_{i=1}^{n} x_i \overline{Z}_i, \tag{2.17}$$

and the corresponding excess property is given by

$$\overline{Z}^E = \overline{Z} - \overline{Z}^{id} = \sum_{i=1}^{n} x_i \overline{Z}_i^E, \tag{2.18}$$

with

$$\overline{Z}_i^E \equiv \overline{Z}_i - \overline{Z}_i^{id}. \tag{2.19}$$

Equation (2.16) is an example of Eq. (2.19) for the Gibbs free energy since $\overline{G}_i = \mu_i$.

$$\overline{S}_i = -(\partial \mu_i/\partial T)_{p,n_j}, \quad \overline{H}_i = \mu_i + T\,\overline{S}_i, \tag{2.20}$$

we have

$$\bar{S}_i^E = -R \ln \hat{\gamma}_i - RT \left(\partial \ln \hat{\gamma}_i / \partial T\right)_{p,n_j}, \quad \bar{H}_i^E = -RT^2 \left(\partial \ln \hat{\gamma}_i / \partial T\right)_{p,n_j} \tag{2.21}$$

Moreover, for the total excess properties,

$$\bar{S}^E = -R \sum_{i=1}^{n} x_i \left[\ln \hat{\gamma}_i + \left(\partial \ln \hat{\gamma}_i / \partial \ln T\right)_{p,n_j}\right],$$

$$\bar{H}^E = -RT \sum_{i=1}^{n} x_i \left(\partial \ln \hat{\gamma}_i / \partial \ln T\right)_{p,n_j},$$

$$\bar{G}^E = RT \sum_{i=1}^{n} x_i \ln \hat{\gamma}_i. \tag{2.22}$$

Note, for completeness, that

$$\bar{H}_i^{id} = \bar{H}_i^o, \quad \bar{S}_i^{id} = \bar{S}_i^o - R \ln x_i, \tag{2.23}$$

The reason for this rather thorough presentation of well-known thermodynamic quantities is that although our experiments are in the dilute solution range, where the infinite dilution standard state and the γ_i activity coefficients are useful, the mixture theories we wish to discuss are cast in terms of the excess functions just listed. For the excess functions the pure component reference states are required by definition, and therefore so are

the $\hat{\gamma}_i$ activity coefficients. Put another way, although our solutions are dilute enough to be very nearly ideal, the activity coefficients are not nearly unity because it is the pure component-based activity coefficients, the $\hat{\gamma}_i$, that we calculate. Indeed, in most of our experiments the γ_i are all unity and the $\hat{\gamma}_i$ are all composition independent constants, namely, $\hat{\gamma}_i^\infty$. The $\hat{\gamma}_i^\infty$ do depend on temperature, however, and we have,

$$\overline{H}_i^{E^\infty} = -RT(\partial \ell n\ \hat{\gamma}_i^\infty / \partial \ell nT)_p, \quad \overline{S}_i^{E^\infty} = -R[\ell n\ \hat{\gamma}_i^\infty + (\partial \ell n\ \hat{\gamma}_i^\infty / \partial \ell nT)_p]. \tag{2.24}$$

C. Lattice Stabilities

Suppose that at a given temperature and pressure, pure component i can exist in two stable phases (crystalline modifications) α and β. Of course only one of these can exist at equilibrium away from a transition point, but instances of supersaturation, supercooling, etc., are plentiful. The relative stability $\mu_i^{\alpha\beta o}$ is defined by

$$\mu_i^{\alpha\beta o} \equiv \mu_i^{\beta o} - \mu_i^{\alpha o}. \tag{2.25}$$

To see the importance of relative lattice stabilities, consider an alloy which undergoes a phase transition from

the α modification to the β modification. Since the mole fractions do not change, the change in Gibbs free energy in the transition is

$$\Delta\overline{G}^{\alpha\to\beta} = \overline{G}^{\beta} - \overline{G}^{\alpha} = \sum x_i \mu_i^{\beta} - \sum x_i \mu_i^{\alpha}$$

$$= \sum x_i \left(\mu_i^{\beta} - \mu^{\alpha}{}_i\right) = \sum x_i [\mu_i^{\beta o} - \mu_i^{\alpha o} + RT\ell n(\hat{\gamma}_i^{\beta}/\hat{\gamma}_i^{\alpha})]$$

$$= \sum_i x_i \mu_i^{\alpha\beta o} + RT \sum x_i \ell n(\hat{\gamma}_i^{\beta}/\hat{\gamma}_i^{\alpha}). \qquad (2.26)$$

Thus, $\Delta\overline{G}$ is due both to changes in the chemical environment, reflected in the activity coefficient terms, and to changes in the structure, reflected in the lattice stability terms. Kaufman (1959, 1967) and Kaufman and Nesor (1973, 1975) have calculated lattice stability energies from phase diagram data for a variety of systems.

D. Models

The Taylor series expansion of $\mu_i^E = RT\ell n\hat{\gamma}_i$ in the mole fractions $x_2 \ldots x_n$ is

$$\mu_i^E = RT\ell n\hat{\gamma}^{\infty} + RT \sum_{j=2}^{n} E_{ij}\, x_j + RT \sum_{j=2}^{n} \sum_{k=2}^{n} P_{ijk} x_j x_k + \theta(x^3), \qquad (2.27)$$

where we use the Lupis and Elliot (1966) notation for the

partial derivative coefficients:

$$E_{ij} \equiv [(\partial \ell n \hat{\gamma}_i / \partial x_j)_{T,P,x_k}]_{x_1=1}$$

$$P_{ijk} \equiv [(\partial^2 \ell n \hat{\gamma}_i / \partial x_j \partial x_k)_{T,P,x_\ell}]_{x_1=1} \qquad (2.28)$$

The coefficients are thus evaluated at infinite dilution. The coefficients are called interaction coefficients by Lupis and Elliott (1966). The expansion was suggested by Wagner (1952) and has been used by Elliott and his students (1966) extensively to describe interactions in liquid metals. Chipman and Brushy (1968) have tabulated the interaction coefficients for carbon in ternary iron alloys at 1000°C. Chipman favors use of the lattice ratio, $Z_i = x_i/(1-2x_1)$, as composition variable rather than mole fraction.

While the infinite Taylor series is mathematically rigorous and can therefore be used in principle to describe any system, the number of parameters becomes very large for $n \geq 3$ even if the series is truncated at second-order terms. In order to reduce the number of coefficients, various simplifying models have been used, especially for dilute solutions and for symmetric binary mixtures.

The regular solution model of Hildebrand is

$$G^E = x_1 \bar{G}_1^{\alpha-\beta} + x_2 \bar{G}_2^{\alpha-\beta} + x_1 x_2 \psi^\alpha$$

where ψ is an interaction parameter due principally to the enthalpy of solution. This works well for many cases, but asymmetric composition dependence of ψ is often observed. Slight modification of Hildebrand's equation to

$$G^E = x_1\bar{G}_1^{\alpha-\beta} + x_2\bar{G}_2^{\alpha-\beta} + x_1x_2(x_1\psi_{12}^{\alpha} + x_2\psi_{21}^{\alpha})$$

permits first-order asymmetric composition dependence in the excess free energy.

One type of desirable equation includes constant terms which are independent of each other. An approach in this direction is the model of Kohler (1960) modified by Kaufman and Nesor (1975) and generalized here for multicomponent systems,

$$\bar{G}^{E\alpha} = \sum_{i=1}^{n} x_i\,\bar{G}_i^{\alpha-\beta} + \sum_{i=1}^{n-1}\sum_{j=i+1}^{n}\frac{x_ix_j}{x_i+x_j}[x_i\psi_{ij}^{\alpha} + x_j\psi_{ji}^{\alpha}] + \sum_{i=1}^{n-2}\sum_{j=i+1}^{n-1}\sum_{k=i+2}^{n}\frac{x_1x_jx_k\psi_{ijk}^{\alpha}}{(x_1+x_2+x_3)} \qquad (2.29)$$

where we omit higher-order interaction terms. Note that in the binary case if $\psi_{ij} = \psi_{ji}$ and if ψ_{ij} is independent of temperature, then Eq. (2.29) reduces to the regular solution model. Differentiation of Eq. (2.29) yields for the partial molar excess Gibbs free energy of component n,

$$\mu_n^{E\alpha} = \bar{G}_n^{E\alpha} = \bar{G}_n^{\alpha-\beta} + \sum_{j=1}^{n-1} \psi_{nj}^{\alpha} \left[\frac{x_n x_j^2}{(x_n+x_j)^2} + \frac{x_n x_j}{x_n+x_j}(1-x_n)\right]$$

$$+ \sum_{j=1}^{n-1} \psi_{jn}^{\alpha} \left[\frac{x_j^2}{(x_n+x_j)} \left(\frac{x_j}{x_n+x_j} - x_n\right)\right]$$

$$- \sum_{i=1}^{n-1} \sum_{j=1}^{n-1} \psi_{ij}^{\alpha} \left(\frac{x_i^2 x_j}{x_i+x_j}\right)$$

$$+ \sum_{\substack{i=1 \\ j>i}}^{n-2} \sum_{j=1}^{n-1} \left[\frac{(x_n x_i x_j)}{(x_n+x_i+x_j)} \psi_{nij}^{\alpha}\right.$$

$$\sum_{\substack{j=1 \\ j\neq i}}^{n-1} \sum_{i=1}^{n-2} x_j \psi_{jni}^{\alpha} \left[\frac{x_i x_j}{x_n+x_i+x_j} - \frac{2x_n x_i x_j}{x_n+x_i+x_j} - \frac{x_n x_i x_j}{(x_n+x_i+x_j)^2}\right]$$

$$+ \sum_{\substack{i=1 \\ j\neq i\neq k \\ k>j}}^{n-1} \sum_{j=1}^{n-2} \sum_{k=1}^{n-1} - \frac{2x_i x_j x_k}{(x_i+x_j+x_k)} (x_i \psi_{ijk}^{\alpha}) \qquad (2.30)$$

To illustrate the physical implications of this model on the chemical potential of a species in a multicomponent system, consider a ternary solution:

$$\mu_3^{E\alpha} = \bar{G}_3^{E\alpha} = \sum_{j=1}^{2} \psi_{3j}^{\alpha} \left[\frac{x_3 x_j^2}{(x_3+x_j)^2} + \frac{x_3 x_j}{x_3+x_j}(1-x_3)\right]$$

$$+ \sum_{j=1}^{2} \psi_{j3}^{\alpha} \left[\frac{x_j^2}{x_3+x_j}\left(\frac{x_j}{x_3+x_j} - x_3\right)\right] - \psi_{12}^{\alpha}\left(\frac{x_2 x_1^2}{x_1+x_2}\right)$$

$$- \psi_{21}^{\alpha}\left(\frac{x_2^2 x_1}{x_1+x_2}\right) + \psi_{123}^{\alpha}(1-2x_3)x_1 x_2. \qquad (2.21)$$

The first two terms in $\bar{\mu}_3^{E\alpha}$ describe the binary interactions of component 1 with the other components in the system. They are due to the heats of solution in the binary mixtures. The next two terms appear to be independent of component three and show that even if only binary interactions are considered all binary interactions affect the chemical potential of a species, not just the terms involving it. The ψ_{123}^{α} term involves ternary interactions, for which there are few data. The ψ_{123}^{α} term can be regarded as the extra heat of solution in the ternary over that predicted from a linear combination of the binaries. A nonsymmetric function in x_1 and x_2 would be more appropriate in the cases where the three-one and three-two interactions are appreciably different.

In the limit as $x_3 \to 0$, Eq. (2.31) yields

$$\lim_{x_3 \to 0} \mu_3^{E\alpha} = \psi_{13}^{\alpha} x_1 + \psi_{23}^{\alpha} x_2 - \psi_{12}^{\alpha} x_1^2 x_2 - \psi_{21}^{\alpha} x_2^2 x_1 \qquad (2.32)$$

If the ψ^{α}_{12} and ψ^{α}_{21} terms are small compared to the ψ^{α}_{23} and ψ^{α}_{13} terms, this equation is analogous to one suggested by Wagner (1952).

In the limit of infinite dilution, with 1 = solvent, Eq. (2.31) yields

$$\lim_{x_1 \to 0} \mu_3^{E\alpha} = \psi^{\alpha}_{13} = RT \ln \hat{\gamma}^{\infty}_3,$$

$$\lim_{x_1 \to 1} RT\, E_{33} = 2\psi^{\alpha}_{31} - 4\psi^{\alpha}_{13},$$

$$\lim_{x_1 \to 1} RT\, P_{333} = 3\psi^{\alpha}_{31} - 5\psi^{\alpha}_{13},$$

$$\lim_{x_1 \to 1} \mu_1^{E\alpha} = 0. \qquad (2.33)$$

Thus, the Kohler equation reduces to Henry's Law for the solute in the limit of a dilute solution and to Raoult's Law for the solvent.

The experiments reported here provide a test of the Kohler formalism and provide data on the solution thermodynamics of nickel-based alloys. Measurements of μ^{E}_{carbon} alone cannot lead to all the interaction energies. The other ones must be obtained from the literature. The solution thermodynamics of the transition metal binary systems of interest have been determined more extensively and more precisely than have the thermodynamics of these same metals with interstitials such as carbon, oxygen, and

nitrogen, so the literature is rich in information on binary metals.

If the model is correct, once precise values of ψ_{ij} and ψ_{ijk}, for a system have been determined, then the chemical activity of all the species at all temperatures and composition can be calculated. When the activity data are coupled with thermodynamic data about precipitate phases, the relative stabilities of the various phases can be calculated as well as the phase diagram.

CHAPTER III

CARBURIZATION THERMODYNAMICS

A. The Choice of the Carburizing Medium

One of two gaseous equilibria is ordinarily used to control the activity of carbon in solids; namely

$$CO_2(g) + C(S.S.) \rightleftarrows 2CO(g),\ K_1 = \frac{P_{CO}^2}{P_{CO_2} A_C} \qquad (3.1)$$

$$2H_2(g) + C(S.S.) \rightleftarrows CH_4(g),\ K_2 = \frac{P_{CH_4}}{P_{H_2}^2 A_C}\ . \qquad (3.2)$$

Samples are placed in a reaction chamber, at a temperature of interest, together with a gas mixture of known, constant composition. Knowledge of the value of the equilibrium constant for the gas reaction allows the activity of the carbon in the sample at equilibrium to be calculated.

There are three difficulties with the CO_2-CO reaction: (1) the amount of CO_2 in the mixture becomes very small at high temperatures, which complicates analysis of the gas composition; (2) before it reaches the sample, carbon monoxide gas tends to decompose in the furnace to carbon dioxide and amorphous carbon, which causes uncertainty in

the carbon activity of the gas at the sample surface; and (3) the presence of a small amount of oxygen in the carbon monoxide-carbon dioxide mixture complicates the analysis because of the reaction

$$2CO_2 \rightleftarrows 2CO + O_2. \qquad (3.3)$$

The CO_2-CO reaction is thus unsuitable for use in studies of materials containing stable oxide formers. Although problems one and two have been avoided by most investigators, the problem of oxide formation cannot be overcome. Reaction (3.3) controls the oxygen partial pressure, and if an oxide is stable at that pressure it will form.

The methane-hydrogen reaction requires a cleaner system, primarily because of the devasting effects small amounts of water or oxygen can have on the gas compositions. Ellis et al (1963) quantified this effect and found that even the addition of a phosphorous pentoxide trap does not eliminate the problem. Bungardt et al. (1964) have shown that results comparable with those obtained from CO/CO_2 studies are possible if sufficient care is taken. The advantage of the H_2-CH_4 reaction is that the oxygen potential can in principle be kept as low as desired.

Since titanium and molybdenum are facile oxide formers, the CH_4-H_2 reaction was used exclusively in this work.

Instead of direct analysis of the gas mixture, the carbon content of a pure iron standard was used to determine the carbon activity. The composition-activity relationship for carbon in iron, determined by the CO/CO_2 method, has been studied extensively in the past 50 years. Dunwald and Wagner (1931) performed the first quantitative experiments on iron-carbon binaries, and the system has been studied by many others including Smith (1946) and Ban-Ya et al. (1969) and (1970).

B. Analysis of the Thermodynamics of the CO/CO_2 Equilibrium

It appears superficially that literature data on the iron-carbon system agrees to within 2%. Close examination, however, shows that the apparent agreement is partially a result of using different values for the equilibrium constant for Reaction (3.1). Smith (1946) determined and used a value 10% lower than that employed by Ban-Ya et al (1970). A literature search undertaken to determine the correct value of the equilibrium constant showed that the disagreement results solely from the use of different values of the absolute entropy, S°_{T}, of carbon monoxide. Ban-Ya et al. (1970) used values determined by Clayton and Giauque (1932) from data taken by Snow and Rideal (1929). Smith (1946), on the other hand, used a value determined from his own experiments. The JANAF Thermochemical

Tables (1971) agree with Smith (1946), while the NBS Series III Tables (1948) used values calculated by Clayton and Giauque (1932). National Bureau of Standards Technical Note TN 270-3 agrees with JANAF for $S^{\circ}_{298.15}$, but no literature reference is given. JANAF uses the value for S°_{T} of carbon-monoxide determined by Belzer and Savedoff (1953) from spectral data of Herzberg and Rao (1949).

In order to determine the correct value of S°_{T}, we checked the quality of the two sets of spectral data by a graphical method due to Herzberg (1939). According to Herzberg, a plot of $\{[\Delta_2 F''(J)]-[4 \tilde{B}_e (J + \frac{1}{2})]\}$ versus J highlights any systematic or random errors in the data $\{[\Delta_2 F''(J)]$ equals $[R(J-1)-P(J+1)]$, and $\tilde{B}_e$ is the equilibrium rotational constant for a rigid rotor. R and P refer to the $J = +1$ and $J = -1$ bands of a vibration-rotation band where J is the rotational quantum number.} Figure 3-1 compares the results of Herzberg and Rao (1949) to those of Snow and Rideal (1929). One would expect a smooth curve with a slightly decreasing slope at high J as the centrifugal distortion constant, $\tilde{D}_e$, becomes more important. Snow and Rideal (1929) quote a resolution of "at most" 0.1 cm^{-1}, while Herzberg and Rao (1949) claim 0.01 cm^{-1}. Snow and Rideal (1929) do not state an absolute uncertainty, while Herzberg and Rao (1949) claim an uncertainty of less than 0.03 cm^{-1}. More recent data on carbon monoxide by

THIS PAGE

WAS INTENTIONALLY

LEFT BLANK

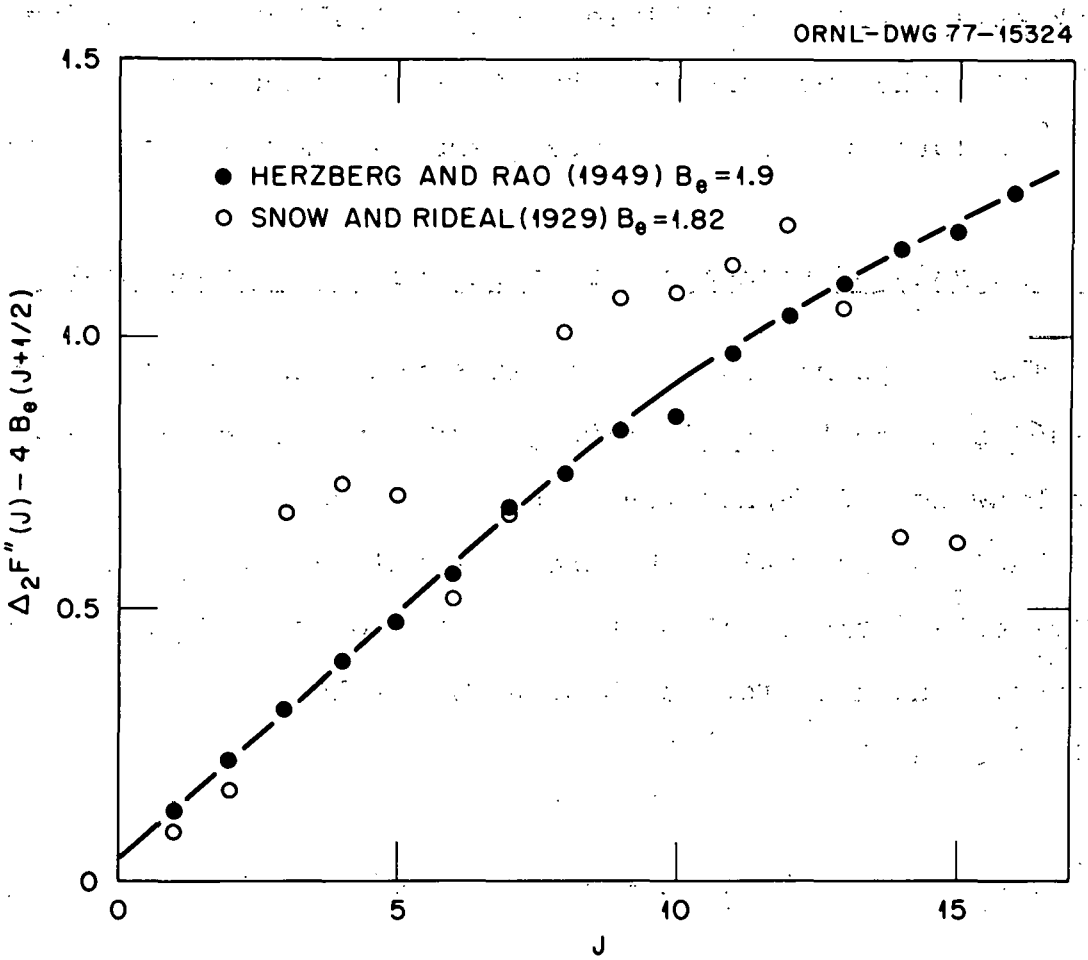

Figure 3.1. The results of Herzberg and Rao (1949) and Snow and Rideal (1929) displayed as $\Delta_2F''(J)-4Be(J+\frac{1}{2})$ versus J, where the terms have been defined in the text. The relatively random appearance of the Snow and Rideal results indicates a lack of internal consistency. The Herzberg and Rao results, however, produce a smooth curve.

Rank et al. (1961) and Plyler et al. (1955) do not differ significantly from the results of Herzberg and Rao (1949). The absolute entropy of Herzberg and Rao is the one to use.

C. Analysis of Literature Data on the Iron-Carbon System

The foregoing analysis dictates that the data of Smith (1946) and Ban-Ya et al. (1969, 1970), Scheil et al. (1961) and Dunwald and Wagner (1931) be reanalyzed.

Table 3-1 contains the thermodynamic quantities used to calculate the equilibrium constant for the CO/CO_2 reaction. The data for log K were fit by least squares, with the result,

$$\log_{10} K = A/T + B + C(T) \qquad (3.3)$$

$$A = -9137\ K,\ \sigma_A = 4.9\ K$$

$$B = 9.602,\ \sigma_B = 8.3 \times 10^{-3}$$

$$C = -2.272 \times 10^{-4}\ K^{-1},\ \sigma_C = 3.38 \times 10^{-6} K^{-1}$$

The carburization data were fit by a non-linear least squares procedure to a model first suggested by Darken and Smith (1946)

Table 3.1. Thermochemical Data for the CO/CO_2 System.[a]

Temp. (K)	ΔG°_f/kJ·mol^{-1}			$\log_{10}K$[d]
	CO(g)[b]	CO_2(c)[c]	C(graphite)	
1000	-200.24	-395.92	0.00	0.238
1100	-209.04	-396.05	0.00	1.046
1200	-217.77	-396.15	0.00	1.715
1300	-226.46	-396.23	0.00	2.278
1400	-235.09	-396.29	0.00	2.757
1500	-243.68	-396.34	0.00	3.170

[a] JANAF Thermochemical Tables, 2nd Ed. (1971).

[b] $\sigma_{\Delta H^\circ_{f,298.15}} = 129$ J·mol^{-1}, $\sigma_{S^\circ_{298.15}} = 0.04$ J·mol^{-1} K^{-1}.

[c] $\sigma_{\Delta H^\circ_{f,298.15}} = 45$ J·mol^{-1}, $\sigma_{S^\circ_{298.15}} = 0.04$ J·mol^{-1} K^{-1}.

[d] $CO_2(g) + C(gr) = 2CO(g)$. $\sigma_{\log_{10}K} = 0.014$ - calculated assuming σ_{S° and $\sigma_{\Delta H^\circ_f}$ are not functions of temperature.

$$\log_{10} A_c = \log \left[\left(\frac{P_{CO}^2}{P_{CO_2}} \right) / K \right] = \log \hat{\gamma}_c + \log y_c, \quad (3.4)$$

$$\log \hat{\gamma}_c = \frac{a}{T} y_c + b + d/T.$$

$$y_c = \frac{x_c}{x_{Fe}} = \text{atom ratio.}$$

Darken (1946) derived this equation from a statistical model for dilute interstitial alloys. In the model it is assumed that the dissolved carbon is in one of two energy states; namely, it has either no or one carbon atom in a nearest neighbor interstitial position. Although very simple, the model does an adequate job of predicting the behavior of carbon in binary metallic solutions.

The data from the four different investigations were fit separately to Equation (3.4). Table 3.2 contains the solubility of graphite in iron at various temperatures and the standard deviation of the data for each investigation. Also in Table 3.2 are the results of Gurry (1942) for the solubility of graphite in iron at 957 and 1104°C and the extrapolated value of Buckely and Hume-Rothery (1963) for the solubility of graphite in iron at the iron graphite eutectic (1153°C). Statistically, the data of Smith (1946) and of Scheil et al. (1961) fit the model best with the data of Ban-Ya et al. (1969, 1970) being almost as good for

Table 3.2. The Solubility of Graphite in Gamma Iron.

Investigator	Temperature (°C) 800	957	1000	1104	1153	Std. Dev. (σ)
			Carbon at %			Std. Dev. % [a]
Smith [b]	3.83	6.01	6.63	8.15	8.87	2.5
Ban-Ya et al. [b,c]	3.64	5.79	6.41	7.92	8.63	3.0
Scheil et al [b]	3.78	5.78	6.37	7.77	8.41	2.7
Dunwald et al [b]	3.62	5.99	6.68	8.40	9.22	5.4
Gurry		6.15		8.10		
Buckley et al					8.98	

[a] σ is the root mean square residual error.

[b] Solubility calculated using the investigators published data and the model suggested by Darken (1946).

[c] Ban-Ya et al's 1300°C and 1400°C data were ignored.

temperatures below 1300°C. If all of the data of Ban-Ya et al. (1969, 1970) are used, the standard deviation jumps to 7%. Chipman (1972) observed that the 1300 and 1400°C data of Ban-Ya et al (1970) are in error. Dunwald and Wagner's (1931) data fit the model with a standard deviation of 5%. When the values for the solubility of graphite are calculated from each set of data it is obvious that while each set is internally self-consistent, the results do not agree with one another. A systematic error must be present in at least three of the data sets and possibily all four. Smith's (1946) results are the only ones that agree with the graphite equilibration data within two standard deviations over the temperature range 800 to 1153°C.

As a result of the systematic deviation among the data sets, it was decided to use only one set of data rather than an average of all the data. Smith's data were chosen for the following reasons:

1. The fit to the model was very good.
2. He obtained the presently accepted value for the CO/CO_2 equilibrium constant using his equipment.
3. Care was used in checking the accuracy of the National Bureau of Standards standard reference material (NBS SRM) used in calibrating his carbon analyzer.

4. His data agree closely with the graphite solubility data of Gurry (1942) and Buckley and Hume-Rothery (1963).

The equation for the activity of carbon in iron derived from Smith's data is:

$$\log_{10} A_c = 10 g_{10} y_c \hat{\gamma}_c = (a/T) y_c + b + d/T + \log_{10} y_c \quad (3.6)$$

$$\sigma_{A_c} = 2.5\%$$

$$a = 3.981 \times 10^3 \text{ K}, \quad \sigma_a = 1.09 \times 10^2 \text{ K}$$

$$b = -8.108 \times 10^{-1}, \quad \sigma_b = 1.33 \times 10^{-2}$$

$$d = 2.212 \times 10^3 \text{ K}, \quad \sigma_d = 1.69 \times 10^1 \text{ K}$$

Smith's (1946) published data are tabulated in Table 3.3. The precision of Smith's (1946) data is 2.5%. It is heartening to note that the graphite and the most precise gas phase carburization data agree.

The results of Smith, Ban-Ya *et al.*, Scheil *et al.*, and Dunwald and Wagner are compared with Equation (3.6) in Figures 3.2, 3.3, 3.4 and 3.5. The x's are experimental points, the zeros, 0, are calculated from Equation (3.6) and the equal signs, =, indicate that the calculated and experimental points differ by less than 1.9%. Smith's

Table 3.3. Data of R. P. Smith (1946) for Activity of Carbon in γ-Iron in Equilibrium with CO/CO_2 Gas Mixtures.

T (°C)	Carbon			
	wt %	at %	y_c [a]	P_{CO}^2/P_{CO_2}
800	0.343	1.58	0.0161	2.25
	0.356	1.63	0.0166	2.46
	0.377	1.73	0.0176	2.65
	0.405	1.86	0.0190	2.85
	0.443	2.03	0.0207	3.11
	0.453	2.07	0.0212	3.12
	0.522	2.38	0.0244	3.63
	0.568	2.59	0.0266	4.21
	0.608	2.77	0.0285	4.50
	0.647	2.94	0.0303	4.87
	0.661	3.00	0.0309	5.11
	0.726	3.29	0.0340	5.54
	0.726	3.29	0.0340	5.64
	0.765	3.46	0.0358	6.07
	0.815	3.68	0.0382	6.55
	0.831	3.75	0.0390	6.75
	0.838	3.78	0.0393	6.81
	0.836	3.77	0.0392	6.89
	0.875	3.94	0.0410	7.24
1000	0.0360	0.167	0.00167	1.98
	0.0487	0.226	0.00227	2.49
	0.0563	0.261	0.00262	3.12
	0.0740	0.343	0.00344	4.21

Table 3.3. Continued.

T (°C)	Carbon			P_{CO}^2/P_{CO_2}
	wt %	at %	y_c [a]	
1000	0.133	0.615	0.00619	7.29
	0.242	1.115	0.0113	13.8
	0.455	2.081	0.0213	27.4
	0.655	2.974	0.0307	43.4
	0.810	3.658	0.0380	56.2
	0.963	4.326	0.0452	70.8
	1.081	4.836	0.0508	84.1
	1.206	5.371	0.0568	99.4
	1.321	5.860	0.0622	113.3
	1.462	6.453	0.0690	130.2
	1.466	6.470	0.0692	131.7
	1.471	6.491	0.0694	132.4
1200	0.0148	0.0688	0.000688	3.75
	0.0141	0.0655	0.000655	3.80
	0.0217	0.101	0.00101	5.83
	0.0252	0.117	0.00117	7.14
	0.0273	0.127	0.00127	7.23
	0.0450	0.209	0.00209	12.46
	0.109	0.505	0.00508	30.3
	0.215	0.992	0.0100	61.4
	0.416	1.905	0.0194	122.5
	0.413	1.892	0.0193	123.1
	0.738	3.341	0.0346	243.6
	0.942	4.234	0.0442	352.2

[a] $y_c = X_c/X_{Fe}$ - atom ratio of carbon to iron.

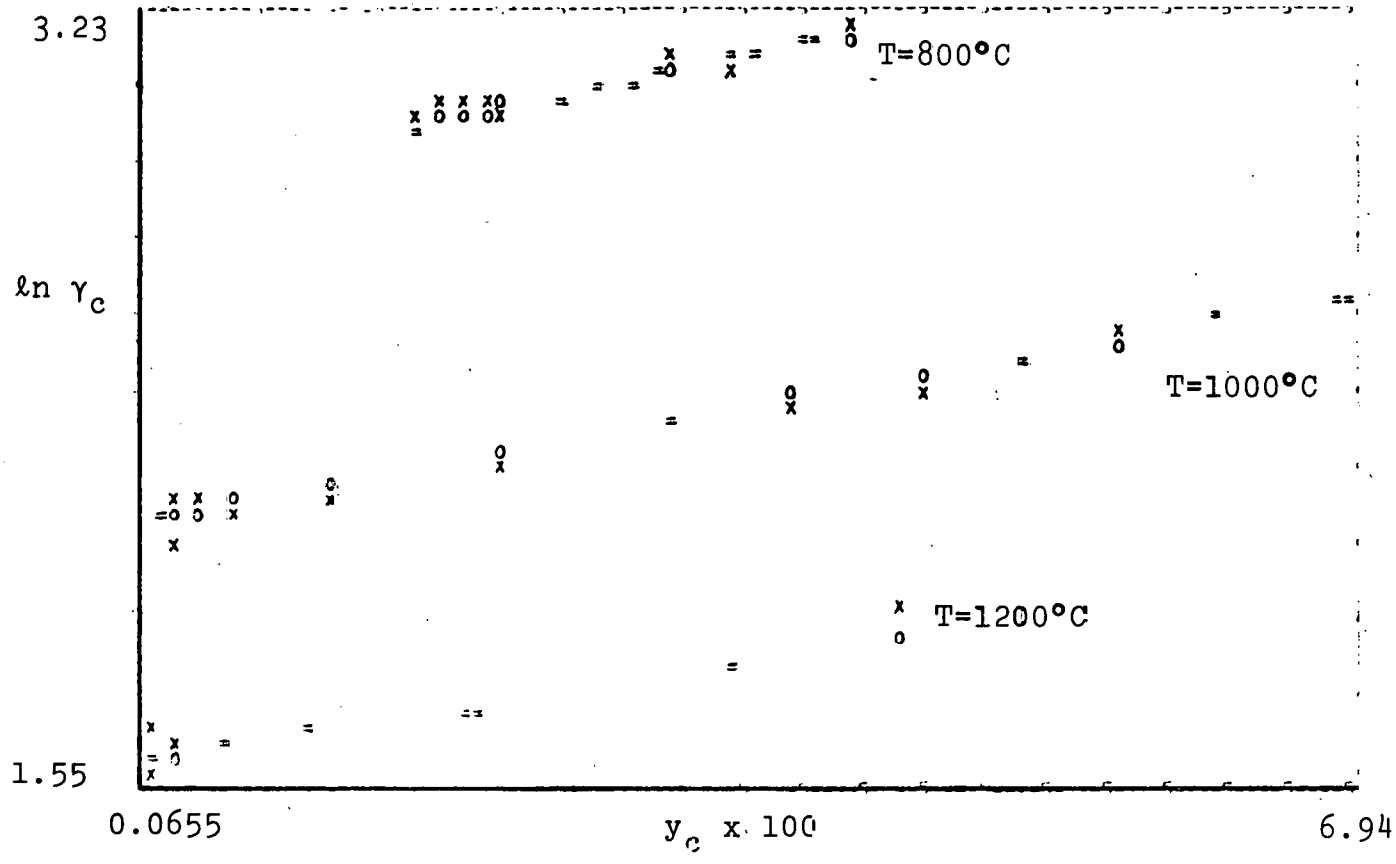

Figure 3.2. The results of Smith (1946) versus Equation (3.5), $\ell n\gamma_c$ vs y_c ($y_c = \frac{x_c}{(1-x_c)}$. The x's are experimental points, the zeros, 0, are calculated points and the equal signs, =, indicate that the calculated and experimental values differ by less than 1.9%.

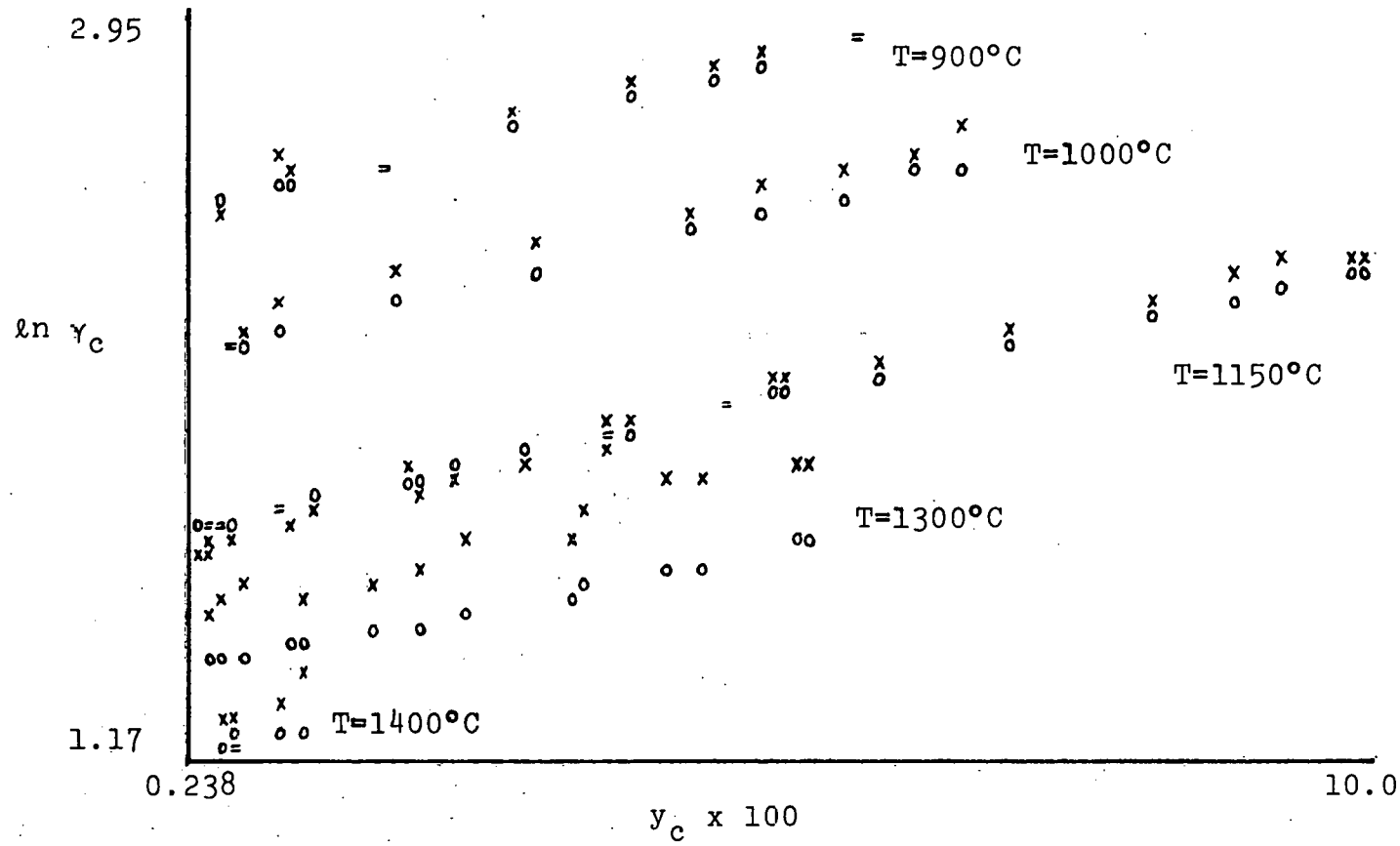

Figure 3.3. The results of Ban-Ya *et al* (1969, 1970) versus Equation (3.6), ℓn γ_c vs y_c [$y_c = x_c/(1-x_c)$]. The x's are experimental points, the zero's, 0, are calculated points and the equal signs, =, indicate the calculated and experimental values differ by less than 1.9%.

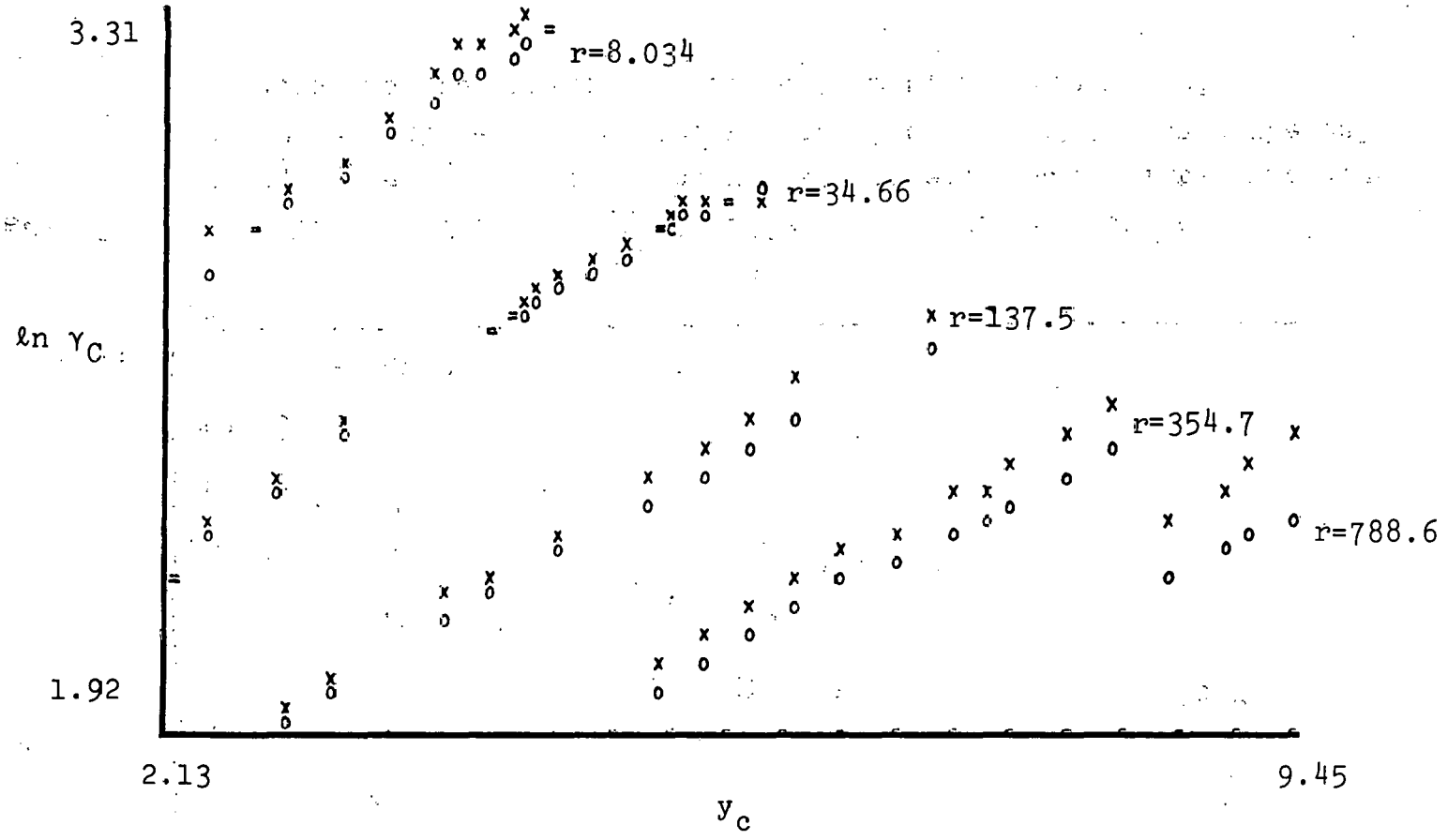

Figure 3.4. The results of Scheil et al (1961) versus Equation (3.6). ℓn γ_C vs. y_c [$y_c = x_C/(1-x_C)$]. Scheil et al performed sets of experiments at constant P^2_{CO}/P_{CO_2} rather at constant temperature. The X's are experimental points, the zero's, 0, are calculated points and the equal signs, =, indicate the calculated and experimental values differ by less than 1.9%. ($P^2_{CO}/P_{CO_2} = r$).

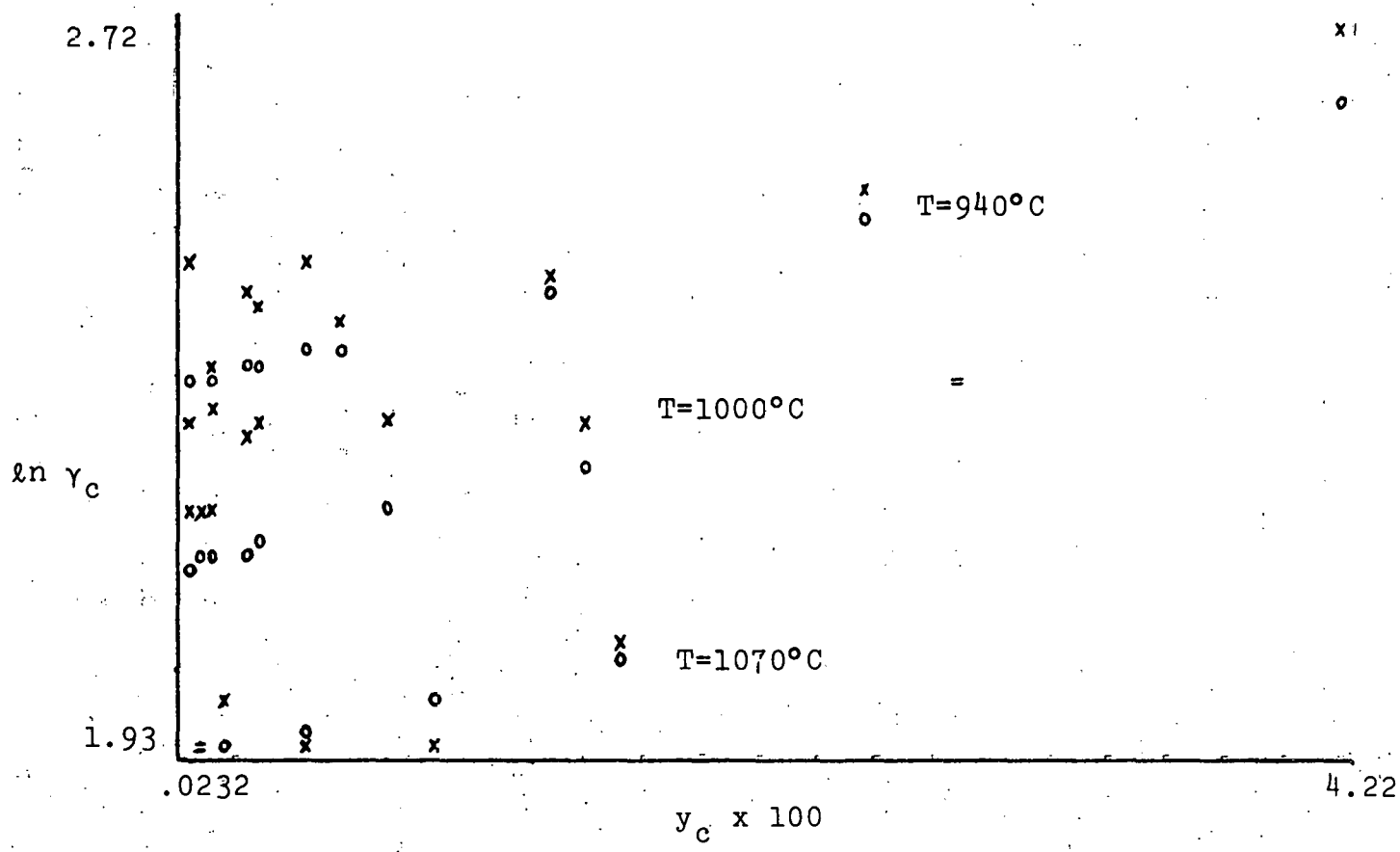

Figure 3.5. The results of Dunwald et al (1931) vs. Equation (3.6), ℓn γ_c versus y_c [$y_c = x_c(1-x_c)$]. The x's are experimental points, the zero's, 0, are calculated points and the equal signs, =, indicate the calculated and experimental values differ by less than 1.9%.

results scatter uniformly about the calculated points and seem to fit the model in both terms of temperature and composition dependence. The results of Ban-Ya et al. for $\ln \gamma_C^{\infty}$ versus y_C, in Figure 3.3 are high compared to Equation (3.6) except at 1150°C, where the results are in better agreement. The residuals at 1150°C, however, are biased as a function of carbon concentration. The results of Ban-Ya et al. at 1150°C were obtained at a different time than those at the other temperatures and this could explain the difference. Figure 3.3 clearly shows that their 1300°C and 1400°C results are not consistent with the model having an intercept which is proportional to 1/T or 1/T plus a constant. This affirms Chipman's (1972) assertion that the high temperature data of Ban-Ya et al. is in error.

The results of Scheil et al (Figure 3.4), like those of Ban-Ya et al., are high compared to Equation (3.6). When fit directly to the model, Equation (3.6), Scheil's results do not seem to fit. The residuals indicate that the intercept would have to be a complicated function of temperature to fit all the results. Dunwald and Wagner's results are also high compared to Equation (3.6). This is especially true at low carbon concentration where their data indicate a zero slope for $\ln \gamma_C^{\infty}$. Given the precision of the other investigators' results, it is likely that Dunwald

and Wagner's results are incorrect at low carbon concentrations.

Mainly, the results of the other investigators beside Smith were systematically higher for $\ln \gamma_C^{\infty}$ than those of Smith. The most probable reason for this is the gas composition or the carbon analyses, either of which could conceal a systematic error that would effectively increase the value of the activity coefficient of carbon. Figures 3.2-3.5 all tend to confirm our decision to use only one set of data, that of Smith, in our experiments.

If greater accuracy is desired for the iron-carbon system, the areas where improvement of technique would be most valuable are: (1) carbon analyses; (2) analyses of the gas mixtures, and (3) experiments at more, different temperatures to obtain a better fit for the temperature dependence of the activity coefficient.

CHAPTER IV

ANALYSIS FOR CARBON

A. Introduction

Analysis for carbon is critical to the results of this work. Considerable effort was expended on developing the combustion method for analysis of carbon and in demonstrating its precision and accuracy. The procedure described here is the culmination of a many step process. The attainable precision of the method is shown to be approximately 1% in Section B; not all analyses were of this precision, however. Section C addresses the question of the accuracy of the analyses. Since the analysis method relies on National Bureau of Standards Standard Reference Materials (NBS SRM), the accuracy of the results depends on the accuracy of the certified analysis of the NBS SRM. Analysis of several NBS SRM's shows that they scatter approximately ±5% relative to their certified concentrations. The scatter in the standards limits the accuracy of the carbon analyses reported here to approximately ±5%.

B. Procedure for Total Carbon Determination by the Combustion-Gas Chromatographic Method

1. Summary

The carbon in the material is converted to carbon dioxide by combustion in an oxygen stream. The carbon dioxide is then trapped on a zeolite column. After the combustion is completed, the trap is heated, and the carbon dioxide is released into a stream of helium and thence to a chromatographic column. The amount of carbon dioxide is measured in a thermistor type conductivity cell. The signal is automatically integrated and displayed on a digital panel. The instrument must be calibrated with material of known carbon concentration.

2. Equipment and Reagents

Reaction crucibles: fired at 1000°C for eight hours and then stored in a desiccator until used.

Acetone: electronic grade, less than 0.0005 percent residue.

Tin metal accelerator: washed in water and acetone to remove organic impurities and then dried at 70 to 100°C.

Cupric oxide: fired at 1000°C for two to three hours in air.

Helium, high purity: passed through a purification train of ascarite, glass wool and Dri-rite.

Oxygen, ultrahigh purity: passed through a purification train of ascarite, glass wool, and Dri-rite.

3. Calibration

NBS Standard Reference Material 121B was used as the calibration standard. Aliquots of less than 20 mg were not used. Homogeneity for aliquots of 20 mg has been demonstrated for National Bureau of Standards Standard Reference Materials (ASTM, E350).

4. Determination of Blank

Before actually determining the blank, the instrument is cycled several times with the standard until a constant response is obtained.

To determine the blank, one scoop (approximately 0.75 gram) of tin granules and then two scoops of cupric oxide are placed in a crucible. The crucible is then placed in the combustion chamber and allowed to sit in the oxygen stream for one to two minutes before cycling the instrument. The blank determination is repeated several times until a reading of ±1 µg is achieved for three consecutive determinations. A blank greater than 15 µg indicates

that there is probably a leak in the system which must be corrected.

5. Procedure

With the instrument stabilized and the average blank determined, the analyses are undertaken according to the following procedure: Each unknown determination is preceded and followed by an aliquot of a SRM. The aliquots of 121B are measured to contain approximately the same numbers of micrograms of carbon as the samples (±100 ug). Aliquots of standard and sample of less than 100 µg or greater than 1000 µg are avoided. The factor $(\frac{\mu g \text{ carbon}}{\text{number of counts}})$ used for calculating the concentration of carbon in the unknown is obtained by averaging the value obtained for the SRM. If the instrument is not run for an hour, or if different batches of gas, tin, copper oxide or crucibles are used, the procedure for determining stability and the blank is repeated before proceeding to new samples.

C. Precision of the Carbon Analyses

Table 4.1 and Figure 4.1 contain data on National Bureau of Standards Standard Reference Material 121B collected in three sets over a period of three weeks. As

Table 4.1. Calibration Data for LECO Gas Chromatograph Carbon Analyzer with National Bureau of Standards Standard Reference Material 121B.[a]

Date	NBS SRM 121B (gms)	Instrument Reading (counts)
2/18/77	0.2213	307.1
	0.3029	425.3
	0.4345	609.4
	0.5209	740.2
	0.6091	848.3
	0.4157	581.3
	0.5192	725.9
	0.4080	576.8
	0.5182	721.6
	0.4184	578.5
	0.6439	899.0
	0.4408	615.0
	0.5134	721.7
	0.4106	579.3
	0.4110	592.0
	0.4423	621.1
	0.5208	734.1
	0.4553	641.9
	0.4030	566.2
3/3/77	0.4150	579.7
	0.2318	319.9
	0.4448	627.0
	0.4249	592.8
	0.6269	875.0

Table 4.1. Continued.

Date	NBS SRM 121B (gms)	Instrument Reading (Counts
3/3/77	0.4550	634.1
	0.2214	305.9
	0.5113	724.0
	0.5465	768.0
	0.5084	718.0
	0.4246	588.0
3/11/77	0.2427	338.7
	0.5513	794.7
	0.4302	598.8
	0.2116	292.3
	0.6144	858.0
	0.3369	477.1
	0.4158	584.0
	0.4273	596.7
	0.4159	592.2
	0.4520	641.8
	0.4199	597.1
	0.4358	617.3
	0.4085	577.0
	0.4322	613.6
	0.2277	324.2

[a]NBS SRM 121B is stated to contain 0.0720 wt% carbon.

THIS PAGE

WAS INTENTIONALLY

LEFT BLANK

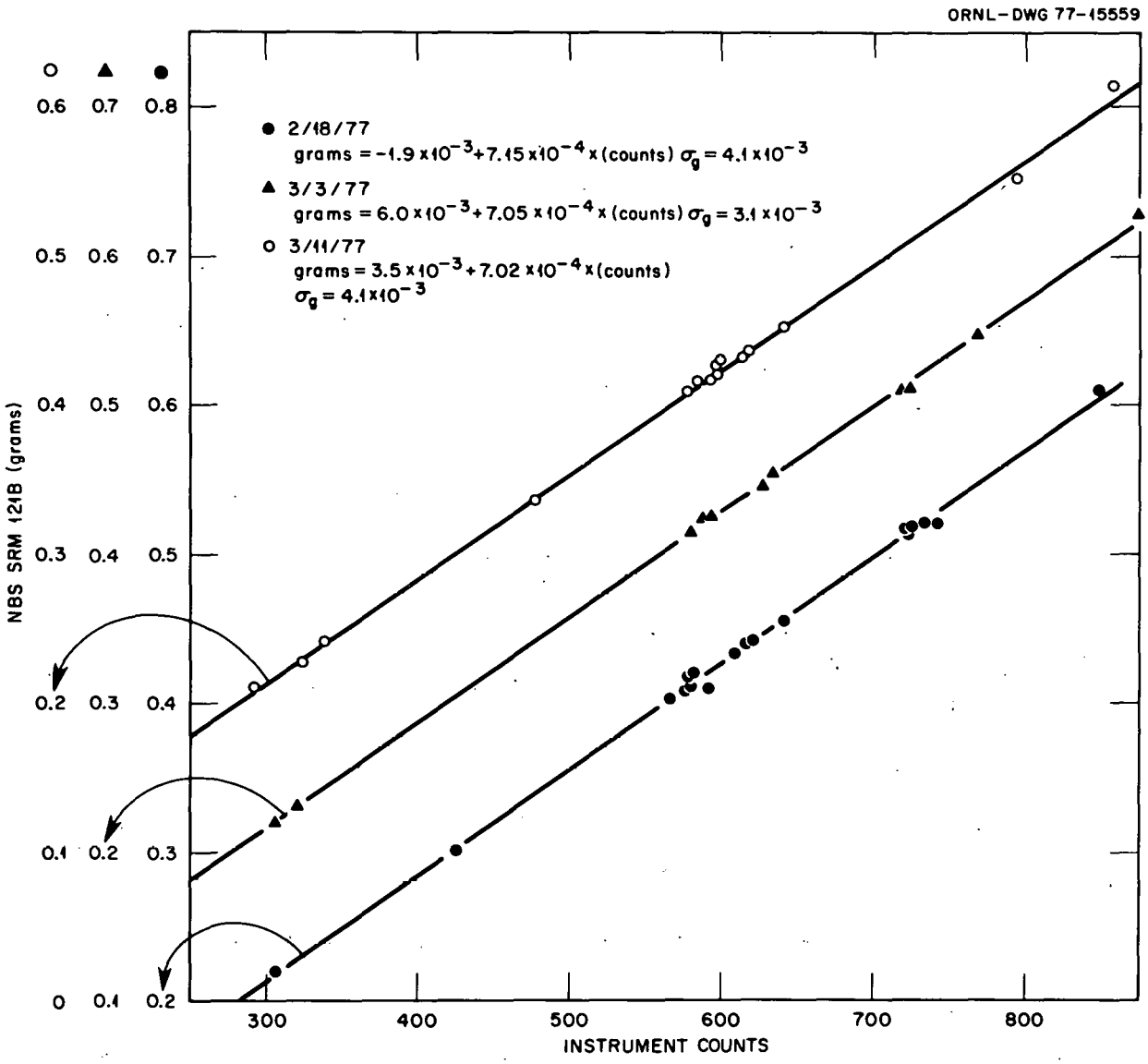

Figure 4.1. Calibration data for the LECO carbon analyzer. The data was taken on three separate days.

shown in the figure the standard deviation in the weight of 121B varied from 3.1 to 4.1 mg. To obtain one percent precision one must use aliquots of 121B with a mass of approximately 0.4 grams or larger. Since 121B has a nominal carbon concentration of 0.0720 weight percent, aliquots of greater than 300 μg of carbon should be used to ensure one percent precision. In practice it is not desirable to exceed 1000 counts on the instruments. Above 1000 counts the amplifiers begin to saturate and become non-linear in their response. If aliquots of greater than 500 micrograms of carbon were desirable for some situation a lower amplifier setting can be used, so that the number of counts per microgram of carbon is decreased.

D. Accuracy of the Carbon Analyses

NBS Standard Reference Materials are used almost universally to standardize instruments for material analysis. These materials undergo a rigorous testing for homogeneity and composition at the Bureau of Standards Laboratory and in private and industrial research laboratories. However, the accuracies of the analyses are not stated or implied by the National Bureau of Standards. The certificate of analysis accompanying the standards shows that in many cases the scatter in the certificate value as reported by the various laboratories is ±5 percent for carbon.

As part of this research effort several NBS Standard Reference materials with certified carbon contents were examined. Some of the results are tabulated in Table 4.2. The instrument used for these analyses is a LECO carbon analyzer with a gas chromatograph-thermal conductivity detector. The following procedure was used to measure the carbon concentrations in the NBS materials. The instrument was cycled several times until the response stabilized and a constant blank was obtained. A NBS SRM was used to calibrate the instrument. An aliquot of the standard reference material preceded and followed each aliquot of sample. The number of micrograms of carbon was approximately the same in both the calibrating standard and the standard being checked.

Table 3.1 shows that the scatter in the data for each standard is less than or equal to ±1 percent of the value. The discrepancy with the certified value is as much as ±7 percent. The relative lack of accuracy in the certified analysis leads to the following problems:

NBS SRM's

1. If one standard is used consistently the precision of results can be greater than 1 percent. The calculated data, however, will contain a systematic error due to the accuracy of the certified analysis.

2. If many different standards are used to calibrate

Table 4.2. Analysis of NBS Standards.

SRM Number	Certificate Analysis Carbon (weight percent)	Carbon[a] (wt. %) Analysis Number 1	2	3	Average	Average % Deviation from NBS Value
20F	0.330	0.395	0.396	0.398	0.396	+4.3
19E	0.197	0.204	0.204	0.205	0.204	+3.7
15D	0.100	0.102	0.102	0.102	0.102	+2.0
101E	0.0540	0.0528	0.0524	0.0534	0.0529	-2.1
160B	0.0460	0.0437	0.0429	0.0425	0.0430	-6.5
101F	0.0140	0.0140	0.0139	0.0138	0.0139	-0.7

[a]The carbon concentrations are relative to NBS SRM 121 B, 0.0720 wt. % carbon.

an instrument, the precision of the measurement will be limited by the scatter in the values of the certified analyses relative to one another.

3. Comparison of data from various investigators is difficult since different groups use different calibrating standards. If different standards are used, discrepancies as high as 10 percent could occur. These problems can be mitigated to some extent if the calibrating standard is cited in the literature. To eradicate the problems, inaccuracies in the standards must be removed. Problems related to inaccuracy have been caused by abuse of the standards rather than by a failure on the part of the NBS. The fact that a scatter of 5 percent is reported on the certification should be sufficient to keep users from claiming accuracies of ±1 or 2 percent.

Initially, NBS SRM 19E was used to calibrate the instrument and, hence, as a basis for analysis of a number of samples. When SRM 19E was exhausted, SRM 121B was used. All the SRM 121B data were converted to the SRM 19E after analysis. The correction is shown in Table 4.2. Thus, the data in Appendix A based on SRM 121B were converted to the SRM 19E base for all subsequent calculations unless otherwise stated.

CHAPTER V

EXPERIMENTAL PROCEDURES

A. Preparation of the Alloys

In working with carbon in alloys containing strong carbide forming elements, special care has to be taken during fabrication. Precipitation of carbides during processing can result in inhomogeneous alloys (Braski and Leitnaker, 1977). The problems of inhomogeneity are not restricted, unfortunately, to the as-fabricated material. It has been found that the carbides cannot be easily removed once formed. The slow diffusion rate of carbide forming metals results in the enrichment of titanium and molybdenum in the former carbide areas even after long anneals. This is demonstrated by the fact that the carbides precipitate in "stringer" like patterns upon aging at temperatures below the solubility limit. Figure 5.1 is an optical photomicrograph showing this so-called "memory effect" in a nickel based alloy similar to those used here.

Braski and Leitnaker (1977) concluded that a way to achieve a homogeneous microstructure was to hot work the material at temperatures in the solid solution regime and that any intermediate recovery anneals after cold working

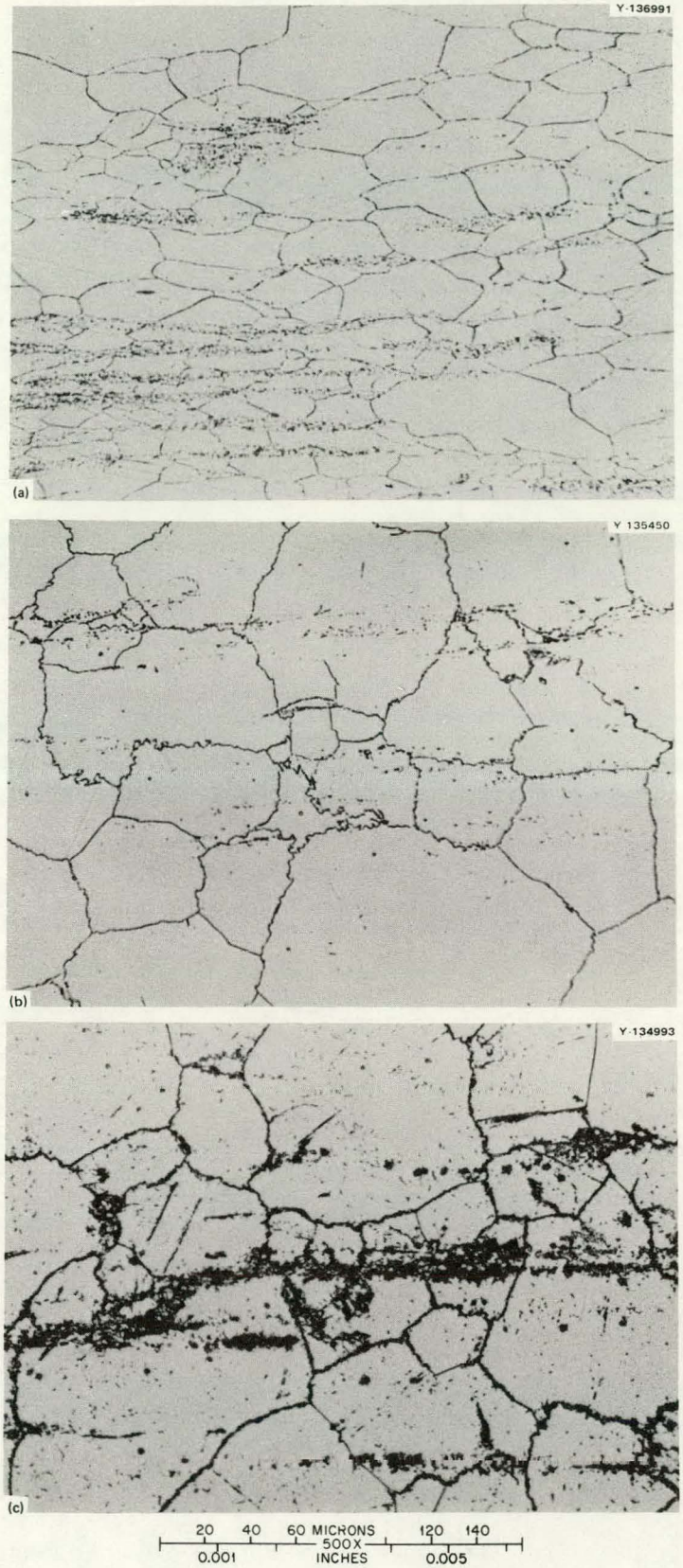

Figure 5.1. Optical photomicrographs illustrating the "memory effect" in Ni-2.5 Ti-8 mo-8 Cr-0.2 (at. %). (a) As swaged. (b) After 1 hour at 1177°C. (c) After 1 hour at 1177°C + 160 hours at 760°C.

THIS PAGE

WAS INTENTIONALLY

LEFT BLANK

should be in the solid solution regime. As a result of their work the eight primary alloys used in this study were prepared using a slightly modified version of the fabrication schedule suggested by Braski and Leitnaker. Table 5.1 lists the procedure followed.

Table 5.2 gives the composition of the melts, as weighed prior to melting, and the composition of the analyzed 3 mm diameter rods. An extra 0.5 weight percent of chromium was added to all of the alloys containing chromium to correct for expected losses through evaporation. The carbon concentration was lowered to one third of its initial value, primarily due to losses during the final deoxidizing anneal. As Table 5.2 shows, the molybdenum and the chromium contents of the alloys were analyzed in several different ways. Quantitative analysis for transition metal elements in the concentration regimes in which this work was performed is a difficult task due to the high concentration of the different elements. The Paschen results for the chromium and molybdenum and the atomic absorption results for molybdenum appear to be unreliable because of the non-reproducibility of these techniques for the elements in question. Table 5.3 gives the values for the composition of the alloys that were judged to be the best. These values are used in all subsequent calculations.

Table 5.1. Fabrication Schedule[a] for Alloys 7261-7268.

Step No.	Fabrication Process	Rod Diameter (mm)	Reduction in Area During Swaging (%)	Heat Treatment[b]
1	Arc melt-drop cast (remelt 5 times)	25.4		
2	Hot swage at 1177°C			
	Pass 1	22.1	24.3	15-min reheat between passes
	Pass 2	18.8	27.6	
	Pass 3	16.3	24.8	
	Pass 4	13.7	29.3	
	Pass 5	12.4	18.1	
	Pass 6	10.9	22.7	
3	Homogenizing anneal			1 hr at 1300°C
4	Cold swage (room temperature)	8.6	37.8	
5	Intermediate anneal			15-min at 1177°C
6	Cold swage (room temperature)	6.4	44.6	
7	Intermediate anneal			15-min at 1177°C
8	Cold swage (room temperature	5.1	36.5	
9	Intermediate anneal			15-min at 1177°C
10	Cold swage (room temperature)	4.1	35.4	
11	Intermediate anneal			15-min at 1177°C
12	Cold swage (room temperature)	3.2	39.1	
13	Deoxidizing anneal in H_2 gas			2 hr at 1100°C

[a]Procedure developed by Eraski and Leitnaker (1977).

[b]Specimen were water quenched after each reheat.

Table 5.2. Alloy Compositions as Determined by Several Methods of Analysis, wt %.

Alloy Melt No.	Titanium			Chromium			Molybdenum				Carbon[g] Direct Combustion
	Paschen[a] Emission	Comp[b] of Melt	AA[d]	Paschen[a] Emission	Volume[e]	Comp[f] of Melt	Paschen[a] Emission	AA[d]	Color	Comp of Melt	
7261	2.00	2.06									0.015
7262	1.95	1.95					12.0	12.79	12.81	12.90	0.014
7263[c]	2.02	2.08		7.78		7.93					0.014
7264	1.95	2.00					6.38	6.78	6.68	6.62	0.015
7265	2.06	2.07		4.09		4.20					0.016
7266	1.91	1.97	7.01	7.58	7.08	7.55	12.7	13.38	12.76	12.02	0.021
7267	1.95	1.96	3.98	4.07	3.77	4.02	12.2	12.95	12.93	12.96	0.016
7268	2.00	2.02	7.29	7.44	7.33	7.73	6.5	7.20	6.66	6.68	0.015
7068	2.97	3.14									0.087
7071	2.80	3.14			8.08	8.50					0.135
7095	3.06	3.14					14.1		14.6	13.9	0.380
A	2.00	1.94					13.6			13.0	0.094
B	1.73	1.94									0.086
C	2.00	1.94		7.40		7.50					0.109
449[h]	2.00	1.94		7.20		7.50	11.5	11.4		13.0	0.035

[a]The 21 ft Paschen-Runge spectrograph at the ERDA Y-12 facility was used for these analyses. The 95% confidence level (2 standard deviations from the mean equals approximately 2.5% of the stated value for Ti, and 3.0% of the stated value for Cr, and 6% of the stated value for Mo. For a description of analytical procedure see Leitnaker et al (1977).

[b]The 750 g melts lost 0.3±0.1 wt % on casting.

[c]Colorimetric analysis for Cr gave a result of 7.2 wt % ±3% of the value.

[d]Atomic absorption has an uncertainty of 3% of the values for both Mo and Cr. Molybdenum spike recovery was poor for alloy 7266 and probably accounts for the high value relative to the colorimetric results. NBS standard reference material 101E was used to prepare the calibration curves.

[e]Volumetric analysis for Cr has an uncertainty of ~1% of the value. It is considered the most accurate method for Cr determination in this concentration range.

[f]Due to the high vapor pressure of Cr, relative to the other elements in the melt, 0.5% Cr was added to the amount desired in the final product. A good approximation would be that all weight loss on casting is attributable to Cr volatilization. Values include the extra 0.5% Cr.

[g]Method used was direct combustion to CO_2. The standard deviation is ±3%.

[h]This alloy also contained 0.2 wt % Fe.

Table 5.3. Composition[a] of Alloys Used for Calculations.

Alloy Melt No.	Element/wt %				
	Ti	Cr	Mo	C	Ni
7068	2.97			0.087	96.94
7261	2.00			0.015	98.0
7262	1.95		12.81	0.014	85.3
7263	2.02	7.78		0.014	90.2
7264	1.95		6.68	0.015	91.4
7265	2.06	4.09		0.016	93.8
7266	1.91	7.08	12.76	0.021	78.2
7267	1.95	3.77	12.93	0.016	81.4
7268	2.00	7.33	6.66	0.015	84.0
7071	2.80	8.08		0.135	89.0
7095	3.06		13.9	0.380	82.7
A	2.00		13.0	0.094	84.9
B	1.73			0.086	98.2
C	2.00	7.40		0.109	90.5
449	1.94	7.36	11.4	0.035	79.0

[a]These values were picked from those in Table 5.1.

B. Carburization

1. Specimen Preparation

For the carburization experiments the 3 mm nickel alloy rods were cut into sections 4 cm long. Each specimen was marked with a vibrator tool with the last two digits of its respective melt number prior to cutting from the parent rod. The specimens were then chemically cleaned in a solution of hydrochloric and nitric acid. The acid cleaning was followed by washings in methanol and, finally, acetone. After they were cleaned and dried, the specimens were weighed on a Mettler semi-micro balance to 0.002 mg.

The samples were next spot welded at each end to loops of nickel wire. It was found that the wire could be removed cleanly from the specimens if the welding was done with the proper energy-input (25 watt-sec for 3 mm rod and 0.5 mm wire worked well). If, however, too large an energy-input was used during the welding or if the sample surface became oxidized, then the wire could not be easily removed after carburization. As many as ten samples were welded to the loops in this fashion. The connected set of samples was lowered into the hot zone of the furnace on a nickel tether attached to an iron slug controlled by magnets, as described in Section 2.

2. Furnace and Auxiliary Equipment

a. The Furnace - The carburizing and annealing furnace was one of the central pieces of equipment used in this study. In order to accommodate the wide range of uses required of it, the furnace was designed according to the following criteria:

(1) It must be capable of being operated safely in an atmosphere of H_2 or Ar.

(2) It must have incorporated in it a vacuum pump to facilitate changes in sample atmosphere and to check the system for leak tightness.

(3) It must allow for cooling rates which vary from a brine quench to a furnace cool. The cooling must be done in an inert atmosphere.

(4) It must be inert relative to the gases, e.g. CH_4 or H_2. Specifically, it must not act as a sink for carbon or a source for any other elements.

(5) It must have a constant temperature zone of 4-6 inches.

(6) It must allow for reproducible mixing of different gases.

(7) It must have unobstructed flow of gas around the samples while they are in the hot zone.

(8) It must have the capability to purify and monitor the purity of the gas stream.

The furnace itself is a platinum resistance heated furnace with a 55 mm bore. The temperature controller used throughout most of the experiments was a Speed-Max G duration adjusting (DAT) controller. The controller maintained a constant temperature to ±2°C. Toward the end of the investigation an Electromax III current adjusting type controller (CAT) was substituted for the DAT. Temperature control of better than ±1°C is possible with the CAT controller.

To insure the inertness of the system the furnace liner is made of DeGussitt-19 recrystallized high-purity alumina. Smith (1946) noted that above 1000°C with a mullite liner the reduction of SiO_2 becomes a major problem. In this work we found that iron can also be transferred from a mullite liner to samples in a reducing atmosphere. Alumina reduction by hydrogen at the temperatures dealt with here (900-1215°C) is not a problem.

The liner is sealed to a copper collar at both ends with a viton O-ring. The water cooled copper collar serves as inlet and exit for gas, as the connection to the vacuum system, and for the removal and introduction of samples. The lower collar contains the vacuum port and connects to the quenching tank through an air-activated

gate valve.

The upper collar contains the vacuum gage and is fitted with an O-ring groove which allows a pyrex extension tube to be sealed to the collar. The pyrex extension functions as the cold zone of the furnace. A magnet is used to lower the samples into the hot zone. If a quench is desired the magnet can be removed and the sample dropped through the gate valve and into the quench tank. The gas system is so arranged that the samples are in a controlled atmosphere until they hit the quenching medium. If slower cooling is desired, the samples can be raised with the magnet into the extension tube.

b. Thermometry - The temperature in the furnace was measured with a calibrated platinum-10% rhodium (Type S) thermocouple. A similar thermocouple was used to control the furnace temperature. Before each set of runs, to insure that the furnace was at the proper temperature, a profile of the furnace temperature was taken. After initially adjusting the resistance across 6 taps the furnace temperature was found to be constant within 2°C over the 100 mm center section of the muffle. No discernible drift in the peak occurred with time.

c. Gases - The piping system to the furnace is designed to allow three different gas cylinders to be used

together or separately. Each of the three lines feeds gas through a Fisher-Porter Tri-flat variable area flowmeter and into a central mixing chamber. The flowmeters, with flow rates of 0-300 cc/min, can be used to mix gases to ratios as low as 1:20 with little difficulty. After passing through the mixing chamber the gas stream either enters directly into the furnace or goes through a purification train and then into the furnace. The purification train consists of a palladium catalyst followed by a column filled with Linde 3A molecular sieve. The palladium converted any free oxygen in the gas into $H_2O(g)$ and then the molecular sieve removed the water. The gas stream was analyzed for water on the exit side of the furnace with a Panametrics Model 1000 hygrometer. Water concentrations of less than 0.5 ppm by volume were obtained with this purification technique.

d. Operating Procedure for Safe Use of the Hydrogen Furnace

1. Starting Up

a. Close bottom gate valve and unplug electrical socket.

b. Set all regulators at ~5 lbs and close all flow meter valves.

c. Make sure vent valves are closed.

d. Evacuate furnace system with fore pump. (If the fore pump is not used to evacuate the furnace system, a minimum of 0.5 cubic feet of argon must flow through the furnace and more than 1.5 cubic feet is not necessary since the furnace volume is only ∿.15 cubic feet.

e. Back fill with argon.

f. Repeat d and e for 3 cycles.

g. Open exit valve to exhaust system. The pressure in the furnace should be atmospheric or very slightly above.

h. Light pilot light and open exhaust hood.

i. Begin flowing hydrogen with argon still flowing.

j. Shut off argon.

2. Shutting Down

a. Start flowing argon.

b. Turn off hydrogen.

c. Flush the furnace with at least 0.5 cubic feet of argon, not more than 1.5 cubic feet is needed. (At the end of this time a platinum wire near the pilot light should not be glowing.)

d. Open furnace to remove or insert samples. Leave argon flowing while furnace is open and reclose the furnace as soon as possible.

e. Shut off pilot light.

f. Shut off argon.

g. Close exhaust hood.

3. Use of Quench Tank

a. Secure quenching tank to the base of furnace with C-clamps or bolts.

b. Flush quench tank with a minimum of 0.7 cubic feet of argon or not more than 2.0 cubic feet.

c. Turn off argon first up stream from quenching tank and then down stream just prior to quenching samples. (It is important not to build-up pressure in the tank which may blow the quenching media up into the furnace chamber when the gate valve is opened.

d. Plug in gate valve.

e. Open gate valve - drop samples into quench tank - close gate valve - unplug gate valve.

C. Annealing

In order to obtain information on the solubility of carbon in the carbide-forming alloys at relatively low temperatures (800-1000°C), a procedure other than carburization was employed. The low solubility of carbon, <0.05 atom percent, and the slow kinetics of the carburization reaction make carburization experiments extremely

difficult at these temperatures. (See Chapter IX for a discussion of the results of the carburization experiments at 900°C in the carbide forming alloys.) To circumvent the problems of carburization, alloys with a fixed concentration of carbon were arc melted and cast. Three (3) millimeter rod sections of these alloys were then annealed at various temperatures.

For annealing, two platinum wound resistance furnaces with Inconel 600 furnace tubes were used. The samples were first cleaned as described in Section II B and then wrapped tightly in a sheet of tantalum. The furnaces were designed to allow a continuous flow of argon through the hot zone. The tantalum foil acted as a getter for the impurities in the gas. When samples were being placed in the furnaces the flow of argon was increased and was kept high for approximately five minutes after closing the furnace. At the end of an experiment the argon flow was again increased, and the samples were quickly pulled from the hot zone of the furnace and plunged into a 10% sodium-chloride brine. A translucent oxide was visible on alloys containing chromium and molybdenum after quenching. Oxidation apparently occurred during the quench rather than during the anneal.

The calibrated platinum-10% rhodium thermocouple used in the carburization experiments was used to measure the

temperature in the annealing furnaces. The current adjusting type of proportional temperature controller was used throughout this series of experiments. The temperature in the region of the furnaces containing the samples was held constant to within ±2°C.

D. Electrolytic Extractions

1. Description - In order to obtain precise information about precipitated phases in metallic matrices, it is necessary to isolate the precipitate. The precipitate phases in the materials of concern have varied from 0.05 wt % to 5 wt %. Since quantitative determination of weight fractions was desired, a highly specific isolation technique was required such that none of the precipitate phases dissolves but all the matrix dissolves. The literature [Donachie (1972) and Andrews (1966)] indicates that anodic dissolution has been shown to be a highly selective technique. Donachie (1972) lists 9 different precipitate phases that have been successfully isolated by the electrolytic technique. Specifically, since MC type phases can be quantitatively recovered and since MC was the phase of primary import in this investigation, it was decided to use anodic dissolution for the concentration of precipitates.

Anodic dissolution involves using the sample material

as the anode and some inert material, such as platinum, as the cathode in an electrolytic cell. The electrolyte most often used, and that used for all this work, is a solution of 10% by volume of concentrated HCl in methanol. Donachie (1972) indicates that in alloys containing tungsten, tantalum or niobium a complexing agent such as tartaric acid must be added to control oxidation since considerable amounts of oxides of these elements can form and precipitate.

In this connection it was discovered during this investigation that nickel oxide forms in small quantities during electrolytic polishing of surfaces. Oxide formation can be a particularly severe problem in sample preparation for the electron microscope or small angle x-ray scattering. The nickel oxide has only been detected by x-ray diffraction in extracted residue which contained very little MC phase. Since the NiO and MC phases have similar structure and lattice parameters 0.420 nm and 0.431 nm, respectively, the carbide phase, if present, would obscure the nickel oxide. That the amount of oxide formed is small is verified by analysis of the extracted material. Nickel varied from a few parts per million to 1000 parts per million but never higher.

Another problem cited in the literature [Andrews (1966) Leitnaker (1977)] is the precipitation of silicon in the form of a gelatinous silica during extraction.

Leitnaker determined that silica was not precipitating in his high alloy steels with silicon concentration of 1 wt %. Since the alloys in question here contained only traces of silicon it is certain that, even if it occurred, it would not pose a problem.

2. Precision - In order to insure that the best precision available from the technique was obtained a strict procedure was developed and followed closely in all extractions. (The procedure is outlined at the end of this section.) As a test of the procedure, two samples that had been thoroughly homogenized by long term aging were extracted several times. Table 5.4 contains the results of these extractions. The standard deviation of the procedure is 0.013 wt %. If 1 gram of material is dissolved, 0.013 wt % corresponds to 0.13 mg. Since each extraction involves the weighing of a centrifuge tube twice with a standard deviation of approximately 0.05 mg, the precision obtained with the following technique is the best that can be expected until a more precise balance and better recovery technique become available.

3. Procedure for Anodic Dissolution of Nickel-Based Alloys for the Concentration of Precipitated Carbide Phases -

Equipment and Reagents

Semi-microgram balance

Table 5.4. Results of Multiple Extractions of 0.64 cm Rod Specimens[a] of Ni + 2 wt % Ti + 0.1 wt % C.

Heat Treatment		Quench	Precipitate Extracted wt %
Temp. (°C)	Time (hrs)		
1100	16	Cz[b]	0.122 0.129 0.103 Avg=0.118, σ^c=0.013
1260	4	Cz	0.128 0.115 0.098 0.108 Avg=0.112, σ^c=0.013

[a]The extraction solution was 10% (volume) HCl in methanol. The voltage was held constant 1.5 V for the duration of the experiment ∿6 hours.

[b]CZ-cold zone cooled.

[c]σ is the root mean square residual.

Constant voltage power supply (0-4 V)

Platinum tipped forceps

Platinum sheet to serve as a cathode

50 x 70 mm pyrex dish

15 ml centrifuge tube

Multi-position centrifuge

Ultrasonic cleaner

Eye dropper

Magnetic stir bar

Plastic wrap

Methanol-analytical reagent grade

Hydrochloric acid-analytical reagent grade

Procedure

1. A solution of 10% hydrochloric acid, by volume, in methanol solution is prepared.
2. Any surface oxide is removed from the sample with sand paper.
3. The sample is cleaned by anodically dissolving it for 1 hour. The specimen is held in the platinum tipped forceps which are connected to the positive terminal of the power supply. A piece of platinum sheet functions as the cathode. It is molded to fit the inside of the 50 x 70 mm dish (see Figure 5.2). The dish is filled with the acid solution so that the sample is well covered. Finally, a

THIS PAGE

WAS INTENTIONALLY

LEFT BLANK

Y-139850

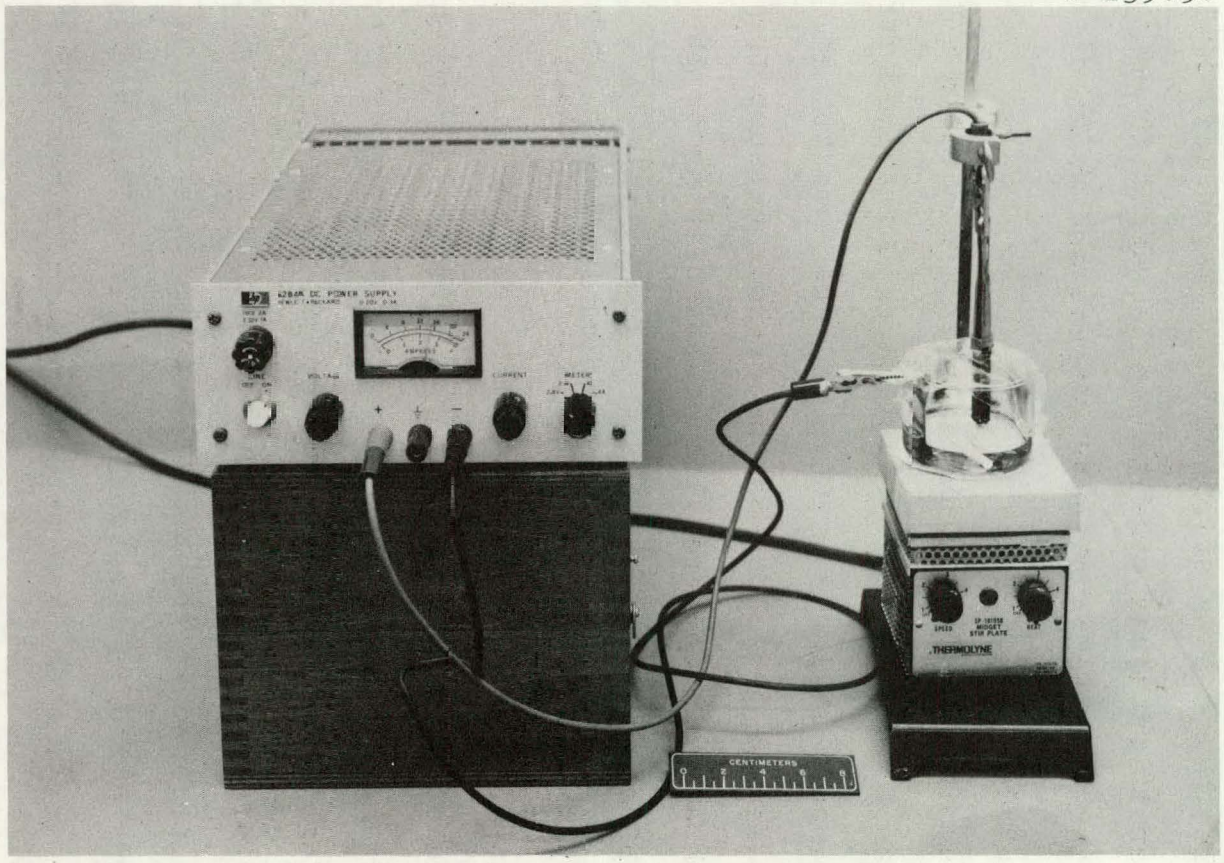

Figure 5.2. Electrolytic extraction equipment constant voltage power supply, Pt tipped forceps, Pt cathode, and magnetic stir plate.

piece of plastic wrap is placed over the dish and around the forceps to help control evaporation of the solution. The dissolution is carried out at 1.5 V. The mixture is stirred with a magnetic stir bar.

4. After it is clean, the sample is washed in methanol in the ultrasonic cleaner, dried, and weighed to 0.05 mg.
5. After it is weighed, the sample is placed in a clean dish with fresh solution and dissolved for 6-8 hours as in (3). Care is taken not to get the sample too close to the cathode because the high current that results causes plating on the cathode.
6. A 15 ml centrifuge tube is cleaned with soap, rinsed several times with methanol, and placed in a vacuum dessicator. After 1 hour it is removed and allowed to equilibrate with the air for 1 hour before weighing to the nearest 0.02 mg. Since the precision of the results depends strongly of the precise weighing of the centrifuge tubes in steps 5 and 9, the tube is weighed twice, and the zero is checked both before and after the weighing.
7. The remaining sample is placed in the preweighed centrifuge tube partially filled with methanol,

and the tube is then placed in an ultrasonic cleaner to remove any precipitate adhering to the rod. The sample is then removed from the tube, dried, and reweighed.

8. The extraction solution in the dish is transferred to the centrifuge tube with an eye dropper and is spun at high speed for at least 2 min. The supernate is decanted.
9. The precipitate in the tube is washed with methanol and centrifuged again. This procedure is repeated until the supernate is clear.
10. The tube containing the clear precipitate is placed in a vacuum dessicator to remove the methanol. After several hours of dessicating, the tube is allowed to equilibrate with the air for at least 1 hour and is then weighed as in Step 5. If any discoloration or film is visible in the tube, Steps 9 and 10 are repeated.

E. Electron Microprobe

1. Introduction

The electron microprobe was used to analyze the carbide precipitates extracted from the nickel matrix. The microprobe offers several advantages over conventional techniques such as atomic absorption spectroscopy or gravimetric analysis. The more conventional techniques

usually require large samples, are destructive, and require equipment that was not readily available for this work. Besides requiring only small samples and being non-destructive, the microprobe permits a rapid analysis which is important when substantial numbers of samples need to be analyzed. A method requiring only a small amount of sample was important in this work because often only 1 mg of material was available and several different types of analysis were desired.

Abdel-Gawad (1966) and E. W. White et al. (1966) have shown that the electron microprobe can be used to analyze quantitatively micro-crystalline powders. The procedure used in this study is essentially that described in their papers. The assumption is that the intensity ratios for elements in the powders are constants for any given composition. A series of powders was analyzed by conventional techniques and then by the microprobe. A calibration chart was then constructed comparing intensity ratios of elements of interest to weight percent ratios. The use of intensity ratios and calibration curves severely restricts the applicability of this technique. Light elements are not detected by the instrument. The calibration curves are complicated with only three elements if a wide range of concentrations are considered. Fortunately, the system of interest here is essentially a two component mixture of titanium and molybdenum. Chromium

and nickel are also present, but amount to only 1.0 and 0.05 wt %, respectively, and were not considered in the calibration curve. Practically, one is limited to the analysis of, at most, three elements of mass greater than sodium.

The instrument used in this investigation was a Materials Analysis Corporation electron microprobe coupled with a Si(Li) energy dispersive x-ray detector and a multichannel analyzer.

2. Procedure for Analysis of Carbide Precipitates

To obtain quantitative results from the microprobe a substrate of atomic number less than 11 is necessary. Elements above sodium emit x-rays that are detectable with the energy dispersive x-ray detector, and there is also a greater chance of absorption and fluorescence interactions between the substrate and the sample at high atomic number. Beryllium appears to be the best material for our purposes. It has a low atomic number (four) and is available in a sheet form that can be mounted in epoxy and polished to a high sheen. Another requirement of the substrate is that it be an electronic conductor because the surface charge that could otherwise result would lead to erroneous results.

The precipitates were dispersed in methanol and then transferred onto the beryllium chip with a Pasteur

pipette. The crystallites adhered to the surface of the polished beryllium after the methanol evaporated. It was not necessary to further bind them to the surface with glue or graphite.

A constant accelerating voltage of 25 keV was used for the electrons. The beam was caused to raster over an area of approximately 10,000 μ^2. A window of 0.3 eV was ordinarily used for each elemental peak. The peaks normally used corresponded to the Kα of titanium and the Lα of molybdenum. In a typical analysis the specimen was counted for 20 seconds (∿10,000 counts) in ten different locations on the substrate. The resultant intensity ratios were then averaged. It was also part of the procedure to check for inhomogeneity in the sample by analyzing very small areas but no gross inhomogeneity was discovered.

3. Calibration Curve

Several different carbide precipitates were analyzed by atomic absorption spectroscopy and with the microprobe. The calibration curve was based on materials of very similar composition and crystal structure to the precipitates. Tables 5.5 and 5.6 and Figure 5.3 are the result of this effort. The data were fit by least squares to

$$\frac{\text{Intensity Mo (L}\alpha)}{\text{Intensity Ti (K}\alpha)} = 0.006+0.980\ (\text{wt } \% \frac{\text{Mo}}{\text{Ti}})-0.016\ (\text{wt } \% \frac{\text{Mo}}{\text{Ti}})^2$$

Table 5.5. Analyses of Precipitates by a Colorimetry or Atomic Absorption Spectroscopy and by an Electron Microprobe Energy Dispersive X-ray Analysis.

	Microprobe[a] I_{Mo}/I_{Ti}	Titanium[b] (wt %)	Molybdenum[c] (wt %)	$\frac{\text{wt \% Mo}}{\text{wt \% Ti}}$[d]
7263[e] A-7783-17 + 8 Cr		37.65		
7264[f] A-7783-17 + 4 Mo	0.91	42.49	41.37	0.97
7262[e] A-7783-19 + 8 Mo	1.27	38.80	48.55	1.25
7266[e] A-7783-19 + 8 Mo + 8 Cr	1.48	36.06	52.91	1.47
7267[e] A-7783-19 + 8 Mo + 4 Cr	1.33	37.17	49.96	1.34
7268[e,f] A-7783-19 + 4 Mo + 8 Cr	0.85	44.35	37.60	0.85
7266[e] A-7783-37 + 8 Mo + 8 Cr	3.19	63.1	17.4	3.62

[a]The intensity ratio is the average of approximately ten measurements. The root mean square residual is ∿±2%. The precipitates were dispersed on a Be wafer to facilitate the analysis.

[b]These analyses were performed by a colorimetric method. The uncertainty is ∿5% of the value.

Table 5.5. Continued.

[c]These analyses were performed by atomic absorption spectroscopy. The uncertainty is $\sim\pm 5\%$. The weight percent ratio is based on atomic absorption results.

[d]By error analysis $\frac{\sigma_{wt\ \%\ Mo}}{wt\ \%\ Ti} = 7\%$.

[e]The base composition is Ni + 2.5 at. % Ti. The additions of the Mo and Cr are in atomic percent of the uncarburized alloy.

[f]The chemical analysis of this precipitate was performed at a later date than the others in this table.

Table 5.6. Analysis of Precipitates by Pashen-Runge Emission Spectroscopy and Energy Dispersive X-ray Analysis.

	Microprobe[a] I_{Mo}/I_{Ti}	Titanium[b] (wt %)	Molybdenum[b] (wt %)	$\frac{\text{wt \% Mo}}{\text{wt \% Ti}}$[c]
7262 A-7603-97 + 8 Mo	1.50	30	50	1.66
7266 A-7603-97 + 8 Mo + 8 Cr	2.88	72	25	3.00
7095 A-7603-106 + 1.2 Ti + 8 Mo	1.74	32	67	2.09

[a]The intensity ratio is the average of approximately ten measurements. The root mean square residual is approximately 2%. The precipitates were dispersed on a Be wafer to facilitate the analysis.

[b]The root mean square residual is approximately 10%.

[c]By error analysis $\frac{\sigma_{\text{wt \% Mo}}}{\text{wt \% Ti}} = 14\%$.

THIS PAGE

WAS INTENTIONALLY

LEFT BLANK

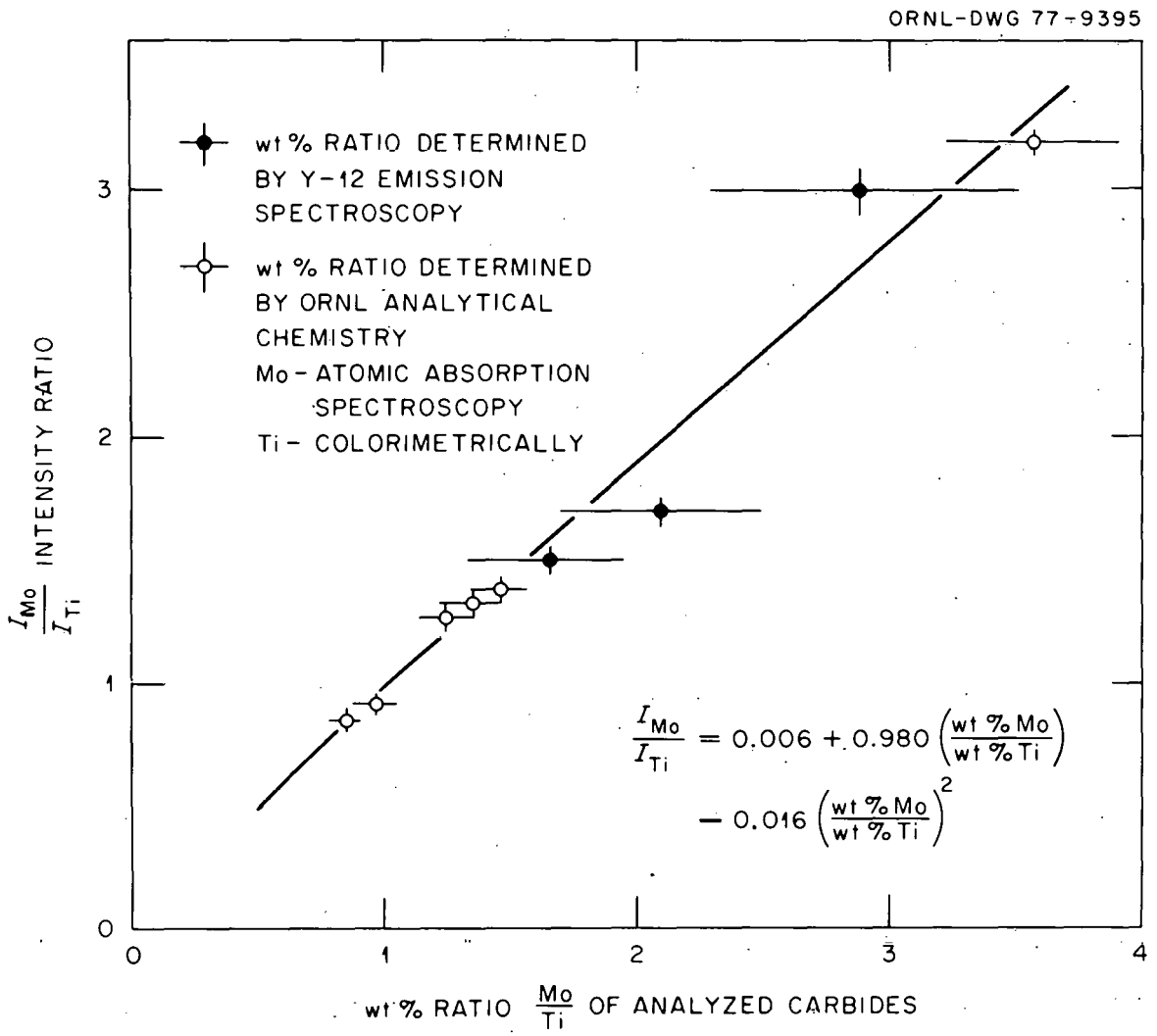

Figure 5.3. The calibration curve for the electron microprobe data. The emission spectroscopy results were not used for determining the shape of the line.

The root mean square residual is 2%.

Initially it was hoped that a calibration curve could be prepared by intimately mixing pure materials such as titanium and molybdenum powders or titanium and molybdenum oxides. Figure 5.4 shows the result of mixing molybdenum oxide (MoO_3) and titanium oxide (TiO_2). A straight line relationship was obtained between intensity ratio (I(Mo)/ I(Ti)) and weight percent ratio (wt T Mo/wt % Ti) however when this result was applied to carbides of a known composition the calibration curve disagreed with the atomic absorption results by a factor of two.

F. X-ray Diffraction

Precipitates were examined by x-ray diffraction as follows: The precipitates were first dispersed in methanol. The suspension was then dropped onto a glass slide and the methanol allowed to evaporate. The dried precipitate was scrapped off the slide and placed on a silicon single crystal wafer. The wafer acts as a substrate in the diffractometer and is oriented so that silicon diffraction peaks were not detected. A small amount of TaC powder, $a_o = 0.445587 \pm 0.000020$ nm, was then sprinkled on the wafer as an internal standard. Finally, a drop of polyvinyl alcohol was used as a binder. A diffracted beam graphite monochromator rejected all wavelengths except

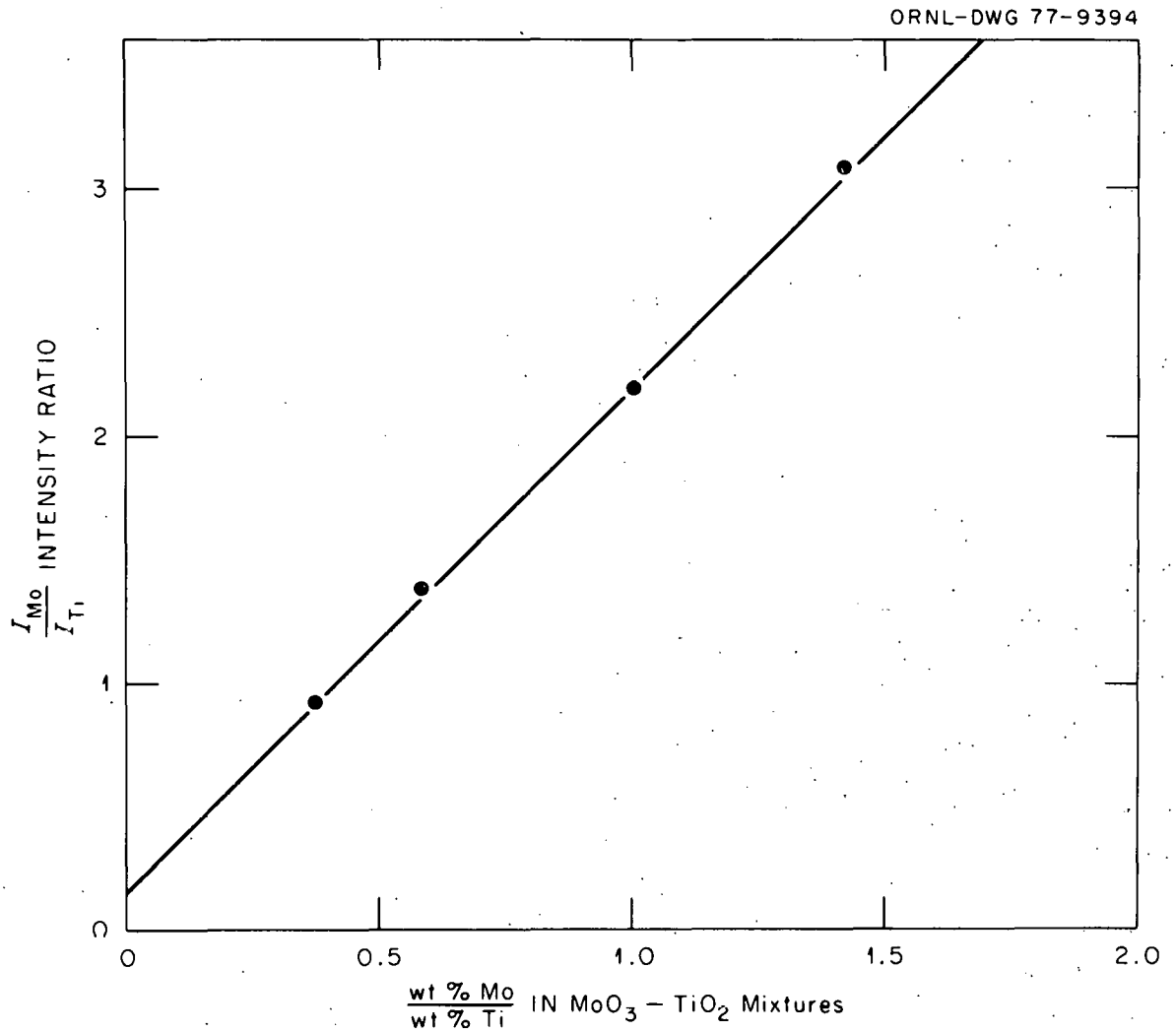

Figure 5.4. Calibration curve for the analysis of MoO_3 and TiO_2 mixture for Mo and Ti with the electron microprobe.

THIS PAGE

WAS INTENTIONALLY

LEFT BLANK

those corresponding to the copper K_α lines. The scan speed was usually 0.25°/min. A typical experiment ran from 20 to 80° 2θ.

CHAPTER VI

THE NICKEL-CARBON SYSTEM

A. Results of the Carburization Experiments

Appendix A contains a precis of all carburization experiments. Table 6.1 contains a summary of the results of these experiments for the nickel-carbon system. In each experiment several specimens were carburized along with an iron standard. Carbon activities relative to graphite, were calculated from Eq. (3.6). The data set numbers in Appendix A and in Table 6.1 refer to the Oak Ridge National Laboratory notebook page numbers where the experiments were recorded.

The activity coefficients in Table 6.1 were obtained by dividing the activities by the respective atom fractions. As Figure 6.1 shows, the activity coefficients scatter uniformly about a constant value at each of the three experimental temperatures. Calculated slopes were of the same magnitude or smaller than the uncertainties. Thus, the activity is proportional to the atom fraction for these experiments - Henry's Law is obeyed. Solute-solute interactions are therefore negligible or of the same magnitude as solvent-solute interactions for the concentrations studied.

Table 6.1. Experimental Results for Carburization of Nickel.

Data Set	Carbon in Iron (at. %)	A_c [a]	Temp. (°C)	Carbon in Nickel (at. %)	$\hat{Y}_c$
A-7603-106	4.40	0.291	1215	0.729	39.9
A-7603-106[b]	4.40	0.291	1215	0.714	40.8
A-7783-37	4.46	0.295	1215	0.739	39.9
A-7783-38	3.28	0.198	1215	0.438	45.2
A-7783-116	2.44	0.138	1215	0.332	41.6
A-7783-120	4.38	0.288	1215	0.676	42.6
A-7783-123[b]	4.17	0.270	1215	0.618	43.7
A-7783-4	1.58	0.113	1100	0.177	63.8
A-7783-14	1.78	0.129	1100	0.186	69.4
A-7783-15	3.49	0.295	1100	0.448	65.0
A-7783-17	6.57	0.709	1100	1.05	67.5
A-7783-18	5.53	0.546	1100	0.869	62.8
A-7783-19	2.71	0.212	1100	0.354	59.8
A-7783-35	4.62	0.422	1100	0.661	63.8
A-7783-32L	5.35	0.520	1100	0.816	63.7
A-7783-32H[b]	5.35	0.520	1100	0.816	63.7
A-7783-33	4.96	0.467	1100	0.739	63.2
A-7783-125[b]	2.49	0.191	1100	0.303	63.1
A-7783-44	3.63	0.601	900	0.449	134
A-7783-45	2.41	0.356	900	0.257	139
A-7783-45[b]	2.41	0.356	900	0.254	140
A-7783-47	1.96	0.278	900	0.201	138
A-7783-48	1.81	0.252	900	0.200	126
A-7783-49	0.854	0.110	900	0.0782	141
A-7783-57	1.39	0.187	900	0.141	133
A-7783-136[b]	2.04	0.291	900	0.211	138

Table 6.1. Continued

[a]Activity of carbon relative to graphite, calculated from Eq. (3.6). The concentration of carbon in iron for each data set is given in Appendix A. NBS SRM 19E is the analytical basis for the above data.

[b]Equilibrium reached by decarburization.

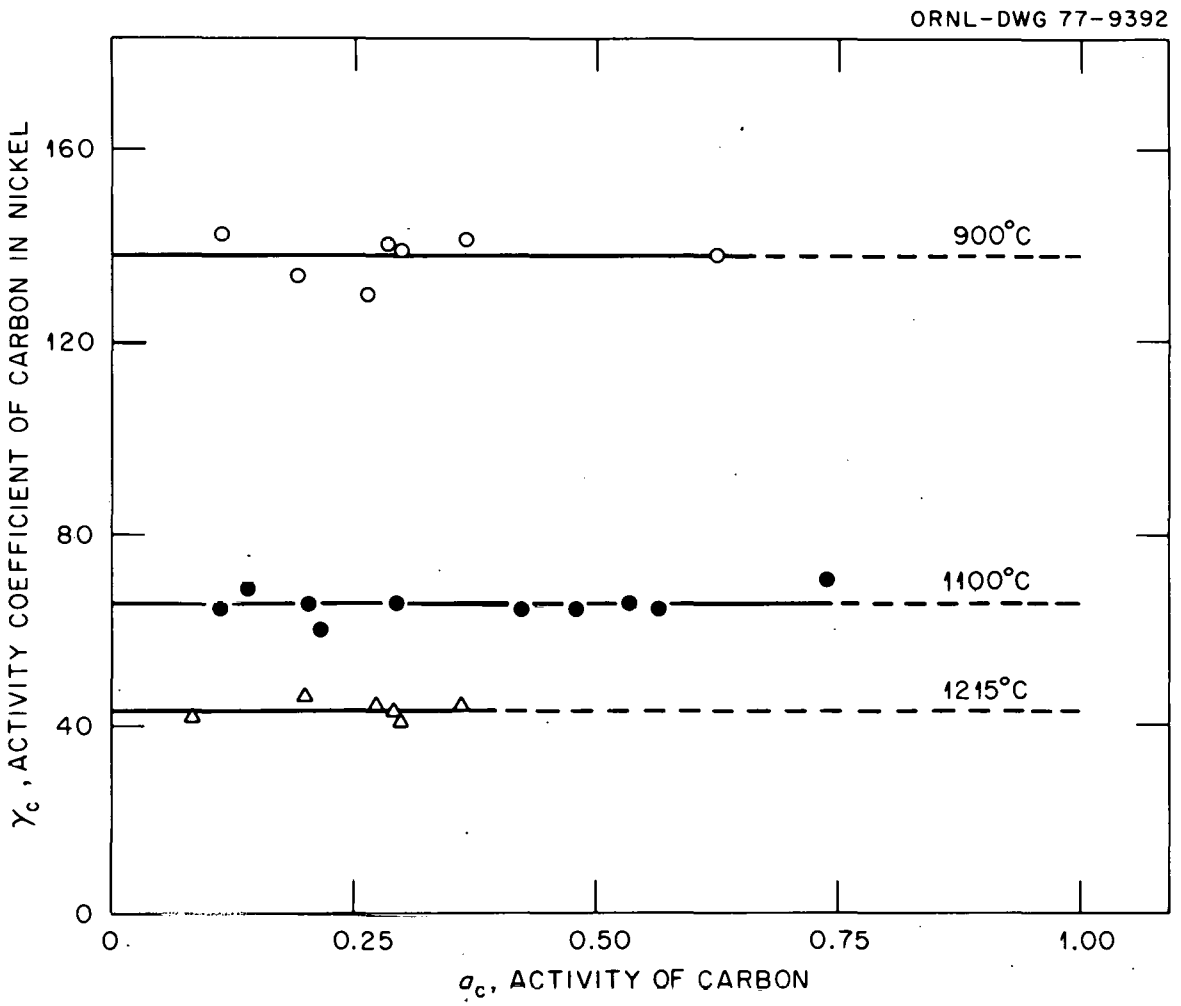

Figure 6.1. Activity coefficient of carbon in nickel as a function of carbon activity. Dashed lines are extrapolations of solid (i.e., experimental lines).

THIS PAGE

WAS INTENTIONALLY

LEFT BLANK

By Equation (2.14), the constant activity coefficient $\hat{\gamma}_c$ is the reciprocal of the solubility $(X_c)_{sat}$, the atom fraction of carbon in a saturated solution in equilibrium with graphite. The linear least-squares fit of $\log_{10} \hat{\gamma}_c$ as a function of reciprocal absolute temperature T thus also yields an equation for the solubility as a function of T^{-1}, viz.

$$-\log_{10} \hat{\gamma}_c = \log(X_c)_{sat} = a + bT^{-1},$$

$$a = 0.260,\ \sigma_a = 0.087,\ b = -2816\ K,\ \sigma_b = 170\ K \quad (6.1)$$

This equation reproduces our $\log_{10} \hat{\gamma}_c$ results with a root-mean-square residual of $\sigma = 0.0081$.

Thermodynamic excess functions can also be determined from the activity coefficients since

$$\Delta\bar{G}_c^E = RT\ \ell n\ \hat{\gamma}_c = \Delta\bar{H}_c^E - T\Delta\bar{S}_c^E \quad (6.2)$$

Figure 6.2 is a plot of $\ell n\hat{\gamma}_c$ versus 1/T for our results as well as for the results of other investigators. From Eq. (6.1), the least squares line through our data, one can calculate with the aid of Equation (6.2)

$$\Delta\bar{H}_c^E = 54\ kJmol^{-1},\ \sigma_H = 3.3\ kJmol^{-1}$$

$$\Delta\bar{S}_c^E = 5.0\ Jmol^{-1}\ K \qquad \sigma_s = 2.4\ Jmol^{-1}\ K \quad (6.3)$$

THIS PAGE

WAS INTENTIONALLY

LEFT BLANK

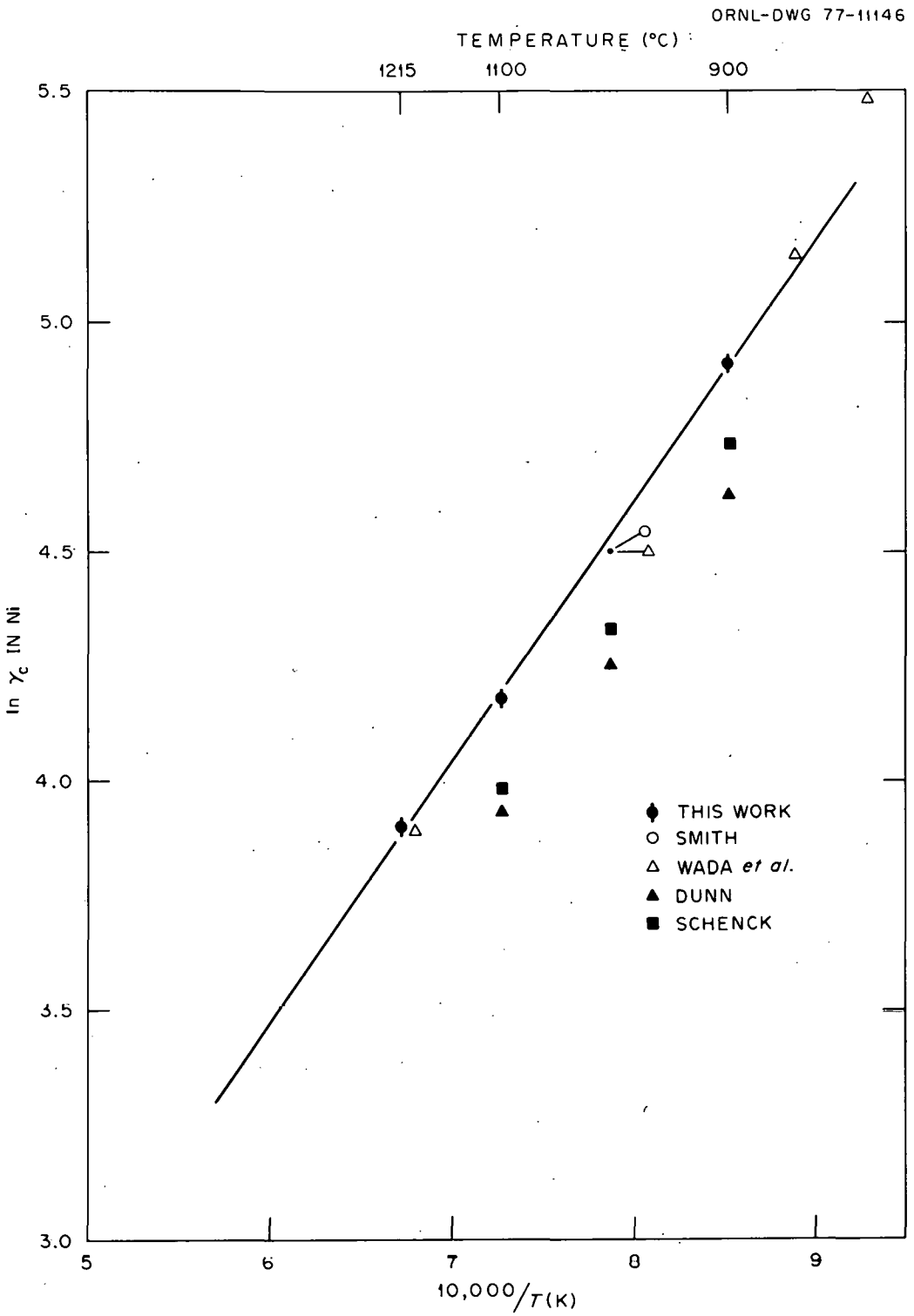

Figure 6.2. $\ell n\ \hat{\gamma}_c$ versus 1/T for carbon in nickel. The results of Smith (1960) and of Wada, et al. (1971) are the corrected results (see text).

B. Comparison with Previous Work

Figure 6.3 shows the activity coefficient results reported by Smith (1960) and by Wada et al. (1971) and the value of $\hat{\gamma}_c$ calculated from Eq. (6.1) for 1000°C. It would appear from their results that Henry's Law is not obeyed for Ni - C system, contrary to our results. The results of Schenck et al. (1965) agree with ours, namely: that the activity coefficient of carbon is independent of composition. Moreover, Henry's Law is valid for dilute solutions of carbon in iron, as shown in Figure 6.4, and one might expect similar behavior in nickel.

Some of the reported results of both Smith (1960) and of Wada, et al. (1971) were incorrectly calculated by the authors. The latter authors used an equation of Ban-Ya et al. (1970) which included the incorrect equilibrium constant discussed in Chapter III. Their results for carburization in the presence of an iron standard are shown in Table 6.2 along with results corrected by use of Equation (3.6). Table 6.3 lists the results of Wada et al. (1971) for carburization in the presence of graphite itself. The corrected results are displayed in Figure 6.5. The least squares line for the corrected results of Wada et al. (1971) at 1000°C is

$$\hat{\gamma}_c = 78.6 + 1270\ X_c \qquad (6.4)$$

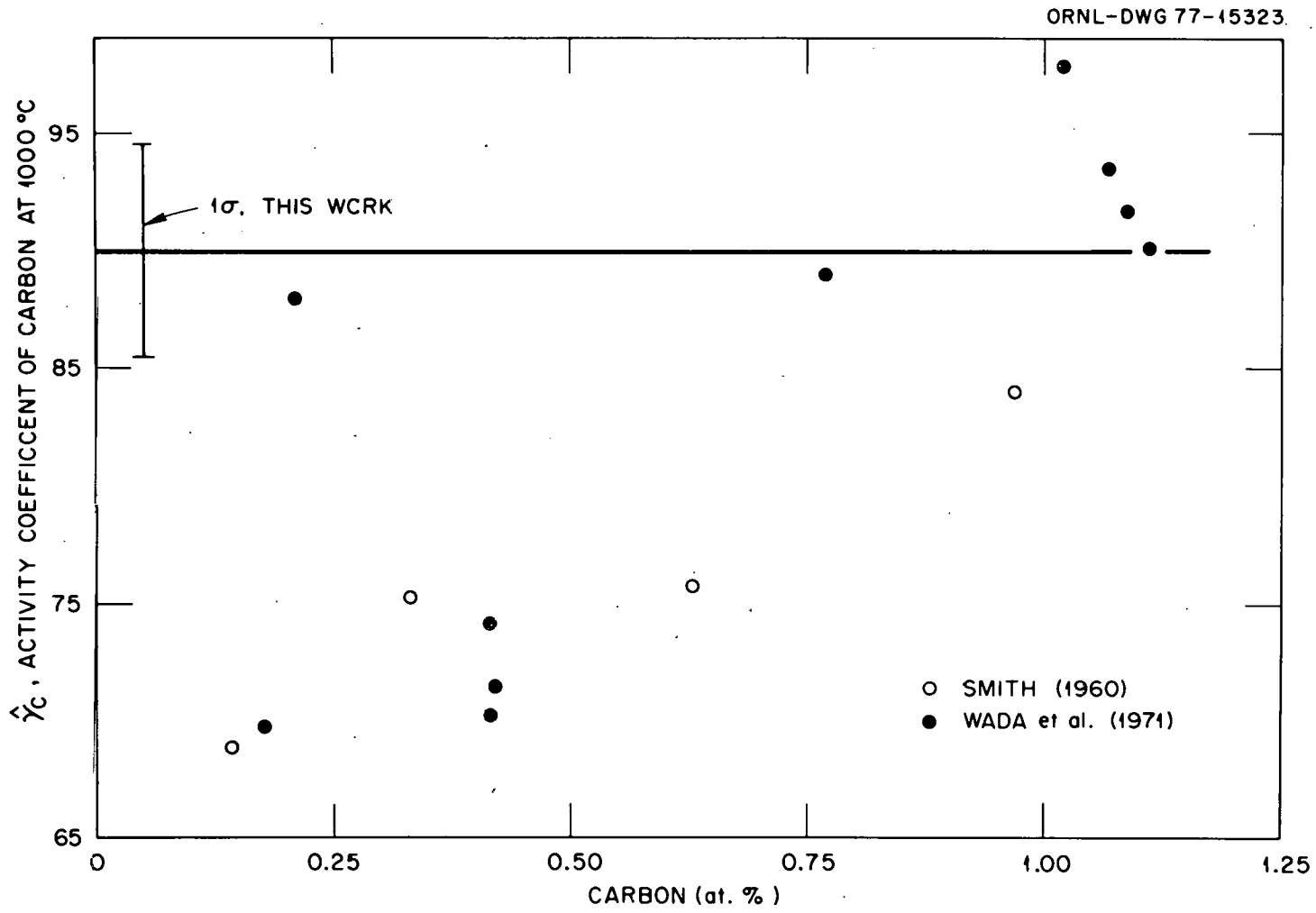

Figure 6.3. The results of Smith (1960) and Wada et al. (1971) at 1000°C, as reported, for the activity coefficient of carbon $\hat{\gamma}_C$ in nickel vs atom percent carbon. Our results are represented by the solid line and the error bars.

THIS PAGE

WAS INTENTIONALLY

LEFT BLANK

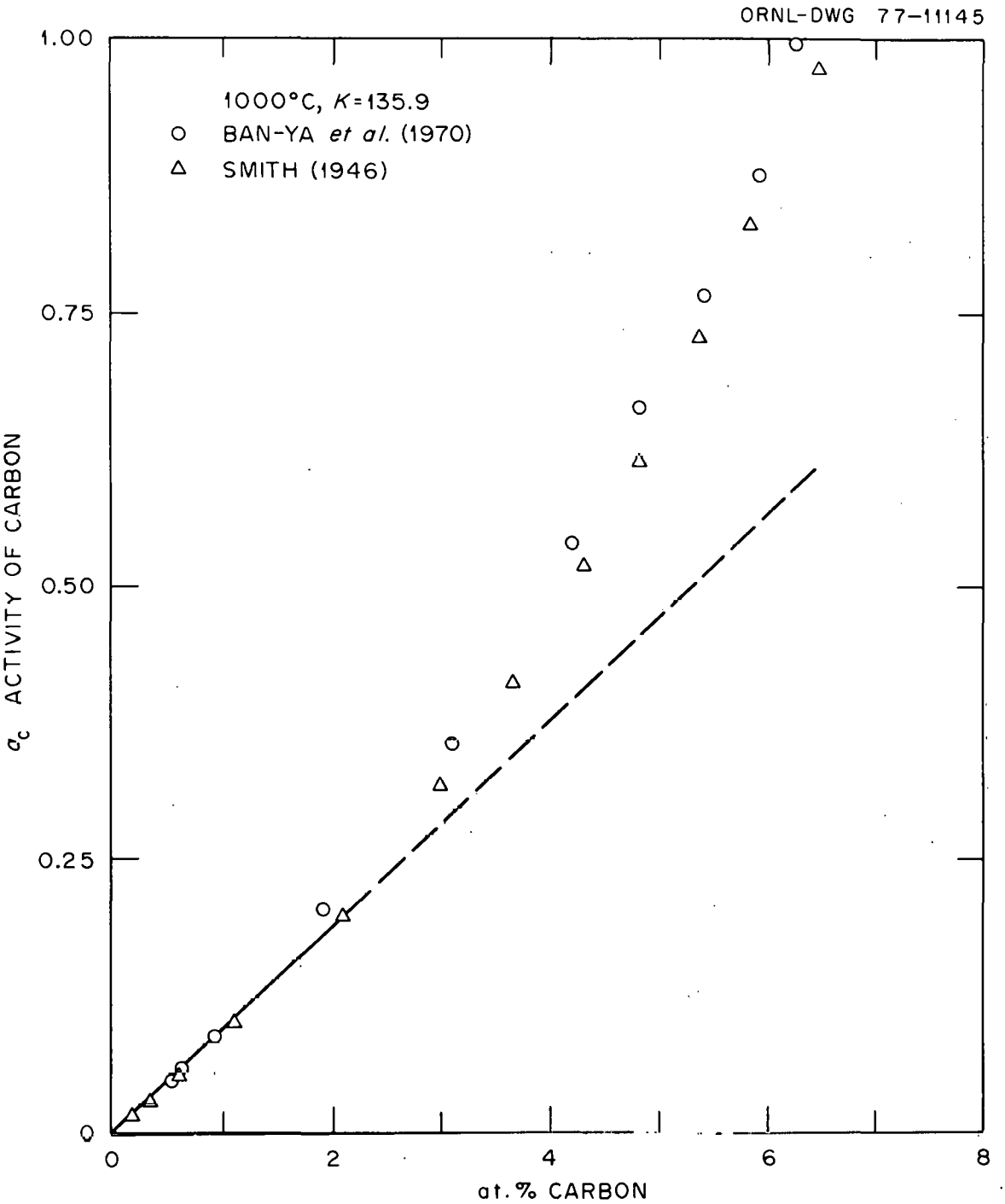

Figure 6.4. Carbon activities in iron, at 1000°C, calculated from data of Smith (1960) and of Banya et al. (1971) and Equation (3.6). The dashed line corresponds to Henry's Law. Note that the departure from Henry's Law does not occur until approximately 2 atom percent carbon is in solution.

THIS PAGE

WAS INTENTIONALLY

LEFT BLANK

Table 6.2. The results of Wada et al. (1971) for the Activity Coefficient of Carbon in Nickel.

			Uncorrected		Corrected[a]	
Temp. °C	At % C, in Fe	At % C, in Ni	A_c	$\hat{\gamma}_c$	A_c	$\hat{\gamma}_c$
800	3.96	0.463	1.03	222	1.042	225
	2.60[b]	0.254	0.583	230	0.596	235
1000	5.43	0.777	0.693	89.2	0.733	94.3
	3.04	0.414	0.307	74.2	0.333	80.4
	3.04	0.424	0.307	72.4	0.333	78.5
	2.91	0.414	0.291	70.3	0.315	76.1
	2.01[b]	0.210	0.185	88.1	0.201	95.7
	1.43	0.178	0.124	69.7	0.136	76.4
1200	5.94	0.97	0.444	45.8	0.460	47.4
	3.57	0.608	0.215	35.4	0.223	37.6
	1.11	0.122	0.0542	44.4	0.0589	48.3

[a]Activities recalculated using Equation 3.6 which corrects for the CO/CO_2 equilibrium constant.

[b]Equilibrated starting from higher carbon content.

Table 6.3. Results of Wada et al. (1971) for the Solubility of Carbon in Equilibrium with Graphite (a_c=1).

Temp. (°C)	At. % C, in Ni	c
850	0.584[b]	171
1000[a]	1.07[c]	93.5
	1.09[c]	91.7
	1.02[b]	98.0
	1.02[b]	98.0
	1.11[b]	90.1
	1.11[b]	90.1
	1.11[b]	90.1
	1.07[b]	93.5
1197	1.87[c]	53.3
	1.83[c]	54.6

[a]Measured at 997°C and corrected to 1000°C.

[b]Specimens were packed with graphite powder in an alumina boat.

[c]Carburized by a controlled CH_4-H_2 mixture with a graphite boat.

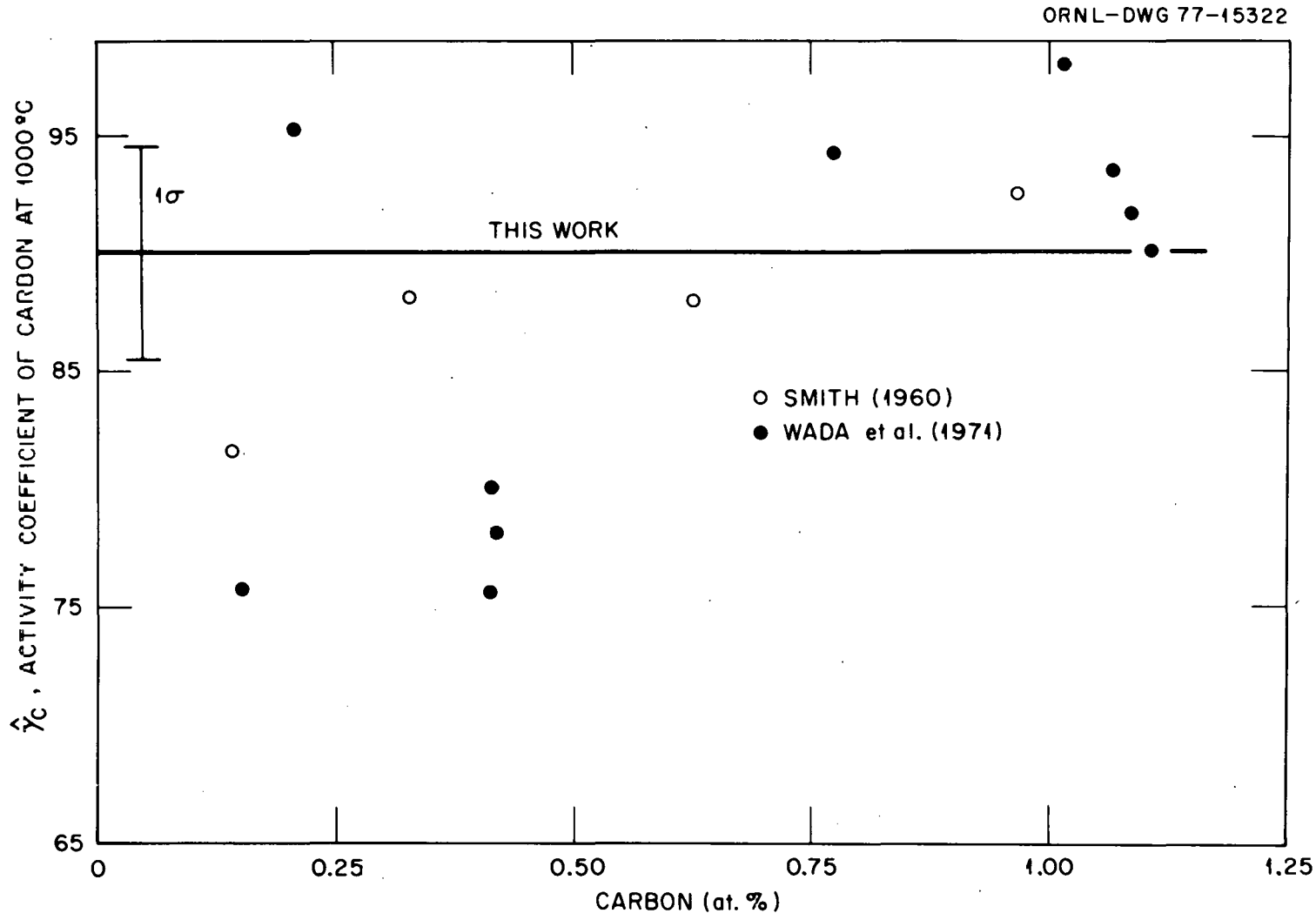

Figure 6.5. The recalculated results of Smith (1960) and Wada et al. (1971) for the activity coefficient of carbon. The results were calculated from their raw data and Equation (3.6).

THIS PAGE

WAS INTENTIONALLY

LEFT BLANK

The uncertainty in the slope (1270) is σ = 670, and the root-mean-square residual in $\hat{\gamma}_c$ calculated from Equation (6.4) is = 6.2. For atom fractions greater than 0.001, activity coefficients calculated from Equation (6.4) are the same as the one calculated from Equation (6.1) within the mutual experimental uncertainties.

Table 6.4 contains the results of Smith (1960) and the values of the activity of carbon calculated using Equation (3.6). Some of the values for the activity of carbon listed in Table 1 of Smith (1960) cannot be calculated from his Equation 1, even after Equation 1 is corrected for the obvious typographical error. Equation 1 of Smith (1960) should read, with $N_i = x_i$,

$$\log \gamma_2 = \log [(a_2)(N_1/N_2)] = 3.37\ (N_2/N_1), \qquad (6.5)$$

where the activity coefficient of carbon is relative to the infinite dilution state of carbon in iron. The activity coefficient $\hat{\gamma}_c$ relative to graphite is calculated from [see Equation (2.10)] $\hat{\gamma}_c = \gamma/\gamma_{sat.}$; likewise, the corresponding activity A_c is calculated from $A_c = a_2/a_{2,sat.}$

The "uncorrected" entries in Table 6.4 are calculated from Smith's Table I, which itself contains two incorrect entries: (1) for 6.61 carbon atomic percent in Fe, Smith

Table 6.4. Results of Smith (1960) for the Activity Coefficient of Carbon in Nickel at 1000°C.

At. % C in Fe	At. % C, in Ni	Uncorrected		Corrected[a]	
		A_c	$\hat{\gamma}_c$	A_c	$\hat{\gamma}_c$
1.24	0.142	0.0979	68.9	0.116	81.7
2.75	0.331	0.250	75.5	0.293	88.5
4.49	0.632	0.479	75.8	0.557	88.1
6.19	0.970	0.816	84.1	0.897	92.5

[a]Activity calculated using Equations (3.6) and the raw data of Smith (1960).

reports 0.141 for a_2 whereas Equation (6.5) gives a_2 = 0.123; (2) for 6.19 carbon atomic percent in Fe, Smith reports 0.115 for a_2 whereas Equation (6.5) gives a_2 = 0.110.

The recalculated, corrected results of Smith (1960) were fit by least squares to

$$\hat{\gamma}_c = 82.0 + 1100\ X_c.$$

The standard deviation of the slope 1100 is 210. The root mean square residual of $\hat{\gamma}_c$ is σ = 1.9. All of Smith's recalculated results, except one point, lie within 1σ of our interpolated results as shown in Figure 6.5.

Schenck, et al., (1965) did not report their raw data, and, although precise recalculation of their results was therefore impossible, they reported Henry's Law behavior up to the saturation limit of carbon. It is clear from Table 6.5, however, that their results differ from those reported here by about 15%.

After analysis of all available nickel-carbon data, we conclude that Henry's Law is obeyed within the precision of the data. The present results and the report of Schenck et al. (1965) indicate the validity of Henry's Law. The corrected results of Smith (1960) and Wada, et al. (1971) show a slight dependence of activity coefficient for any particular composition agrees within

Table 6.5. Comparison of Activity Coefficients,[a] Excess Enthalpies, and Excess Entropies of Carbon in Nickel.

	Investigator				
Temperature/°C	Schenck et al.[b]	Dunn et al.[b]	Wada et al.[d]	Bradley[e]	Smith[f]
$\hat{\gamma}_c$, 900	114	102	138	136	
$\hat{\gamma}_c$, 1000	76.1	70.5	88.3	89.6	87.7
$\hat{\gamma}_c$, 1100	53.9	51.4	65.0	64.3	
$\hat{\gamma}_c$, 1215	38.3	37.7	46.3	42.0	
ΔH_c^E/kJ·mol^{-1}	50.2	46	50.3	54	
ΔS_c^E/J·mol^{-1}·K^{-1}	3.4	0.47	1.9	5.0	

[a] Calculated using iron standards and Equation (3.6).

[b] No estimate of the error was stated by the author. The graphite and the CH_4/H_2 carburization techniques were used.

[c] σ_γ=4.5%, σ_H=1.0 kJ·mol^{-1}, σ_s=0.08 J·mol^{-1}·K^{-1}. The graphite carburization technique was used.

[d] σ_γ=4.2%, σ_H=3.5 kJ·mol^{-1}, σ_s=2.7 J·mol^{-1}K^{-1}. The graphite and the CH_4/H_2 carburization techniques were used.

[e] σ_γ=1.9, σ_H=3.3 kJ·mol^{-1}, σ_s=2.4 J·mol^{-1}K^{-1}, the CH_4/H_2 carburization technique was used.

[f] σ_γ=2.2%, the CO/CO_2 carburization technique was used.

experimental error with the corrected results of Smith (1960) and of Wada, et al. (1971).

Table 6.5 is a comparison of the average value of $\hat{\gamma}_c$ obtained by five investigators. To obtain the value of $\hat{\gamma}_c$ at non-experimental temperatures the average values of $\hat{\gamma}_c$ were fit by least squares to Equation (6.1). Table 6.5 also contains the values of ΔH_c^E and ΔS_c^E calculated from these fits to the data.

Dunn and McLellan (1968) have the largest set of data from which ΔH_c^E and ΔS_c^E have been calculated, and it is apparent from the small size of the uncertainty in their values for the excess functions that their data are internally consistent. However, their activity results are quite different from ours and from those of Wada, et al. (1971) and Smith (1960). The differences are outside the experimental uncertainties of the various sets of data. It appears likely, then, that Dunn and McLellan (1968) have a systematic error in their data.

CHAPTER VII

CARBON PRECIPITATION IN NICKEL AND NICKEL-TITANIUM ALLOYS

A. Discovery of the Carbon Phase

In the course of some of the aging experiments described in Chapter V, electrolytic extraction of specimens of alloy B(Ni + 1.7 wt % Ti + 0.09 wt % C) yielded a black residue which we attributed initially to the presence of titanium carbide in the specimens. This inference was contrary to the Stover and Wulff (1959) nickel-titanium-carbon phase diagram, which showed that the specimens could contain neither titanium carbide nor graphite.

Thorough examination of the residue revealed: (1) The residue had a lower density than that of titanium carbide; (2) the residue lacked the characteristic metallic appearance of titanium carbide; (3) x-ray experiments on the residue gave diffraction patterns of much lower intensity than patterns from similar quantities of titanium carbide, and the lines were shifted to higher 2θ values. (4) Table 7.1 shows that the concentration of the residue is not a function of temperature, whereas the solubility of most carbides in metals increases rapidly as a function of temperature. Clearly, the residue was not titanium

Table 7.1. Results of the Extraction of Alloy B (Ni+1.7 wt % Ti + 0.09 wt % C) Annealed at Temperatures from 1260 to 760°C.

Alloy	Sample Number	Temp./°C	Annealing Time/hrs.	Bulk[a] Carbon (wt %)	Precipitate (wt %)
B	B-15	1260	16	0.08	0.14
	B-15A	760	168	0.08	0.16
B	A-7604	1100	16	0.09	0.12
	A-7604	1260	4	0.09	0.11

[a]Specimens were analyzed after aging.

carbide.

Some remaining possibilities for the residue are: (a) It is not present in the alloy specimen but is instead a product of the extraction process; (b) it is free carbon that has precipitated from solution during quenching; (c) it is an amorphous phase produced by precipitation of alloy impurities such as oxides and sulphides.

B. Chemical Analysis of Additional Residues

New alloys containing only small concentrations of carbon were prepared. The carbon content was adjusted to any desired level by annealing the specimens in CH_4/H_2 mixtures. The low carbon concentrations provided an easy check of possibility (c) above and also provided homogeneous materials which could be examined by electron microscopy.

The results of the electrolytic extraction of the gas-carburized alloys are presented in Table 7.2 along with the analyses of the extracted residue for carbon. Some observations on and inferences from the table are: (1) No measurable residue is collected from uncarburized nickel. That is, no carbon means no residue, and possibility number (c) above is eliminated. (2) The residue is approximately 46 to 75 wt. % carbon. (3) Most of the carbon, both in the nickel and in the nickel-titanium alloys, is

Table 7.2. Results on Extraction of Ni-270 and Ni-270 + Ti Alloys Carburized at 1215°C and Then Quenched.

1	2	3	4	5	6	7	8	9	10	11
	Carburization				Extraction[b]					
Alloy	Time (hr)	Quench	Specimen Weight Change	Carbon[a] Wt.% by Analysis	Specimen Weight Change (g)	Residue Collected (g)	(%)	Carbon in Residue Wt. % of Residue	Carbon in Residue Wt. % of Specimen	Carbon Not Collected in Residue Wt. % of Specimen
Ni A-76C3-132	As Rec.			0.0020	0.77753	-.00003				
Ni A-76C3-121	46	Argon	0.041	0.050	0.94700	0.00068	0.072	75.4	0.054	-0.003
Ni A-76C3-106	36	Argon	0.141 0.11	0.147 0.150	0.67918 0.34883	0.00149 0.00095	0.219 0.27	53.4	0.117	0.030
Ni A-76C3-97	38	Water	0.128	0.139	0.90901 0.60160 0.39749	0.00182 0.00128 0.00103	0.20 0.21 0.26	45.9	0.096	0.043
Ni-2.4 at. % Ti A-76C3-97	38	Water	0.124	0.140	1.08390 0.40205	0.00196 0.00120	0.18 0.30	63.5	0.114	0.026
Ni-2.4 at. % Ti A-76C3-121	46	Argon	0.035	0.0383	0.9470	0.00068	0.047	58.3	0.0274	0.011
Ni 3.6 at. % Ti A-76C3-106	36	Argon	0.056[e]	0.149	0.63558	0.00145	0.228	66.6	0.152	-0.003

[a] Carbon was determined on a LECO thermal conductivity apparatus. σ=0.03%, is the root mean square residual.

[b] % = col 7/Col 6 x 100, = 0.015 %. σ is the root mean square residual.

[c] The scatter in the concentration of carbon in the residue can be traced to the non-reproducible fashion in which chlorine is absorbed by the residue.

[d] Obtained by difference of the bulk and the carbon in the precipitate. This number is sensitive to errors in the other determinations. The average amount of carbon in solution after the quench is 0.017 wt. %, σ = 0.019 wt. %, σ is the root mean square residual.

[e] Alloy 7068 contained ~0.09 wt. % C prior to the gas carburization.

recovered in the residue. The amount of carbon not obtained as a residue from the electrolytic extraction of the quenched alloys is 0.017±0.019 wt % and there is no statistically significant difference in the specimens with and without titanium. (4) From column 11, the concentration of carbon remaining in solution after the quench is slightly higher in the water quenched specimens. However, the difference is probably not significant because of experimental uncertainty and the small number of experiments. (5) Chlorine analysis and metal analysis on both of the A-7603-97 alloys gave a metal to chlorine atom ratio of 3 to 5. The chlorine contamination is a result of the extraction procedure. The precipitates were difficult to separate from the supernates due to their low densities. There is little doubt that the chlorine is present in the form of nickel and titanium chlorides, and that if the chlorides were absent only carbon would remain. The non-reproducibility of chlorine is related to the scatter in column 9. (6) X-ray experiments on the residue yielded extremely weak, unidentified diffraction patterns in the case of the residues from the nickel-titanium alloys and no diffraction at all in the residue extracted from samples of carburized nickel.

C. Electron Microscope Results

Examination of the quenched specimens in the electron microscope did not clarify the nature of the residue. In bright field the matrix of the specimens appeared to be one phase (Figure 7.1). Selected area diffraction revealed the presence of a second phase in both alloys (Figure 7.2). However, the phase indexed as face centered cubic with a lattice parameter $a_o \sim 0.42$ nm, the same as nickel oxide. Coatings of oxide have been recognized in other nickel-based alloys (Kenik and Carpenter, 1977). Stereoscopic examination of the micrographs did not place the precipitates conclusively. While it seemed clear that many were on the surface, some particles appeared to one of the three observers to be within the foil. Attempts to adjust the sample preparation technique to avoid oxide formation proved fruitless. The electron microscope work indicates only that if a precipitate phase is responsible for the residue, then the precipitates are smaller than the 2.5 nm diameter particles shown in Figure 7.2.

Small angle x-ray scattering experiments undertaken to determine whether precipitates exist in the alloy matrix also failed to yield conclusive results, for the same reason viz., scattering of the nickel oxide layer on the surface of the specimens.

THIS PAGE

WAS INTENTIONALLY

LEFT BLANK

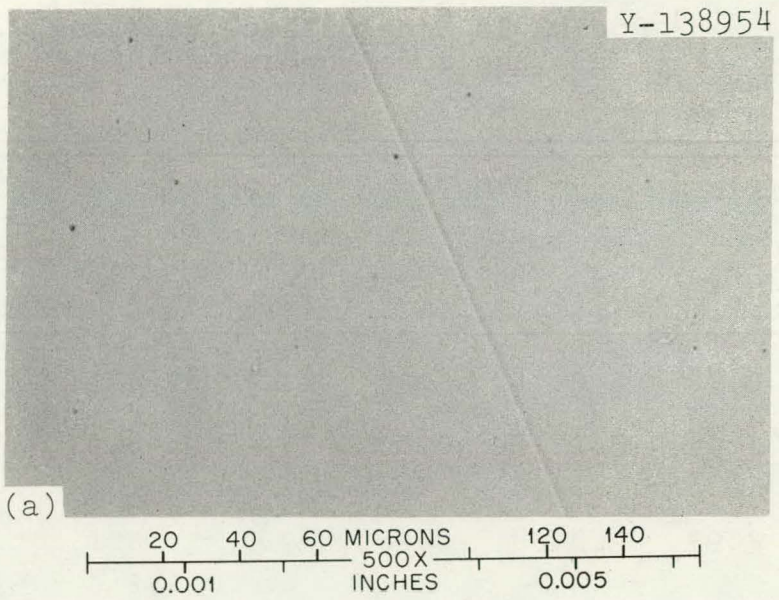

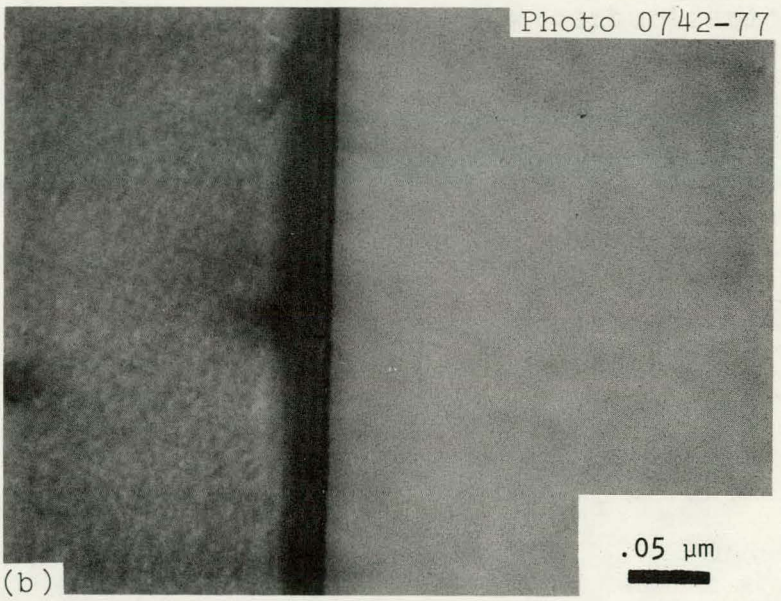

Figure 7.1 (a) Optical micrograph of nickel-0.139 wt % C specimen quenched in water after 38 hours at 1215°C.

(b) Bright field electron micrograph of nickel-0.139 wt % C specimen quenched in water after 38 hours at 1215°C.

THIS PAGE

WAS INTENTIONALLY

LEFT BLANK

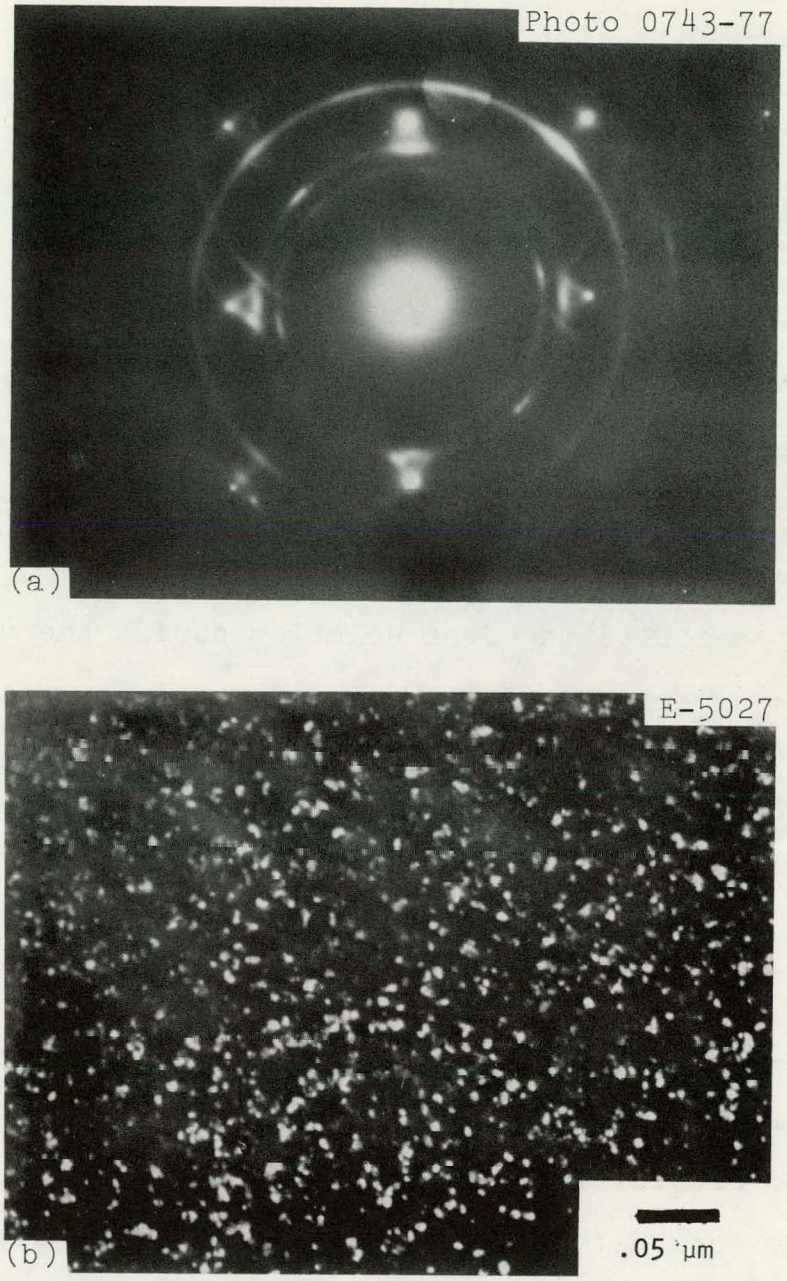

Figure 7.2 (a) Selected area diffraction pattern of a Ni + 0.139 wt % C specimen quenched in water after 38 hours at 1215%.

(b) Dark field electron micrograph from the area marked by the circle in (a). The average precipitate diameter is approximately 2.5 nm.

D. Discussion

We have shown that a carbon residue is electrolytically extracted from quenched specimens of nickel and nickel-titanium initially at 900 to 1200°C. The cooling rates used have no measurable effect on the amount of carbon precipitated, and all but 0.017 wt % is in the residue. There remain two possible explanations for the behavior (1) the isolated carbon atoms in the matrix form the residue during the electrolytic extraction process, or (2) the carbon is precipitating from solution during the quench. Hydrolysis experiments, discussed in the next paragraph, show that the extracted residue is carbon that precipitates during the quench.

1. Hydrolysis of Dissolved Carbon

Hydrolysis experiments on heavy metal carbides (not alloys) by Bradley, Pattengill and Ferris (1965) and Ferris and Bradley (1965) have shown that carbides hydrolyze to form methane and other alkanes in basic and neutral aqueous solutions and to form carbon dioxide and organic acids in acidic solutions. The authors state that they have no experimental evidence to suggest that graphite forms, during the hydrolysis, and moreover think graphite formation unlikely because radicals such as HCO, :CO and CH_2 form instead of graphite.

The nickel-carbon solid solutions studied here are essentially substoichiometric carbides with even less carbon-carbon bonding than in the carbides discussed by Ferris and Bradley (1965). If the carbon in our samples were in solid solution, the hydrolysis experiments indicate that the individual carbon atoms would be oxidized to carbon dioxide. On the other hand, if the carbon is present in the alloy specimens as an elemental phase, then the extraction process would not affect it. Since the extraction experiments resulted in the isolation of a carbon residue, the carbon must not have been in solid solution; i.e., the carbon precipitated during the quench.

2. Diffusion Mechanism for Precipitation of Carbon

In this section we show that the diffusion rate of carbon is fast enough to account for the observed agglomeration during the time of cooling. Diffusion is a strong function of temperature. Smith (1966) reported that the diffusivity, D, of carbon in nickel varies with absolute temperature, T, according to

$$D = 0.366\ e^{-17,900/T}\ cm^2\ sec^{-1} \qquad (7.1)$$

During diffusion carbon atoms migrate from solution at a rate proportional to $e^{-t/\theta}$ (deGroot, 1951), where the

relaxation time, θ, is given by

$$\theta = d^2/\pi^2 D, \qquad (7.2)$$

with d the distance over which diffusion occurs. Diffusion is 99% complete when $t \geq 4\theta$.

In the precipitation experiments under discussion here, the specimens were cooled at a rate of approximately 170 K sec^{-1} (Beck and Bigot, 1965). The specimen temperature thus decreases by one degree in about 6 milliseconds. When 4θ is smaller than 6 msec, the diffusion process is fast enough to be completed during the time interval required for a one degree temperature decrease. When 4θ is larger than 6 msec, the diffusion process is too slow to be completed during the time interval, and precipitation begins to cease. When the temperature falls low enough that 4θ is very large compared to 6 msec, carbon atoms diffuse so slowly that no further precipitation is observable.

Figure 7.3 is a plot of 4θ versus absolute temperature on the assumption that the diffusion path length is 10 nm. This estimate is based on Figure 7.2 where any carbon particle cannot be larger than the 2.5 nm particles observed. Assuming, then, that the precipitates are 2.5 nm in diameter with a graphite crystal structure, we may estimate the diffusion path length for the carbon as follows: Graphite has a density of approximately

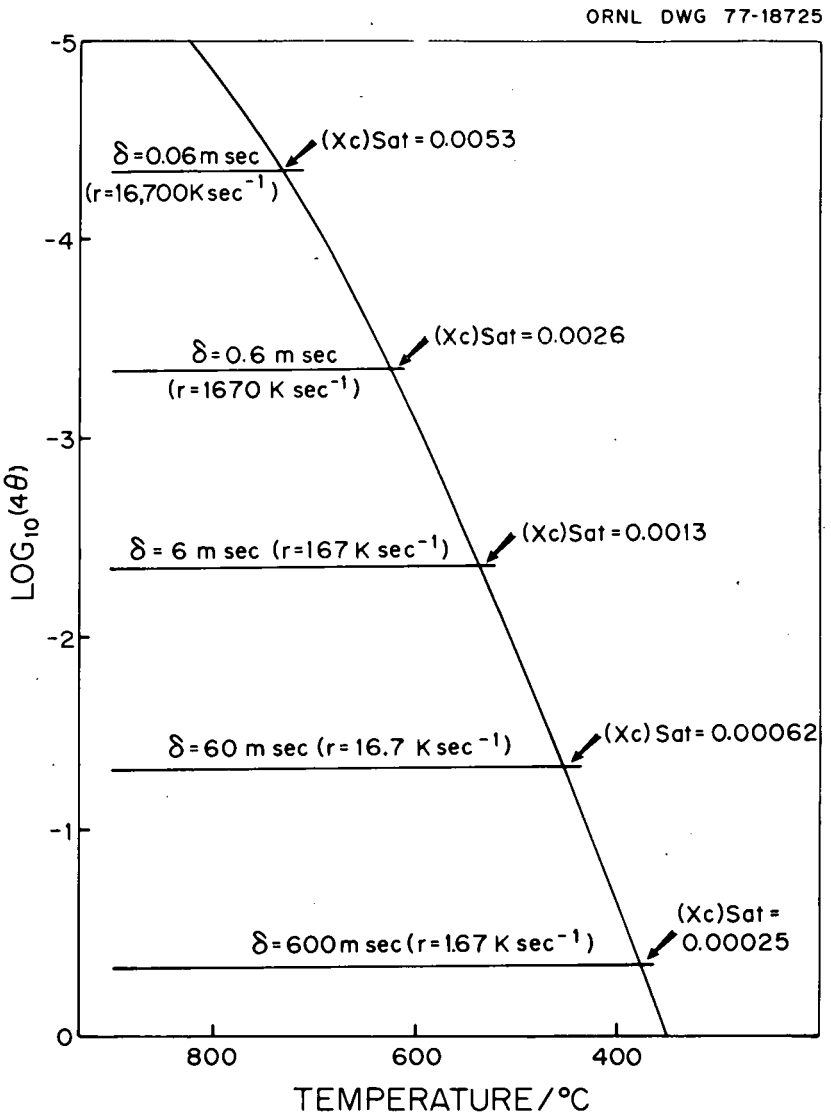

Figure 7.3. $\text{Log}_{10}\ 4\theta$ (the time required to achieve equilibrium) versus T/K (δ is the time required for the temperature to drop one degree, r is the quench rate and $(x_c)_{sat}$ has been defined by Equation (7.4). The intersection of the horizontal lines with the $\log_{10}\ (4\theta)$ versus T curve is the temperature below which, with the quench rate indicated, equilibrium cannot be maintained by diffusion, e.g., at r = 167 $K \cdot sec^{-1}$ diffusion can keep the system at equilibrium down to 535°C and at r = 16.7 $K \cdot sec^{-1}$ down to 450°C.

THIS PAGE

WAS INTENTIONALLY

LEFT BLANK

2 $\mu g/cm^{-3}$ or an atom density of 100 atoms nm^{-3}. Nickel has a density of 90 atoms nm^{-3}. A 2.5 nm diameter sphere has a volume of 8 nm^3 and contains 800 atoms of carbon. If the carbon concentration is 0.0073 atom fraction (0.15 wt %), a volume containing 800 carbon atoms would contain 1.1×10^5 nickel atoms. A sphere containing 1.1×10^5 nickel atoms has a radius of 6.6 nm. The precipitates are taken to be at the center of spheres 20 nm in diameter. The diffusion path length is then 10 nm.

The horizontal lines in Figure 7.3 are the time intervals required for the temperature to fall by one degree at various cooling rates. If for some temperature $4\theta < \delta$ (δ is the time required for the temperature to drop one degree), equilibrium is maintained and carbon precipitates to the extent dictated by its solubility in nickel at that temperature. When $4\theta > \delta$, solubility equilibrium cannot be attained by diffusion. Carbon continues to precipitate, but slower and slower since the temperature continues its rapid decline.

An independent estimate of the temperature below which precipitation ceases is obtained from the experimental result that the atom fraction of carbon remaining in solution is 8.3×10^{-4} (0.017 wt %). The solubility of graphite is given by Equation (6.1),

$$\log_{10} (x_c)_{sat} = 0.260 - 2816/T \qquad (7.3)$$

According to Spear and Leitnaker (1969), graphitic carbon which forms at temperatures below about 2000 K has a Gibbs free energy approximately 2.1 kJ mol^{-1} greater than true graphite. To account for this fact we add 2100/R $J \cdot k^{-1}$ to the enthalpy in term in the solubility equation. Equation (7.3) thus modified reads:

$$\log_{10} (x_c)_{sat} = 0.260 - 2563/T \qquad (7.4)$$

The temperature corresponding to $x_c = 8.3 \times 10^{-4}$ is 756 K. At this temperature, 4θ is 20 nsec and is rising rapidly. A slow quench rate, less than 50 deg sec^{-1}, would be required for equilibrium to be maintained at this temperature. Until the time when 4θ exceeds δ, (i.e., at temperatures above about 800 K), diffusion is sufficiently rapid that equilibrium is maintained.

3. Previous Results

Previously, Shriver and Wuttig (1972), Ulitchny and Gibala (1973), and Stover and Wulff (1959) have used optical metallography to infer that no precipitation has occurred in their quenched specimens. Our results indicate, however, that neither optical metallography at

1000x nor bright field TEM at 175,000x provides positive evidence that precipitation has not taken place; neither technique is always adequate.

Shriver and Wuttig (1972) have measured the magnetic disaccommodation amplitude (the difference between the magnetic permeability preceding and immediately following demagnetization) of a Ni-0.3 wt % C Alloy. The magnetic disaccommodation amplitude is, according to Shriver and Wuttig (1972), proportional to the square of the amount of carbon in solid solution. This implies that the amplitude should continue to increase until all of the carbon is in solution. Their Figure 2 shows no change after 550°C; this indicates that the amount of carbon in solution was not changed by anneals at temperatures above 550°C. Equation 6.1 indicates that 0.3 wt % carbon is not completely soluble until approximately 1070°C. After annealing at temperatures exceeding 550°C, the carbon in specimens of Shriver and Wuttig (1972) must have precipitated on cooling to approximately the equilibrium level at 550°C. Although Wuttig (1977) admits that precipitation occurred in his samples prior to the magnetic measurements he assumes it occurred at the annealing temperature. Since nickel carbide is not stable at the annealing temperature (Hansen and Anderko, 1958) and since carbon has been shown to obey Henry's Law to the solubility limit in nickel, the possibility of the formation of a precipitate which would

lower the solubility of carbon to that at 550°C seems remote. If carbon were precipitating at the annealing temperature, the alloys would not reach equilibrium with graphite until all of the metal for the hypothetical carbide had been used up or all of the graphite had been transformed to the precipitate phase with the lower carbon activity.

Ulitchny and Gibala (1973) measured the internal friction of several iron-nickel-carbon austenitic alloys. Internal friction peaks in austenitic alloys "have their origin in the stress induced reorientation of interstitial solutes which are paired (or clustered in larger numbers) with other point defects", (Ultichny and Gibala, 1973). Large changes are observed in internal friction peak heights as a function of quenching temperature and quenching rate. If the carbon clusters responsible for the peaks were the same as the residue we extract from nickel alloys, quenching temperature and rate would not affect the peak heights. Ultichny and Gibalas (1973) specimens contained 2 atom percent carbon. From Smith's results (1960) the solubility of carbon in iron-36 at % nickel alloys at 1000°C is 1.75 at % and by extrapolation is 1.15 at % at 900°C. Thus, all of the carbon was not in solution at two out of three of Ulitchny and Gibala's experimental temperatures. When the correction for the amount of carbon in solution before the quench is made,

the peak height per atom percent carbon in solution becomes approximately independent of temperature, in agreement with our results.

According to Ulitchny and Gibala the peak height is decreased by a factor of approximately 5 on slowing the quench rate from 170 K sec^{-1} to 0.017 K sec^{-1}. Now, the peak height is proportional to the number of carbon clusters and not to the number of carbon atoms in solution. By optical microscopy Ultichny and Gibala observed graphite precipitates in the slowly quenched specimens. Since the size of the precipitates increases during the slow quench, the number of precipitates decreases and the lower peak height results. The results of Ulitchny and Gibala (1973) are thus consistent with our both in terms of temperature dependence and quench rate dependence.

E. Summary

The fact that a carbon residue can be electrolytically extracted from nickel and nickel-titanium alloys containing carbon has been established. The most likely explanation for the residue is that the carbon is precipitating during the quench in a first step in the dissolution of the super-saturated solution. This interpretation is consistent with the results of Shriver and Wüttig (1972) and of Ulitchny and Gibala (1973). The carbon "clusters"

that these sets of investigators discuss are very likely the residue that we have extracted.

One consequence of the precipitation of free carbon is that analysis of electrolytically extracted carbides for carbon is considerably more difficult since carbon is present in two different phases.

CHAPTER VIII

THE NICKEL-TITANIUM-CARBON SYSTEM

A. Results of the Carburization Experiments

The results of the carburization of two nickel-titanium solid solutions are summarized in Tables 8.1 and 8.2 and displayed in Figures 8.1, 8.2, and 8.3. The addition of titanium to nickel increased the concentration of carbon, relative to that in pure nickel, at all temperatures studied (Table 8.1). At 1215°C, 2.4 atom percent titanium increases the equilibrium carbon concentration by 3.0%, at 1100°C by 9.0%, and at 900°C by 7.9%. Increasing the titanium concentration by 50%, to 3.6 atom percent, approximately doubles the increase in the carbon concentration.

These results agree in magnitude and sign with the only literature values, those of Golovanenko et al., (1973). They reported the percent change in the concentration of carbon relative to pure nickel at 800, 1000 and 1200°C in an alloy containing 3.4 atom percent titanium and found, according to a plot in their paper, that the carbon concentration was increased 18% at 1200 and 800°C and by 10% at 1000°C. They did only one experiment at each temperature and used only one composition, so that uncertainty

Table 8.1 Experimental Results of the Carburization of Nickel-Titanium Solutions.

Data Set	Temp./°C	Composition: Ni — C, at %[a]	Ni + 2.4 at % Ti — C, at %[a]	Ni + 2.4 at % Ti — Percent Increase	Ni + 3.6 at % Ti — C, at %[a]	Ni + 3.6 at % Ti — Percent Increase
A-7783-44	900	0.449	0.468	4.2	0.498	10.9
A-7783-45		0.256	0.285	11.1	0.292	14.0
A-7783-47		0.201	0.215	7.0	0.238	18.3
A-7783-136[b]		0.211	0.230	9.1		
				Avg=7.9(1.5)[c]		Avg=14.4(2.1)[c]
A-7783-4	1100	0.177	0.198	11.9		
A-7783-17		1.05	1.14	8.6		
A-7783-18		0.869	0.941	8.3	1.03	18.5
A-7783-19		0.354			0.408	15.2
A-7783-20		0.108			0.123	13.9
A-7783-35		0.661			0.825	24.8
A-7783-32		0.816			0.949	16.3
A-7783-125[b]		0.303	0.324	7.0	0.348	14.8
				Avg=9.0(1.0)[c]		Avg=17.3(1.5)[c]
A-7603-97	1215	0.637	0.653	2.6		
A-7603-118		0.161	0.164	1.8	0.172	6.8
A-7603-121		0.211	0.215	1.9	0.215	1.9
A-7603-123		0.178	1.85	4.0	2.07	16.2[c]
A-7783-116		0.332	0.350	5.4	0.366	10.3
A-7783-120		0.676	0.687	1.6	0.710	5.0
A-7783-123[b]		0.618	0.639	3.4	0.666	7.8
				Avg=3.0(0.5)[c]		Avg=6.4(1.4)[c]

[a] Concentrations are relative to NBS SRM 19F.

[b] Equilibrium achieved by decarburization.

[c] Parenthesized uncertainties are $\sigma_{pI} = \sigma/\sqrt{n}$ where σ_{pI} is the root mean square residual.

[d] Precipitation of TiC may have occurred in this specimen. The result was not used in the calculation of the average.

Table 8.2. Activity Coefficient[a] of Carbon in Nickel-Titanium-Carbon Solutions.

Composition (at %)	900°C			1100°C			1215°C		
	$\hat{\gamma}_c$	n^b	σ_γ^c	$\hat{\gamma}_c^a$	n^b	σ_γ	$\hat{\gamma}_c^a$	n_b	σ_γ^c
Ni	136	8	1.4	64.3	11	0.8	42.0	7	0.8
7261 Ni+2.4 Ti	128	4	1.5	61.0	5	1.5	41.1	7	0.4
7068 Ni+3.6 Ti	120	3	1.5	54.0	6	0.9	39.3	6	0.7

[a]Activity Coefficient calculated from carburization data and Equation (3.6).

[b]Number of measurements.

[c]$\sigma_\gamma = \frac{\sigma}{\sqrt{n}}$, where σ is the root mean square residual.

THIS PAGE

WAS INTENTIONALLY

LEFT BLANK

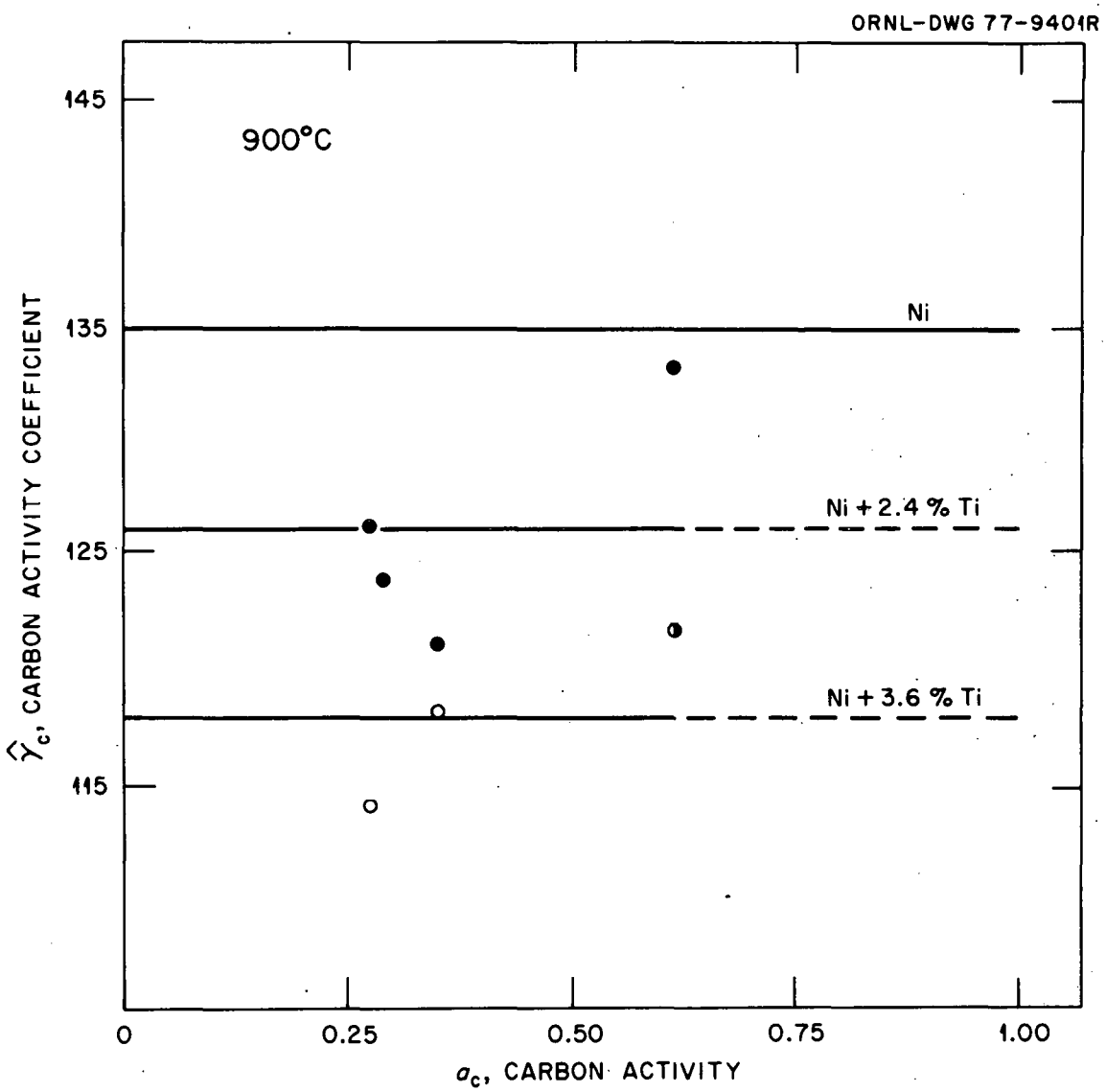

Figure 8.1. Activity coefficient of carbon in nickel-titanium alloys at 900°C. ● Ni + 2.4 at. % Ti; ○Ni + 3.6 at. % Ti; top line from Figure 6.1. Note that experimental error is exaggerated in that $\hat{\gamma}_c$ rather than ℓn $\hat{\gamma}_c$, is plotted.

THIS PAGE

WAS INTENTIONALLY

LEFT BLANK

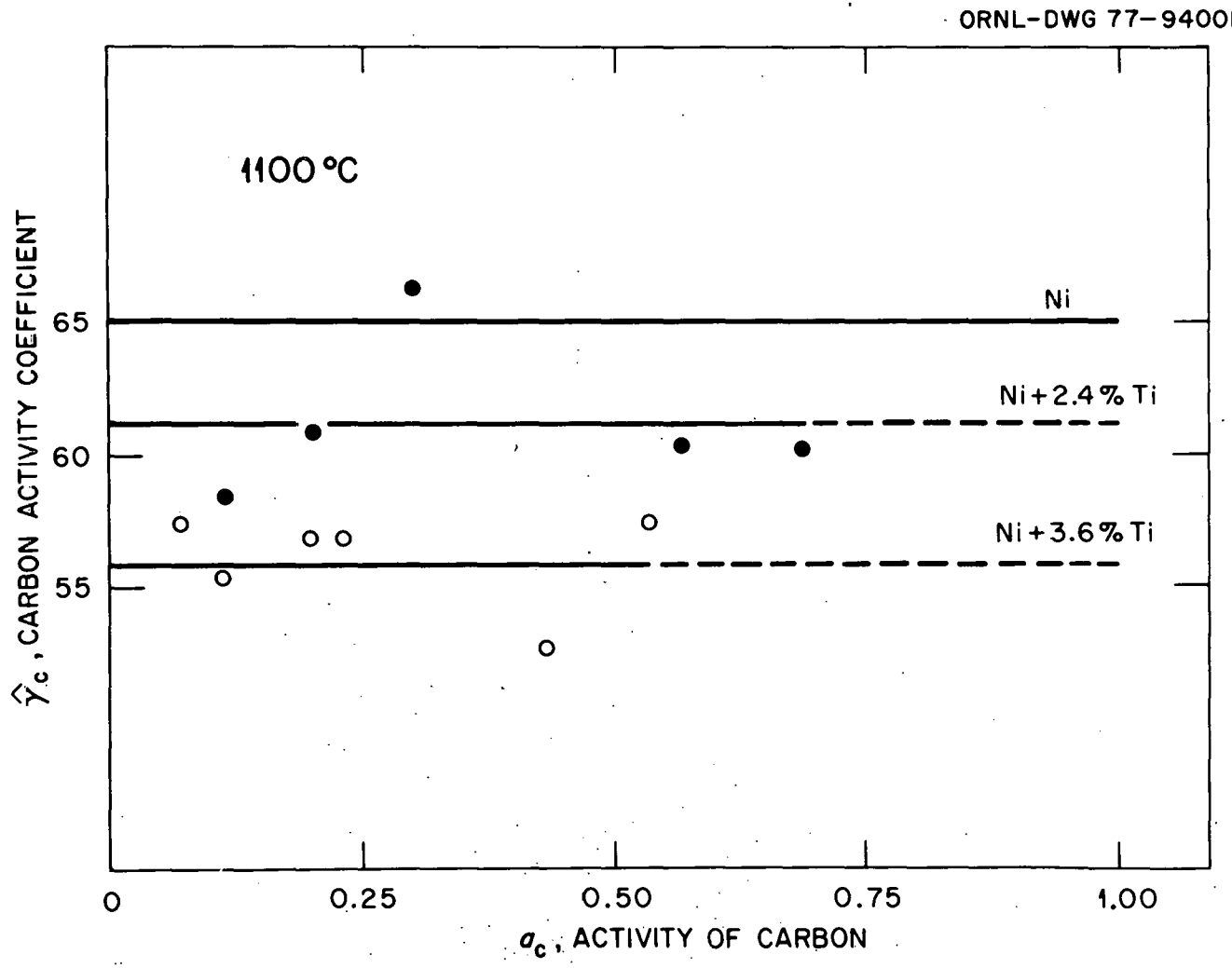

Figure 8.2. Activity coefficient of carbon in nickel titanium alloys at 1100°C. Ni + 2.4 at. % Ti, ONi + 3.6 at. % Ti, top line Figure 6.1. Note that experimental error is exaggerated in that $\hat{\gamma}_C$ rather than ℓn $\hat{\gamma}_C$ is plotted.

THIS PAGE

WAS INTENTIONALLY

LEFT BLANK

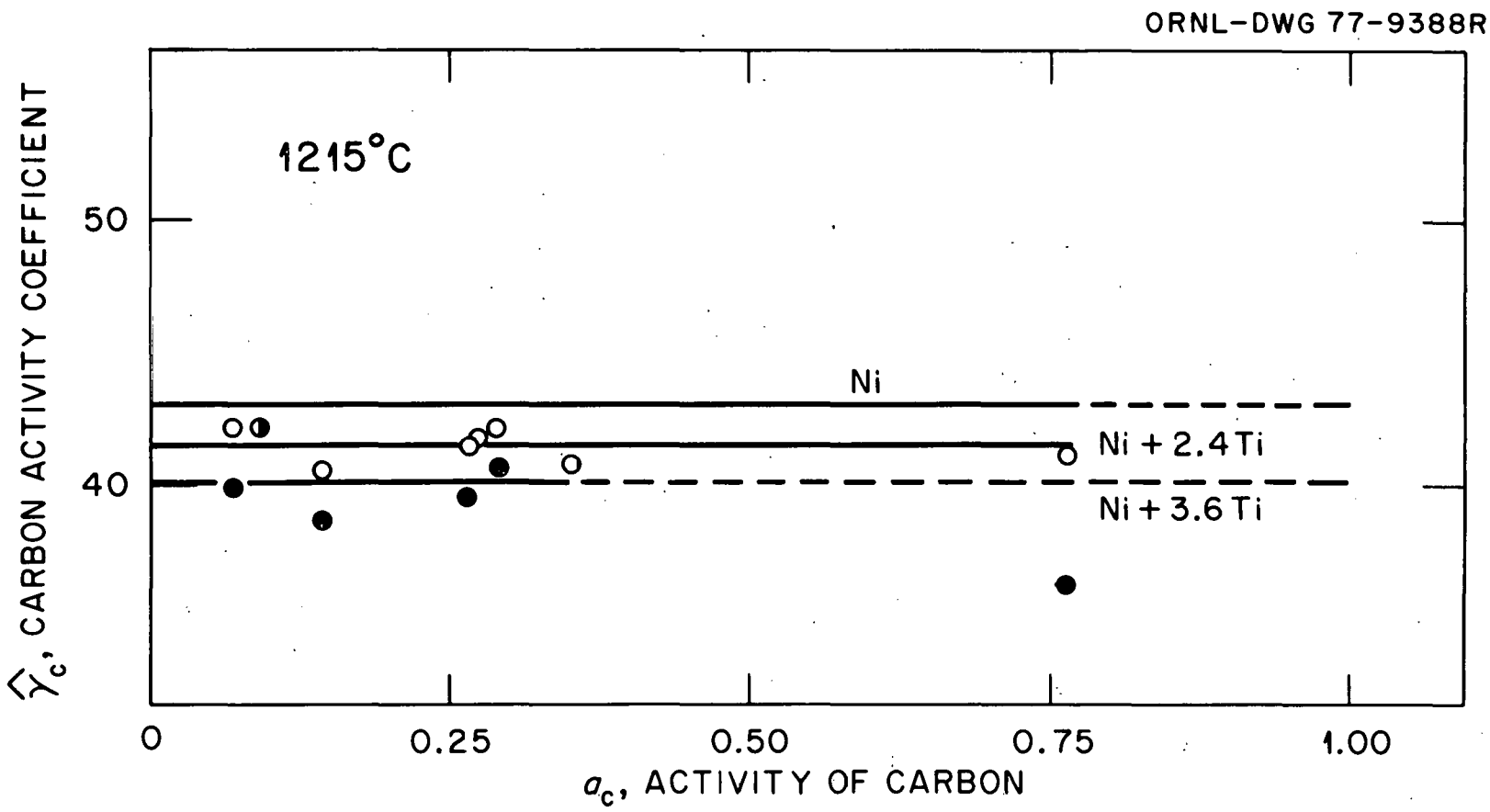

Figure 8.3. Activity coefficient of carbon in nickel titanium alloys at 1215°C. ●Ni + 3.6 at. % Ti, ○Ni + 2.4 at. % Ti, top line Figure 6.1. Note that experimental error is exaggerated in that $\hat{\gamma}_c$, rather than $\ell n\ \hat{\gamma}_c$, is plotted.

and composition dependence are unknown.

Figures 8.1, 8.2, and 8.3 show the scatter, approximately 3% at 900, 5% at 1100°C and 3% at 1215°C, and they show further that the carbon activity coefficient can be taken as independent of the carbon concentration over the ranges investigated.

The decrease in the carbon activity coefficient (Table 8.2) upon the addition of titanium to nickel results in an increased solubility of graphite in the solid solution (because $(x_c)_{sat} = \hat{\gamma}_c^{-1}$). Above a certain level of titanium, precipitation of titanium carbide occurs in nickel-titanium-carbon systems (Stover and Wulff, 1959). When the activity of titanium is large enough, titanium carbide can exist in equilibrium with both the nickel solution and graphite. Addition of more titanium to the system at this tricritical point at the same time decreases the value of the carbon activity coefficient and decreases the solubility of carbon in the solution.

Table 8.3 contains the values of $\Delta\overline{H}_c^E$, $\Delta\overline{S}_c^E$ and the parameters describing the temperature dependence of $\ln \hat{\gamma}_c$ in the nickel-titanium-carbon solutions studied. From the results in Table 8.3 the composition dependence of $\ln \hat{\gamma}_c$ could be fit with an equation of the type

$$\ln \hat{\gamma}_c = \ln \gamma_c(Ni)\ \gamma_c(Ti)$$

$$= \ln \gamma_c(Ni) + \ln \gamma_c(Ti)$$

Table 8.3. The Temperature Dependence of $\hat{\gamma}_c^a$ and the Values of $\Delta\overline{H}_c^E$ and $\Delta\overline{S}_c^E$ in Nickel-Titanium-Carbon Solutions.

	Ni[b]	Ni+2.4 at % Ti[b]	Ni+3.6 at % Ti[b]
A	-0.60 (.29)[c]	-0.49 (0.20)	-0.51 (0.15)
B/K^{-1}	6490 (400)	6277 (270)	6201 (205)
$\Delta\overline{S}_c^E/K^{-1}\cdot J\cdot mol^{-1}$	5.0 (2.4)	4.1 (1.7)	4.2 (1.2)
$\Delta\overline{H}_c^E/kJ\cdot mol^{-1}$	54.0 (3.4)	52.2 (2.2)	51.6 (1.7)

a) $\ell n\ \hat{\gamma}_c = A + B\ (T)^{-1}$.

b) $\sigma_{\ell n\hat{\gamma}_c} = 0.019$.

c) Parethesized uncertainties are root mean square residuals.

where

$$\ell n\ \gamma_C(Ti) = C \cdot x_{Ti} + D \cdot x_{Ti}\ T^{-1}$$

However, the composition range studied so far is too small to warrant such a fit.

B. The Solution Thermodynamics of Titanium in Nickel-Titanium-Carbon Solid Solutions

Stover and Wulff (1959) made a careful phase diagram of the nickel-rich corner of the nickel-titanium-carbon system. When their data are combined with titanium carbide data from the JANAF Thermochemical Tables (1971) the activity coefficient of titanium at the graphite, titanium carbide, nickel solid solution tricritical point can be calculated, as follows:

The equilibrium constant K_f for the formation reaction Ti(s) + C (graphite) = TiC(s) is the same as the equilibrium constant for

$$Ti(\text{in Ni}) + C(\text{graphite}) = TiC(s).$$

Thus, for the three phase equilibrium here,

$$A_{Ti} = K_f^{-1}$$

since

$$A \text{ (graphite)} = 1 = A_{TiC}.$$

(An additional point noted by Stover and Wulff (1959) and confirmed in this study (see Chapter IX) is the minuscule solubility of nickel in titanium carbide. The low solubility of nickel in the carbide justifies the assumption that the activity of titanium carbide can be set to unity.)

Table 8.4 contains the resulting activity coefficient values. One notes immediately that the partial molar excess free energy of titanium is large and negative. To calculate the partial molar excess entropyaand enthalpy a temperature dependent regular solution model is assumed. The values of the regular solution parameter, A, in Table 8.3 allow the excess functions at $X_{Ti} = 0$ to be calculated.

$$\ell n\ \ddot{\gamma}_{Ti} = -20.6\ T^{-1} - 2.5,\ \sigma_{\ell n \gamma_{Ti}} = 0.001$$

$$\Delta\bar{S}^{E}_{Ti} = -21\ J\cdot mol^{-1}\ K^{-1},\ \sigma_S = 0.8\ J\cdot mol^{-1}\ K^{-1}$$

$$\Delta\bar{H}^{E}_{Ti} = -171\ kJ\cdot mol^{-1},\ \sigma_H = 1.3\ kJ\cdot mol^{-1}$$

The assumptions in these calculations are that (1) nickel and titanium behave like a regular solution over the range

Table 8.4. Activity Coefficient of Titanium in Nickel-Titanium Carbon Solid Solutions in Equilibrium with Graphite and TiC.

Temp./°C	K_f[a]	x_{Ti}[b]	x_c[b]	$\hat{\gamma}_{Ti}$	$\Delta\bar{G}^{ex}_{Ti}$/kJ·mol^{-1}	A^e/kJ·mol^{-1}
600	2.66×10^{10}	0.020	0.0020	1.9×10^{-9}	-145.75	-152.4
800	2.40×10^{8}	0.024	0.0064	1.7×10^{-7}	-139.05	-147.9
900	4.08×10^{7}	0.028	0.0090	8.8×10^{-7}	-135.97	-146.6
1000	9.01×10^{7}	0.031	0.012	3.5×10^{-6}	-132.95	-145.2
1100	2.47×10^{6}	0.033	0.016	1.2×10^{-5}	-129.34	-143.0
1200	8.06×10^{5}	0.034	0.021	3.6×10^{-5}	-125.30	-140.3
1260	4.42×10^{5}	0.034	0.026	6.7×10^{-5}	-122.53	-138.7

[a]Calculated from JANAF Thermochemical Tables (1971).

[b]Values taken from Stover and Wulff (1959). Approximate uncertainty $\pm(0.1)\cdot x_{Ti}$, $\pm(0.1)\cdot x_c$.

[c]Calculated from $\hat{\gamma}_{Ti} = (x_{Ti}K_f)^{-1}$.

[d]By $\Delta\bar{G}^{ex}_{Ti} = RT \ln \hat{\gamma}_{Ti}$.

[e]Temperature dependent regular solution model, $\Delta G^{ex}_{Ti} = A(T)x^2_{Ni}$. The contribution of carbon has been neglected.

of 0-3.4 atom percent titanium, that (2) the contribution of carbon to the activity coefficient of titanium is negligible and that (3) $\Delta\overline{H}^{E}_{Ti}$ and $\Delta\overline{S}^{E}_{Ti}$ are independent of temperature. The fit of the equation appears to be very good. The large negative $\Delta\overline{S}^{E}_{Ti}$ would usually be taken to indicate that a large amount of order exists in the system. This is consistent with the fact that several ordered phases (Ni_3Ti, $NiTi_2$ and $NiTi_2$) exist in the nickel-titanium binary system. The values of the titanium partial molar excess Gibbs free energy are used in Chapter X to obtain the value for the Kohler-Kaufman interaction energy ψ_{NiTi}.

CHAPTER IX

NICKEL-TITANIUM-MOLYBDENUM-CHROMIUM-CARBON SYSTEMS

A. Results of the Carburization Experiments

Table 9.1 and Figures 9.1 and 9.2 contain the activity coefficients of carbon calculated from experiments on solid solutions containing nickel, titanium, molybdenum, chromium, and carbon. Within experimental error, the activity coefficient of carbon is independent of the carbon concentration in all of the alloys. Thus, Henry's Law is obeyed, as it is for the nickel-carbon and nickel-titanium-carbon systems. Taken at face value some of the data in Figures 9.1 and 9.2 could be fit with a line of finite slope. However, in light of the indications in Chapters 6 and 8 that Henry's Law is obeyed in Ni-C and Ni-Ti-C alloys, more data are required before a linear least-squares fit is justifiable. As indicated in Table 9.1 too few successful carburization experiments were performed in the solid solution region on these alloys at 900°C to warrant a plot.

The solid solution range in nickel-titanium-molybdenum-carbon alloys is limited because of the ability of molybdenum carbide to form a solid solution with titanium carbide.

Table 9.1. Activity Coefficient of Carbon as a Function of Temperature and Composition in Ni-Ti-Mo-Cr-C Solid Solutions.

Alloy[a]	900°C $\hat{\gamma}_c^b$	900°C n[c]	900°C σ_γ^d	1100°C $\hat{\gamma}_c^b$	1100°C n[c]	1100°C σ_γ^d	1215°C $\hat{\gamma}_c^b$	1215°C n[c]	1215°C σ_γ^d
7262 Ni+2.5 Ti+8.2 Mo	172	1	7.0[e]	75.8	3	3.2	48.1[f]	3	1.8
7263 Ni+2.4 Ti+8.0 Cr	127	2	7.0	53.3	4	1.8	35.8	6	0.4
7264 Ni+2.4 Ti+4.2 Mo	160	1	3.2[e]	72.8	3	1.4	46.3	6	1.0
7265 Ni+2.5 Ti+4.6 Cr	130	4	3.0	59.5	5	0.4	38.9	7	0.8
7267[f] Ni+2.5 Ti+8.2 Mo+ 4.4 Cr				62.0	2	2.1	37.5	2	0.4
7268[f] Ni+2.5 Ti+4.1 Mo+ 8.4 Cr				51.4	2	2.2	33.3	2	0.3
Ni	136	8	1.4	64.3	11	0.8	42.0	7	0.8

[a] Compositions in atom percent.

[b] Activity coefficient calculated from carburization data and Equation 3.6 is used to determine the activity of carbon for each data set. See Table 8.2 for the activity coefficients of Ni + 2.4 Ti.

[c] Number of measurements.

[d] $\sigma_\gamma = \sigma'/\sqrt{n}$ where σ' is the root mean square residual.

[e] Approximate, calculated from average percentage errors at 1100 and 1215°C.

[f] Activity coefficient calculated relative to the activity coefficient of carbon in nickel due to absence of iron data.

THIS PAGE

WAS INTENTIONALLY

LEFT BLANK

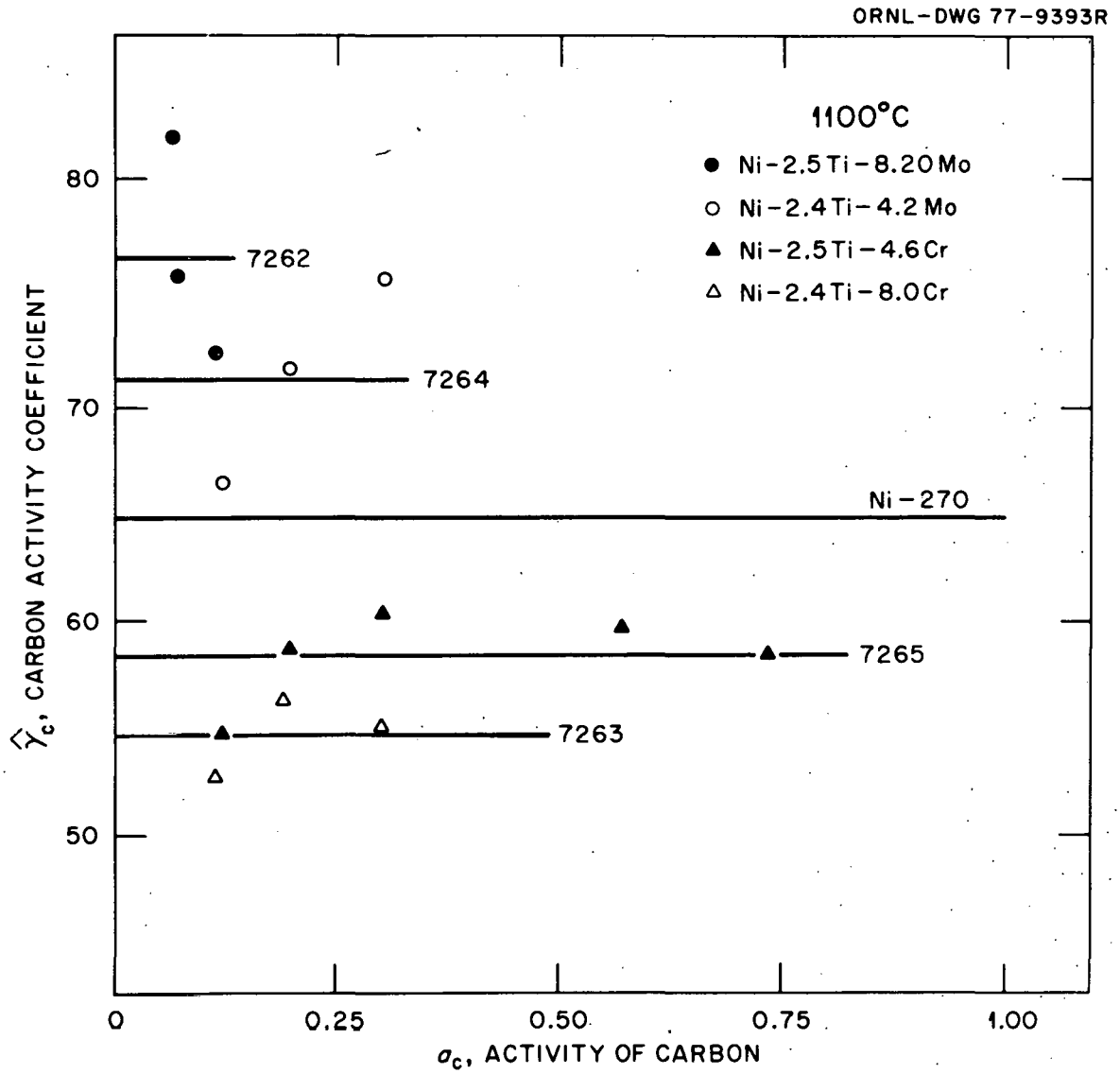

Figure 9.1. Activity coefficient of carbon in nickel-titanium-molybdenum-chromium alloys at 1100°C. The lines represent average values. More data are required in light of the indications in Cahpters VI and VIII that Henry's Law is obeyed in Ni-C and Ni-Ti-C alloys, before a least squares fit is justifiable.

THIS PAGE

WAS INTENTIONALLY

LEFT BLANK

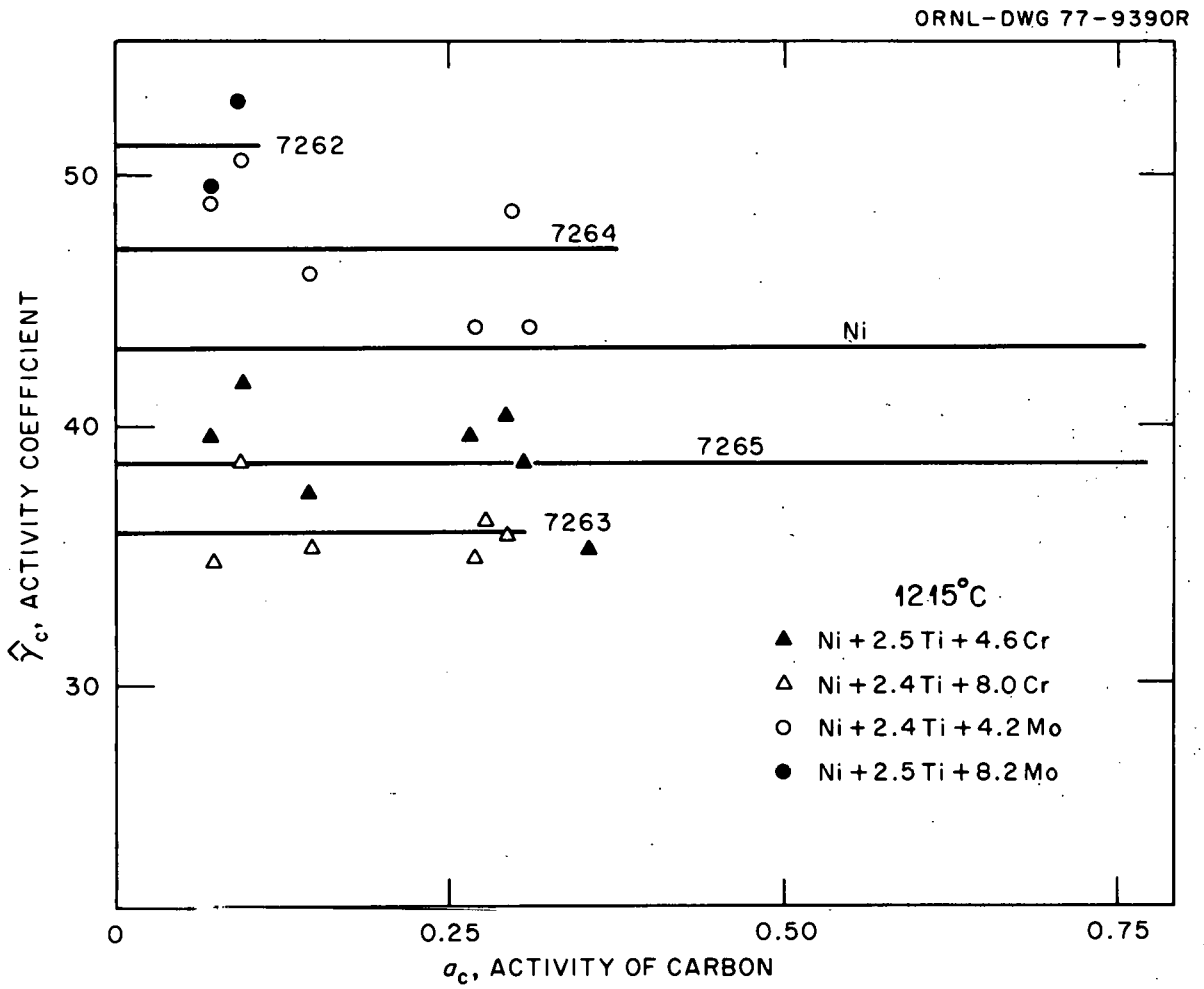

Figure 9.2. Activity coefficient of carbon in nickel-titanium-molybdenum-chromium alloys at 1215°C. The lines represent average values. More data are required, in light of the indications in Chapters VI and VIII that Henry's Law is obeyed in Ni-C and Ni-Ti-C alloys, before a least squares fit is justifiable.

The narrowness of the solid solution region increases the difficulty of the carburization experiments. In particular, alloy 7266, which contains the largest concentrations of both molybdenum and chromium has a single phase region so narrow that quantitative data on the solution phase were not obtained from carburization experiments. Instead, annealing experiments discussed in Section B.2 were performed in order to obtain data on this limited region. Although alloys 7267, 7268 and 7262 also have small carbon solubilities, it was possible to obtain quantitative carburization data on all three solutions at 1100 and 1215°C.

To determine effects of alloying additions on the activity coefficient of carbon two procedures can be followed: (1) compare the activity coefficients of carbon as determined with the iron standard equation (3.6); or (2) compare directly the difference in carbon concentration of two alloys in equilibrium with the same gas composition. The second method is necessary for some of this work because not all of the alloys were present in every run and therefore the effect of the iron standard does not cancel out. Such comparisons are shown in Table 9.2.

Compared to nickel + 2.4 titanium, molybdenum decreases the equilibrium concentration of carbon from 12% to 19% at the 4 atom percent level and from 15% to 25% at the 8 atom percent level (Table 9.2). Percentage increases

Table 9.2. Comparison of Equilibrium Concentrations of Carbon in Ni-Ti-Mo-Cr-C Solutions.

Alloy Pair	Change In Composition	900°C Percent[a] Change	900°C n^b	900°C σ_r^c	1100°C Percent[a] Change	1100°C n^b	1100°C σ_r^c	1215°C Percent[a] Change	1215°C n^b	1215°C σ_r^c
7263/7261	8.0 Cr	0.0	2	5.0	14	4	2.5	15	6	1.2
7265/7261	4.6 Cr	-2.0	4	1.5	3.1	4	2.0	5.0	6	1.2
7263/7265	3.4 Cr	1.3	2	0.3	10	3	1.1	10	5	1.3
7262/7261	8.2 Mo	-25[d]		5.4[e]	-20[d]	1	6.0[e]	-15	3	3.5
7264/7261	4.2 Mo	-19[d]	1	2.9[e]	-14	2	2.0	-12	5	2.2
7264/7262	4.0 Mo	+7.7		5.0	4.6[d]		4.4[c]	2.0	3	1.7
7267/7261	8.2 Mo + 4.4 Cr				-3.1[d]		5.7[d]	9.9	2	1.1

Table 9.2. Continued.

Alloy Pair	Change In Composition	900°C Percent[a] Change	900°C n[b]	900°C σ_r[c]	1100°C Percent[a] Change	1100°C n[b]	1100°C σ_r[c]	1215°C Percent[a] Change	1215°C n[b]	1215°C σ_r[c]
7267/7265	8.2 Mo				-5.1[d]		4.6[e]	6.8		1.5
7268/7261	4.1 Mo + 8.4 Cr				14.5[d]		4.7[e]	23.6	2	0.8
7268/7264	8.4 Cr				38.9[d]		7.1[e]	44.8		1.1

[a] Percent Change: $\frac{\text{Alloy1}}{\text{Alloy2}} = \frac{C_1 - C_2}{C_2} \times 100$, where C_i is the carbon concentration in the indicated alloy.

[b] Number of measurements.

[c] $\sigma_r = \sigma/\sqrt{n}$ where σ is the root mean square residual.

[d] Due to a lack of data for direct comparison the activity coefficients in Tables 8.2 and 9.1 were used. Percent change = $\frac{\gamma_2 - \gamma_1}{\gamma_2} \times 100$.

[e] $\sigma_r^2 = \sigma_{\gamma_2}^2 \cdot (1/\gamma_1^2) + \sigma_{\gamma_2}^2 \cdot (\gamma_2/\gamma_1^2)^2$. σ_r was calculated in this fashion due to a lack of data on the two solutions at the same activity.

are larger at lower temperatures. No literature exists on the effect of molybdenum on the equilibrium carbon concentration in nickel solutions. The value for the Kohler-Kaufman parameter (ψ_{MoC}) estimated by Kaufman and Nesor (1975) indicates that molybdenum should decrease the equilibrium concentration of carbon in nickel solutions, as found here. Wada et al. (1972) indicate that molybdenum increases the equilibrium concentration of carbon in iron solutions, opposite to the effect on nickel solutions.

Compared to alloy 7261, chromium increases the equilibrium concentration of carbon in nickel at 1100 and 1215°C but has no effect at 900°C (Table 9.2). The decrease is from 3% to 6% at the 4.6 % level and from 14% to 15% at the 8.0 % level. Golovenenko et al. (1973) measured the equilibrium concentration of carbon, relative to nickel, in a solution containing 4.0 at % chromium at 800, 1000 and 1200°C. They found that chromium decreased the equilibrium concentration of carbon by 15% at 800°C, 6% at 1000°C and 3% at 1200°C. Neither the temperature dependence nor the sign of the effect of chromium on the equilibrium concentration agrees with our results. Golovenenko et al. (1973) did not estimate the size of their errors. Chipman and Brushy (1968) reviewed the data on the effect of chromium in iron and indicate that 8 atom percent chromium increases the equilibrium concentration

of carbon in nickel by about 7%. The reason for this large difference is discussed in Chapter X.

In the more complex solutions containing both chromium and molybdenum, the effect of additions on the equilibrium concentration of carbon is more complicated. The addition of 8 at. % chromium to a solution containing 4 at. % molybdenum (7264 + 8 at. % Cr → 7268) increases the equilibrium carbon concentration by as much as 45% (Table 9.2). From the previous discussion one would expect the carbon concentration to be increased by ∿15%. Similarly the addition of 8 at. % molybdenum to a solution containing 4 atom percent chromium (7265 + 8 at. % Mo → 7267) has little effect at 1100°C and increases the equilibrium concentration of carbon by 6.8% at 1215°C. The results for the addition of 8 at. % molybdenum to alloy 7261 suggest that the equilibrium concentration should be decreased by from 15% to 20% upon the addition of 8 at. % molybdenum. The relative change in the equilibrium concentration of carbon depends on the amount of both molybdenum and chromium added (Table 9.2). In the case of chromium a much bigger relative change takes place upon the addition of 8 at. % than 4.6 at. %. The addition of 4 at. % molybdenum on the other hand has larger relative effect than the addition of 8 at. %.

B. Carbide Precipitates

The solubility of carbon in equilibrium with the metal carbide that forms in these alloys was determined in two different ways. In one set of experiments alloys of fixed composition were annealed at the desired temperature and then quenched. The amount of carbon in solution was determined from knowledge of the bulk carbon concentration, the weight percent of precipitate in the alloy and the concentration of carbon in the precipitated phase. This method is particularly suited to alloys with low carbon solubility. In the second method, the solubility of carbon was determined from the break in the concentration versus activity curve obtained from gas phase carburization experiments. The concentration above which the atom percent carbon in the alloy is no longer directly proportional to the activity of the carbon is the solubility limit. This method is better suited for alloys of high carbon solubility.

1. Carbide Composition

The precipitates extracted from the carburized alloys were analyzed with an electron microprobe, by the method described in Chapter V. Table 9.3 contains the results of these analyses together with the lattice parameter

Table 9.3. The results of the Analysis of the Carbide Precipitates by the Electron Microprobe and x-ray Diffraction.

Alloy	Sample Number	Temp. (°C)	Wt.%[a] Precipitate in the Alloy	Wt.% C[b] in the Precipitate	Atom %[c] of Mo	Atom %[c] of Ti	Mo/Ti	Atom %[d] of Cr	Atom %[e] of Ni	C:Metal[f] Ratio	Lattice[g] Parameter of Carbide Ao/nm
7262	A-7603-97	1215	1.57	13	24	30	0.80	<0.05	<0.05	0.85	0.4315
Ni+2.4 Ti	A-7783-37	1215	2.17	15	22	28	0.79			1.02	0.4313
+8.2 Mo	A-7783-15	1100	2.14	12	23	29	0.79			0.75	
at. %	A-7783-19	1100	0.945	12	23	29	0.79			0.75	0.4318
7266	A-7603-97	1215	6.05[h]	12	33	20	1.65	2.7	0.3	0.89	
Ni+2.4 Ti	A-7783-37	1215	7.20[h]	11	35	20	1.75	3.7		0.82	0.4299
+8.1 Mo+	A-7783-38	1215	3.62	14	25	26	0.96			0.96	0.4300
8.3 Cr	A-7783-4	1100	1.36[h]	11	23	36	0.64			0.69	0.4311
at. %	A-7783-15	1100	6.53[h]	11	32	24	1.33			0.85	
	A-7783-19	1100	3.84[h]	14	23	29	0.79			0.92	
7264	A-7603-123	1215	2.55	13	21	34	0.62			0.82	0.4326
Ni+2.4 Ti	A-7783-17	1100	2.14	13	18	38	0.47			0.79	0.4321
+4.2 Mo	A-7783-35	1100	0.475	12	17	41	0.41			0.69	0.4324
At. %											
7267	A-7783-37	1215	4.42[h]	12	28	28	1.0			0.82	0.4303
Ni+2.5 Ti	A-7783-38	1215	1.85	15	22	28	0.79			1.00	0.4310
+4.4 Cr	A-7783-14	1100	0.385	12	21	37	0.57			0.75	
+8.2 Mo	A-7783-15	1100	3.99	12	24	33	0.73			0.79	
At. %	A-7783-19	1100	2.95	13	22	32	0.69			0.85	0.4314
7268	A-7783-38	1215	0.39	19	13	33	0.39			1.17	0.4318
Ni+2.5 Ti	A-7783-15	1100	2.39	14	16	38	0.42			0.85	
+8.4 Cr	A-7783-19	1100	1.52	13	17	39	0.44			0.79	0.4319
+4.1 Mo											
At. %											

[a] σ=0.015 wt. % where σ is the root mean square residual.

[b] σ=10% by error propagation. Values determined from a knowledge of the bulk carbon concentration, the activity coefficient of carbon in the alloy, the activity of carbon in the alloy and the weight percent precipitate.

[c] σ=5%, ratios determined with the electron microprobe. Absolute values obtained from knowledge of the carbon concentration wt.% (Mo+Ti) + wt. % C = 100.

[d] Cr determined by atomic absorption. σ=0.05%, where σ is the root mean square residual.

[e] Ni Determined by spark source mass spectrometry. σ=100% where σ is the root mean square residual.

[f] σ=0.22 where σ was obtained by error propagation.

[g] σ=0.0001 nm where σ is the root mean square residual. Specimens were normally scanned with diffractometer from 20° to 80° 2θ.

[h] The carbide phase consisted of an Unidentified phase and the cubic MC phase.

of the precipitate phase as determined by powder x-ray diffraction. The weight percent carbon in the precipitate phase was calculated through a knowledge of the bulk carbon concentrations, the weight percent precipitate, the activity of carbon in the specimens and the activity coefficient of carbon in the alloys. In this way the concentration of carbon in solution is calculated directly and the concentration of carbon in the precipitate by difference. The method for calculating the molybdenum and titanium concentration is contained in Chapter V. From Table 9.3 it appears that the Mo/Ti ratio in the precipitate depends on the amount of molybdenum in the matrix. It also appears that the ratio increases as the weight percent precipitate in the alloys increases.

The Mo/Ti atom ratio in the cubic precipitates formed in the alloys containing 4 atom percent molybdenum (7264, 7268) is 0.42 ± 0.003. The value of 0.62 obtained for alloy 7264 A7603-123 (Table 9.3) is inexplicably high. The lattice parameter of the 7264 A-7603-123 precipitate is not different from those of the other two 7264 specimens, both of which have lower molybdenum concentrations. Doubling the molybdenum concentration in the matrix, to 8 at. %, increases the Mo/Ti atom ratio in the cubic precipitate phase by almost 100% to 0.79±0.01.

Nickel and chromium are minor elements in the

precipitate phase. Chromium is more soluble in the carbide than nickel, but it is likewise depleted in the precipitate phase relative to the matrix.

Figure 9.3 shows the effect of changing the molybdenum concentration in the carbide on its lattice parameter. Over the range explored (Mo/Ti atom ratio 0.4 to 1.0), the lattice parameter is a linear function of the Mo:Ti ratio in the precipitate. The addition of molybdenum decreases the lattice parameter of the carbide.

Alloys 7268 and 7267 differ from alloys 7264 and 7262, respectively, only in that they contain 8 at. % more chromium in the matrix. The addition of the 8 at. % chromium to the matrix lowers the precipitate lattice parameter by approximately 0.0005 nm. The effect of chromium on a per atom percent basis is larger than that of molybdenum, presumably because of chromium's smaller atomic radius (Slater, 1964).

As shown in Table 9.3 the carbon-to-metal atom ratio in the precipitate was almost always less than 1. The average value is 0.85, σ=0.11, and $\sigma/\sqrt{n}$=0.03. The Ti-Mo carbide might be viewed as a solid solution between nearly stoichiometric TiC and Mo_3C_2. Molybdenum increases the lattice parameter of nickel at a faster rate than does titanium, yet molybdenum is observed to decrease the lattice parameter of TiC. Since the lattice parameter

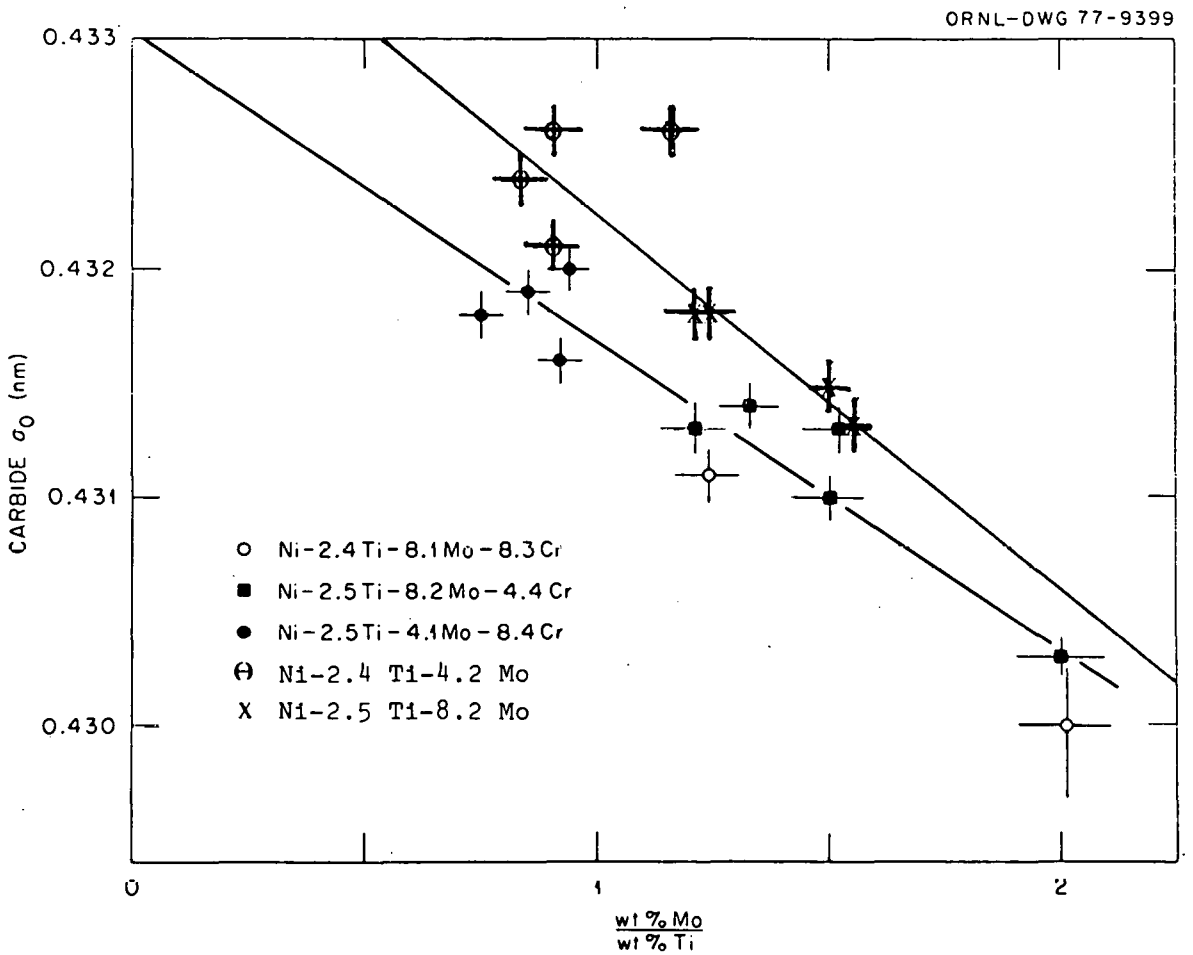

Figure 9.3. Lattice parameter of the carbide precipitate as a function of Mo/Ti in the carbide. The line was determined by a least squares fit of the data in Table 9.3.

THIS PAGE

WAS INTENTIONALLY

LEFT BLANK

of Mo_3C_2 is 0.428 nm and that of TiC is 0.433 nm, a ready explanation is provided by a TiC-Mo_2C_3 solid solution for both the lowering of the carbon lattice parameter by molybdenum and the substoichiometry.

2. Annealing Experiments

Table 9.4 and Figure 9.4 contain the results of the annealing experiments. Since the weight percent precipitate extracted from alloy B (Ni + 2.1 at. % Ti) did not change as a function of temperature, we infer, with the help of the evidence of Chapter VII, that the extracted material precipitated on cooling. This means that at least 0.08 wt % carbon is soluble, in alloy B, at all the temperatures investigated.

Alloy C (Ni + 2.4 at. % Ti + 8.2 at. % Cr + 0.5 at. % C) behaves like alloy B at high temperatures. The weight percent precipitate extracted from alloy C annealed at 1100°C is equal to that from specimens annealed at 1260°C. At 760°C, however, the weight percent precipitate increases by a factor of two. The solubility of carbon in alloy C at 760°C was calculated on the assumption that the precipitate was stoichiometric TiC and that 0.07 wt % of the precipitate formed during cooling (see Chapter VII). The value of 0.045 wt. % for the carbon solubility at 760°C should be considered a minimum estimate since

Table 9.4. Results of the Annealing Experiments.

Alloy at. %	Specimen Number	History	Temp./°C	Annealing Time/hr	wt. %[a] Carbon in Annealed Specimen	wt. %[b] Precipitate in Annealed specimen	wt. %[c] Carbon in Solid Solution Solubility
B Ni+2.1 Ti	B15	As received	1260	16	0.08	0.141[d]	0.08
	B15A	16 hr at 1260	760	168	0.08	0.157[d]	0.08
C Ni+2.4 Ti +8.2 Cr	C-6	As received	1200	16	0.103	0.149[d]	0.1
	C-7	As received	1200	16	0.098	0.117[d]	0.1
	C-6-A	16 hr at 1200	760	168	0.104	0.359	0.045[e]
A Ni+2.6 Ti +8.4 Mo	B2A	As received	1260	4	0.083	0.037	0.078[f]
	A-8	As received	1260	16	0.102	0.093	0.090
	A-10	As received	1260	16	0.092	0.037	0.087
	BA1H	As received	1200	1	0.102	0.104	0.088
	BA2H	As received	1200	2	0.102	0.095	0.090
	A-7783-147	4 hrs at 1160	1100	18	0.083	0.328	0.040
	A-7783-5	As received	1000	72	0.078	0.421	0.023
	A-7783-5	As received	900	114	0.083	0.533	0.013
	A-7783-5	As received	800	500	0.084	0.626	0.002
	A-8-A	16 hr at 1260	760	100	0.096	0.732	-----
449			1177	2	0.035	0.050	0.028
Ni+2.5 Ti	A-7783-147	4 hrs at 1160	1100	18	0.0265	0.070	0.017
+7.2 Mo	A-7783-5	As received	1000	72	0.0275	0.126	0.011
+ 8.8 Cr	A-7783-5	As received	900	114	0.0303	0.223	0.001
	A-7783-5	As received	800	500	0.0306	0.233	-----
			760	100	0.035	0.28	-----

[a] σ = 3% where σ is the root mean square residual.

[b] σ = 0.015 wt. % where σ is the root mean square residual.

[c] The solubility of carbon in alloys 449 and A was calculated on the assumption that the weight percent carbon in the precipitate was 13%. This was based on the assumption that all of the carbon in the specimens annealed at 760 had precipitated. Solubility = bulk carbon concentration - (wt. % ppt) x 0.13. The results for the weight percent carbon in the precipitate found in Table 9.3 indicate a value of ~10% for σ.

[d] This precipitate was free carbon as described in Chapter VII.

[e] The solubility of carbon in alloy C was calculated on the assumption that the precipitate was stoichiometric TiC and that 0.07 wt. % precipitate resulted from the precipitation of free carbon (see Chapter VII).

[f] The solubility for this specimen appears low. It may be that the precipitate was free carbon.

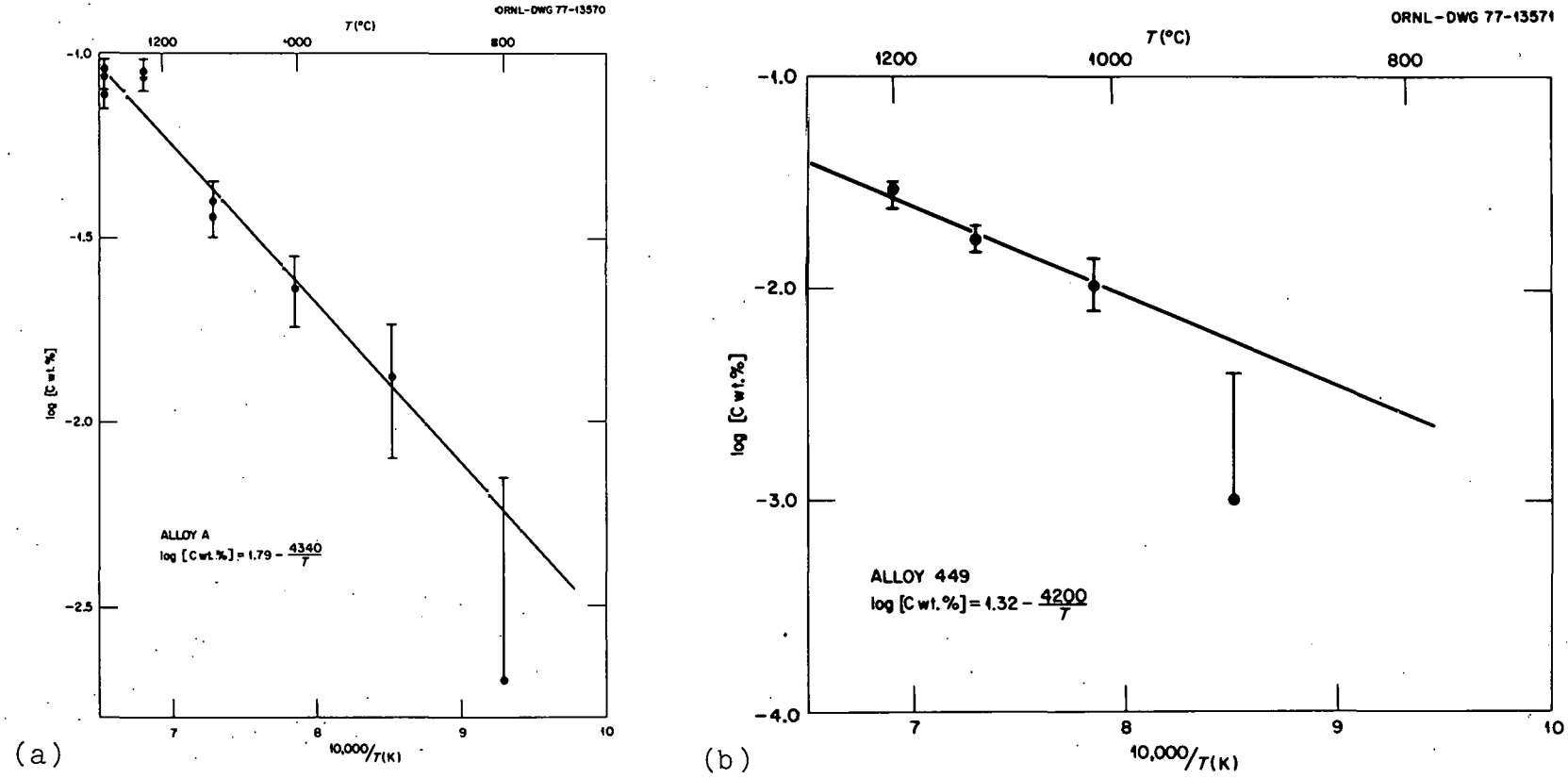

Figure 9.4. (a) The concentration of carbon in alloy A (Ni + 2.6 at. % + 8.4 at. % Mo) in equilibrium with the cubic carbide phase as a function of temperature. σ = 10% of the bulk carbon concentration.

(b) The concentration of carbon in alloy 449 (Ni + 2.0 at. % Ti + 8.3 at. % Mo + 8.4 at. % Cr) in equilibrium with the cubic carbide phase as a function of temperature. σ = 10% of the bulk carbon concentration.

THIS PAGE

WAS INTENTIONALLY

LEFT BLANK

TiC is often substoichiometric in carbon.

Alloy A (Ni + 2.6 at. % Ti + 8.4 at. % Mo + 0.5 at. % C) has considerably smaller carbon solubility than either B or C. Figure 9.4a is a plot of the logarithm of the carbon solubility versus the reciprocal of absolute temperature. The solubility was determined on the assumption that the solubility of carbon at 760°C is zero and that the weight percent carbon in the precipitate is not a function of temperature. The addition of molybdenum lowers the solubility of carbon from something over 0.08 weight percent at 760°C in alloy B to something less than 0.001 weight percent in alloy A. Molybdenum lowers the carbon solubility relative to the carbide by three different processes: (1) molybdenum dilutes the nickel-titanium solution and thus increases the titanium activity; (2) molybdenum forms a solid solution with TiC (see IX B.1) and the activity of the carbide is thus lowered; (3) the molybdenum-carbon interaction is weak relative to the nickel-carbon and titanium-carbon interactions, and the addition of molybdenum to the solution increases the carbon activity coefficient. All three of these effects tend to displace the reaction

$$Ti(Ni) + C(Ni) \rightleftarrows TiC(solid)$$

to the right.

Alloy 449 (Ni + 2.0 at. % Ti + 8.3 at. % Mo + 8.4 at. % Cr + 0.18 at. % C) results from the replacement of 8.4 at. % nickel with 8.4 at. % chromium in alloy A. Alloy 449 and 7266 are essentially the same. Table 9.4 and Figure 9.4b show that the addition of the 8.4 at. % chromium lowers the solubility of carbon relative to that in alloy A by a factor of approximately 3 at 1215°C. The decreased solubility of carbon in alloy 449 is due primarily to diluting the nickel-titanium interaction which results in a higher titanium activity. That is, the Gibbs free energy of mixing for titanium and chromium is much less negative than for titanium and nickel. The chromium does not form an appreciable solid solution with the carbide phase, and therefore the addition of chromium does not alter the activity of the carbides.

3. Carburization Experiments

Table 9.5 and Figures 9.5, 9.6 and 9.7 contain the result of the gas carburization experiments undertaken to determine the solubility of carbon in various nickel alloys. Since it has been shown in Chapters VI, VII and IX that the carbon in solid solution in these alloys obeys Henry's Law, any negative deviation from Henry's Law can be considered evidence that carbide precipitation has taken place. The solubility limit is the concentration at which the

Table 9.5. Solubility of Carbon in Several Nickel-Based Alloys as Determined from Carburization Experiments.

Temp. (°C)	900		1100		1215	
Alloy Comp. At. %	$A^{a}_{C(sat)}$	$C_{(sat)}$ wt.%	$A^{a}_{C(sat)}$	$C_{(sat)}$ wt.%	$A^{a}_{C(sat)}$	$C_{(sat)}$ wt.%
7262	0.17	0.019	0.18	0.046	0.18	0.073
7264	0.36	0.045	0.38	0.10	0.32	0.14
7266[b]			0.046	0.016	0.067	0.037
7267			0.10	0.032	0.095	0.050
7268			0.11	0.043	0.13	0.079

7262 Ni + 2.5 Ti + 8.2 Mo

7264 Ni + 2.4 Ti + 4.2 Mo

7266 Ni + 2.4 Ti + 8.1 Mo + 8.3 Cr

7267 Ni + 2.5 Ti + 8.2 Mo $\pm$ 4.4 Cr

7268 Ni + 2.5 Ti + 4.1 Mo + 8.4 Cr

[a]The solubility was determined from the following equation $A_{C(sat)} = \hat{\gamma}_c \, x_{C(sat)}$. Activity coefficient of carbon was obtained from Tables 8.2 and 9.1.

[b]The activity coefficient of carbon in alloy 7266 was not experimentally determined therefore an approximate value had to be used. The activity coefficient of carbon in alloy 7266 was taken to be the average of those for alloys 7267 and 7268. This seems to be appropriate since alloy 7267 and 4 at. % more Mo than 7268 and Mo and Cr have opposite effects.

THIS PAGE

WAS INTENTIONALLY

LEFT BLANK

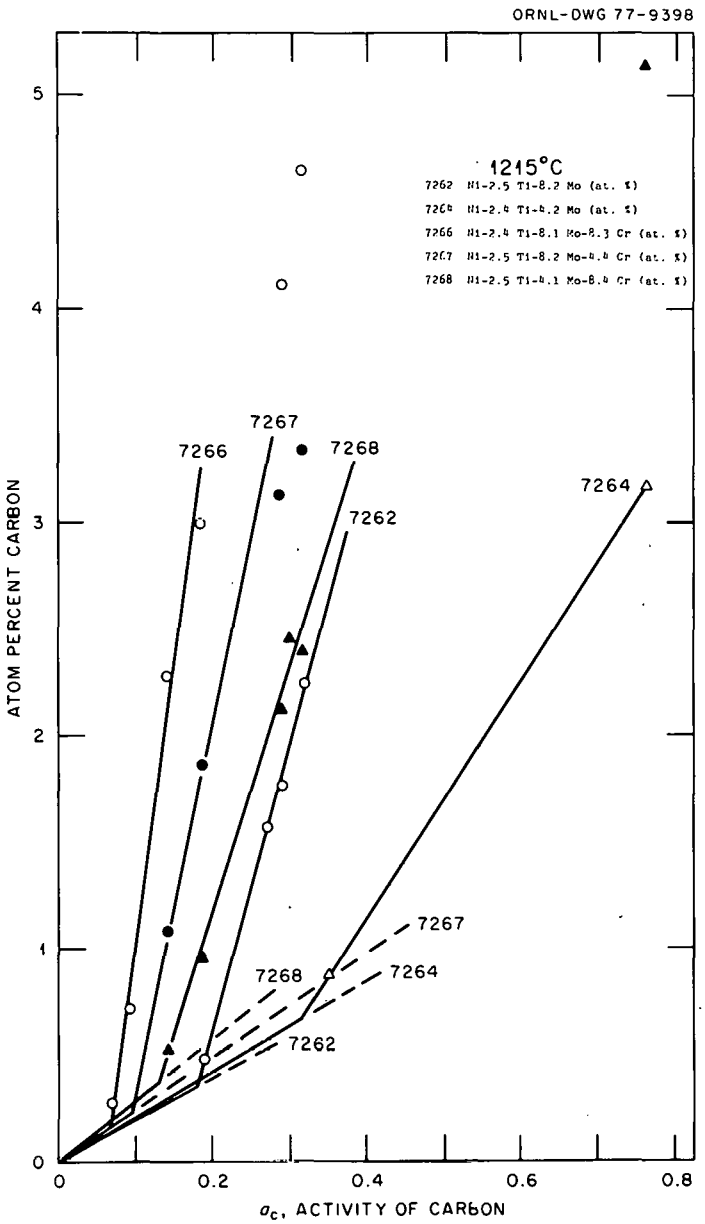

Figure 9.5. Atom % carbon versus activity of carbon in several nickel-based alloys at 1215°C. The intersection of the two lines, with the same label, is the solubility limit of carbon relative to the carbide phase. The lower line represents the solid solution where the slope is $100/\hat{\gamma}_C$ ($x_C = A_C/\hat{\gamma}_C$). The dashed lines are an extrapolation of the solid solution lines and represent the amount of carbon in solution at any given activity. The upper lines have been fit by least squares to the data from the two phase region, points that diverged from the straight line behavior exhibited near the intersection were ignored.

THIS PAGE

WAS INTENTIONALLY

LEFT BLANK

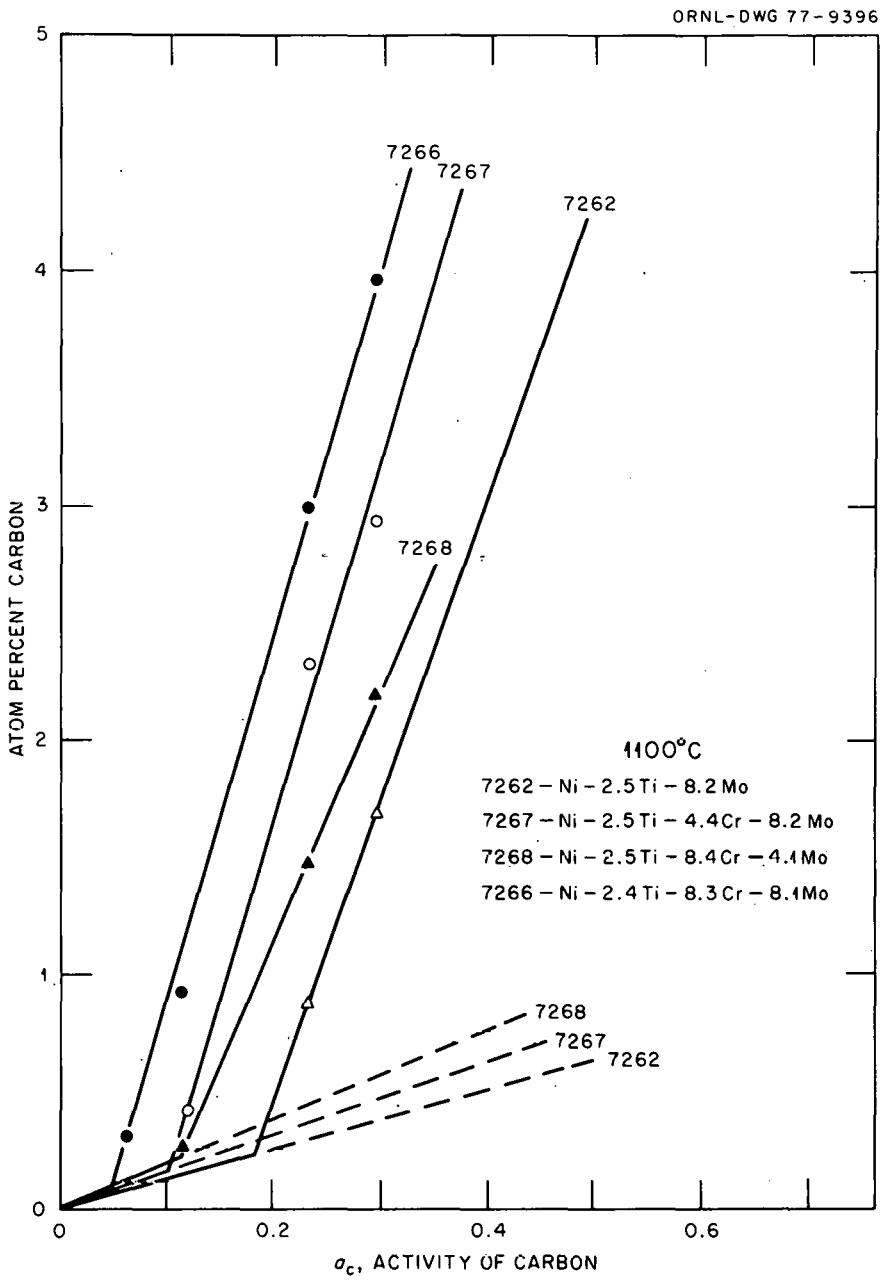

Figure 9.6. Atom % carbon versus activity of carbon in several nickel-based alloys at 1100°C. The intersection of the two lines, with the same label, is the solubility limit of carbon relative to the carbide phase. The lower line represents the solid solution where the slope is $100/\hat{\gamma}_C$ ($x_C = A_C/\hat{\gamma}_C$). The dashed lines are extrapolations of the solid solution lines and represent the amount of carbon in solid solution at activities exceeding the solubility limit. The upper lines were fit by least squares to the data from the two phase region.

THIS PAGE

WAS INTENTIONALLY

LEFT BLANK

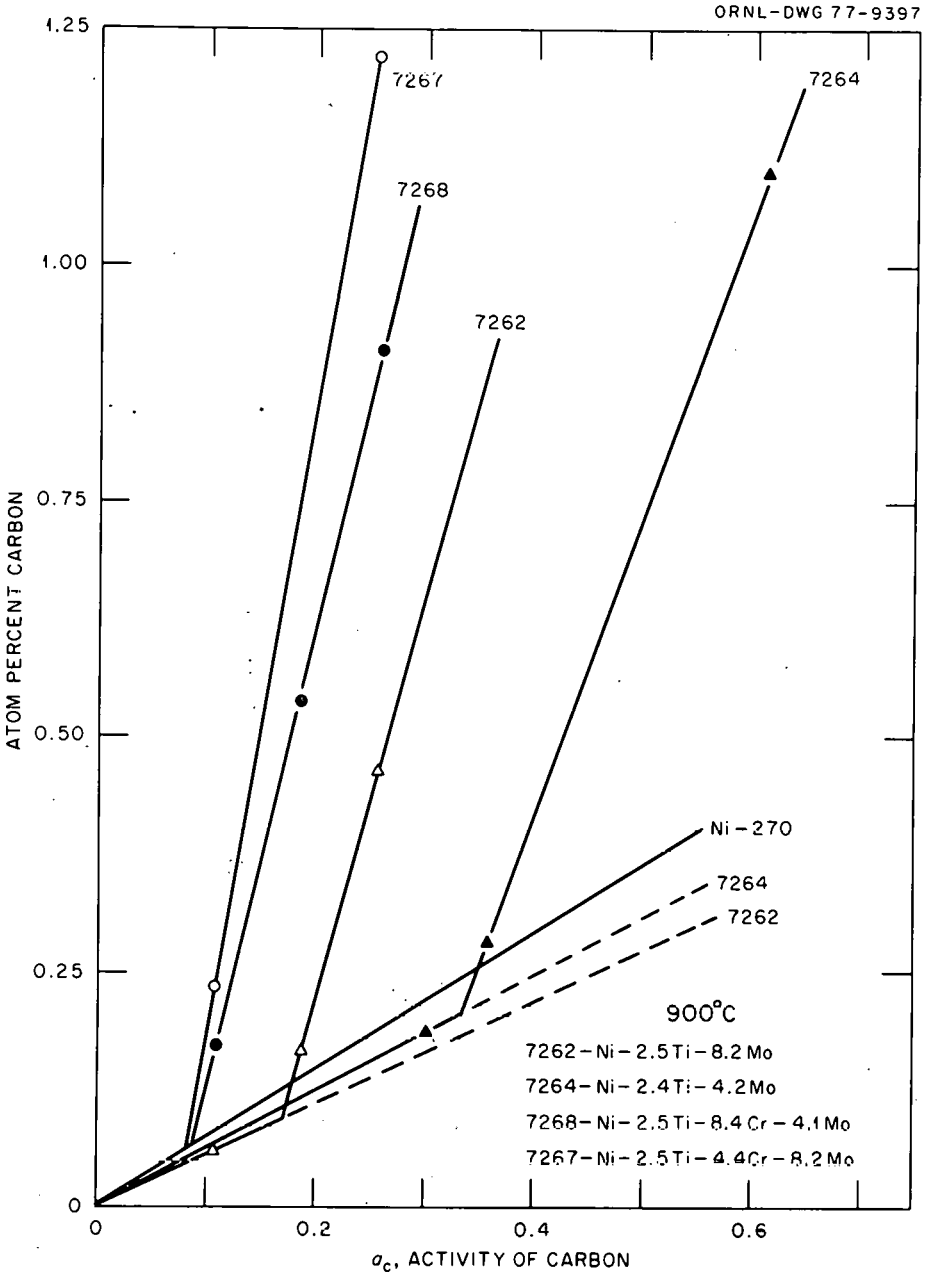

Figure 9.7. Atom % carbon versus activity of carbon in several nickel-based alloys at 900°C. The intersection of the two lines, with the same label, is the solubility limit of carbon relative to the carbide phase. The lower line represents the solid solution where the slope is $100/\hat{\gamma}_C$ ($x_C = A_C/\hat{\gamma}_C$). The dashed lines are extrapolations of the solid solution lines and represent the amount of carbon in solid solution at activities exceeding the solubility limit. The upper lines were fit by least squares to the data from the two phase region.

concentration versus activity line for carbon in the alloy has a change in slope. In Figures 9.5, 9.6 and 9.7 the solubility limit has been determined by fitting the solid solution carburization data and the carburization data from the two phase region with least squares lines and calculating their intersection.

The solubility of carbon in molybdenum-free alloys was not determined by this technique because either the carbide phase does not exist in the alloys at the temperatures and activities investigated or only one data point in the two phase region existed. The solubility limit of carbon in alloys 7266, 7267 and 7268 was not determined at 900°C because a diffusion barrier, possibly a layer of chromium oxide, slowed the rate of carburization so much that carburization experiments were impractical.

As Table 9.5 indicates, doubling the molybdenum concentration reduces the carbon solubility by a factor of 2. The result of adding chromium to the carbide forming alloys has a similar effect. Both the decrease in solubility of carbon upon addition of chromium and the values of the solubilities agree with results obtained for similar alloys in the annealing experiments discussed in the previous subsection.

The effects of additions of chromium and molybdenum on the solubility of carbon relative to the carbide phase

in the alloys already forming a carbide phase thus follow a regular pattern: doubling the molybdenum or chromium concentration decreases the carbon solubility by a factor of about two.

C. An Unidentified Phase of High Carbon Content

In alloys 7266 and 7267 some specimens contained an unidentified carbide phase (see Table 9.3). The Mo/Ti atom ratio is approximately 1.6 and the carbon to metal ratio in the two phase precipitate is approximately 0.8. Microprobe examination of precipitates, in the matrix (see Figure 9.8) revealed that the precipitates with the needle like morphology had the same composition as the more rounded precipitates. The new phase does not correspond to any of the low carbon carbide such as M_2C, M_6C or $M_{12}C$.

Attempts to index the x-ray diffraction characteristic of the phase have failed as have attempts to identify it with the ASTM x-ray card file. Tables 9.6 and 9.7 contain the 2θ values and relative intensities of the diffraction peaks in the spectrums for 7266 specimens A-7603-97 and A-7783-37. Figure 9.8 is an optical micrograph of the precipitates in alloy specimen 7266 A-7603-97: the needle-like morphology is not characteristic of TiC precipitates.

Table 9.6. X-ray Diffraction Data on the Unidentified Phase Alloy 7266 A-7783-97[a].

2θ	I
27.29	11
36.70	1100
41.48	85
44.30	25
46.35	20
51.11	130
54.82	80
58.95	30
61.37	30
63.17	48
67.67	15
72.43	54
78.07	100

[a]Copper K_α radiation was used. The spectrometer travel speed was 1/4° 2θ per min.

Table 9.7. X-ray Diffraction Data on the Unidentified Phase in Alloy 7266-A-7783-37.[a]

2θ	I	2θ	I
27.30	7	63.28	18
33.02	2	67.74	4
35.56	7	72.45	22
36.70	870	72.65	14
37.04		73.73	6
39.00	4	76.84	4
41.53	21	77.10	3
44.41	6	78.11	100
46.37	9	78.33	
51.12	2	88.20	2
51.29	1	88.35	2
59.00	9	88.43	1
61.45	6	90.38	2

[a]Copper K_α radiation was used. The spectrometer travel speed 1/4° 2θ per min.

THIS PAGE

WAS INTENTIONALLY

LEFT BLANK

Y-138956

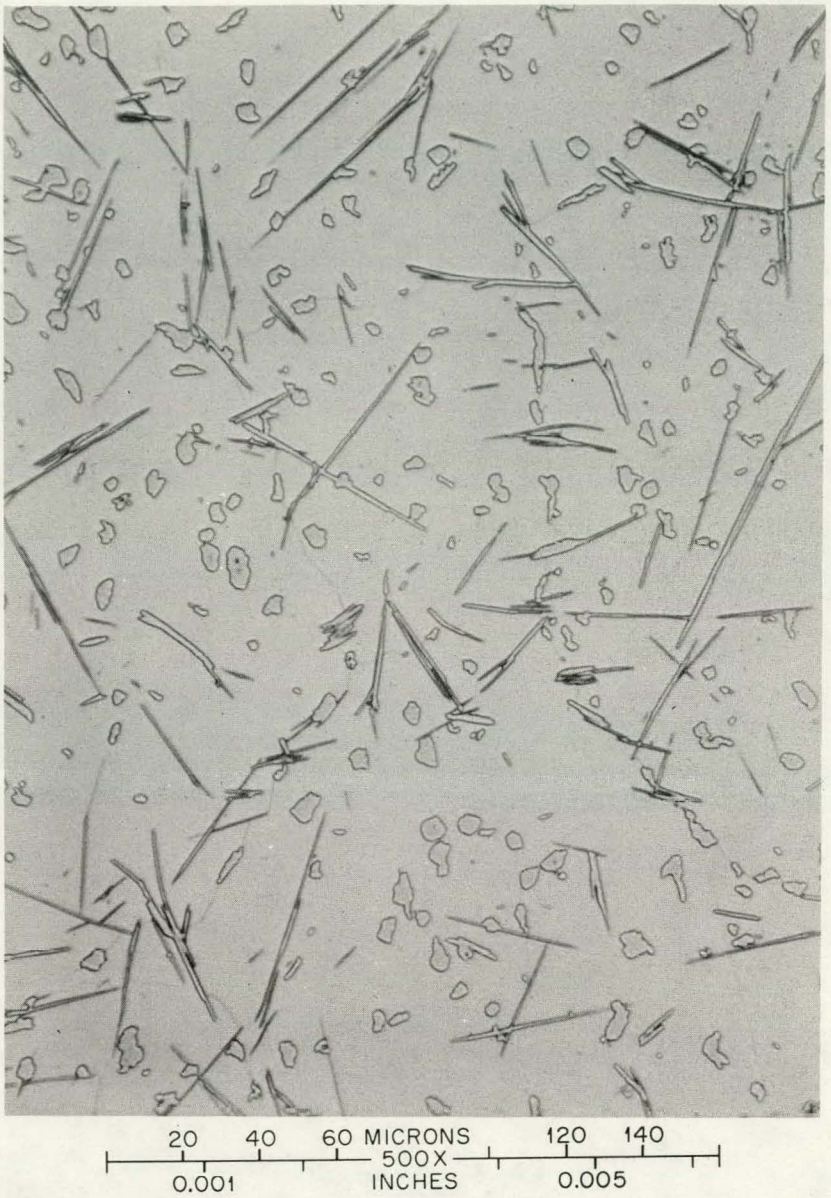

Figure 9.8. Specimen number 7266 A-7603-97 equilibrated at 1215°C at A_c = 0.268. Note the needle like precipitates which are characteristic of the unidentified phase. The other precipitates are the MC phase.

CHAPTER X

THE KOHLER-KAUFMAN EQUATION

A. Calculation of the Nickel-Carbon and the Iron-Carbon Interaction Energies

Table 10.1 contains the values of the 4 interaction energies that describe the nickel-carbon and the iron-carbon systems. The relative lattice stabilities are listed in Table 10.2. The equations used to calculate the interaction are from Equation (2.30). For each temperature

$$\overline{G}^{E}_{C(Ni)} = RT \ln \hat{\gamma}_{C(Ni)} = \overline{G}_{C}^{FCC-gr} + x_{Ni}^{2}(1-2x_C)\,\psi_{NiC} + 2x_C x_{Ni}^{2}\,\psi_{CNi}$$

$$\overline{G}^{E}_{C(Fe)} = RT \ln \hat{\gamma}_{C(Fe)} = \overline{G}_{C}^{FCC-gr} + x_{Fe}^{2}(1-2x_C)\,\psi_{FeC} + 2x_C x_{Fe}^{2}\,\psi_{CFe}. \qquad (10.1)$$

To obtain ψ_{NiC} and ψ_{FeC}, Equations (10.1) are solved at $x_C = 0$, where

$$\psi_{NiC} = RT \ln \hat{\gamma}^{\infty}_{C(Ni)} - \overline{G}^{FCC-gr}$$

$$\psi_{FeC} = RT \ln \hat{\gamma}^{\infty}_{C(Fe)} - \overline{G}^{FCC-gr} \qquad (10.2)$$

Table 10.1. Calculated Values of Nickel-Carbon and Iron-Carbon Interaction Energies, ψ_{ij}^{FCC}.[a]

	A_{ij} kJmol^{-1}	B_{ij}/Jmol^{-1}K^{-1}	C_{ij}/Jmol^{-1}K^{-2}·10^{-3} d_{ij}
ψ_{NiC}[b]	-135.52	87.31	-29.29
ψ_{CNi}[b]	-163.7	14.0	c
ψ_{FeC}[d]	- 96.15	-0.88	0.0
ψ_{CFe}[d]	-156.1	0.0	0.0

[a] $\psi_{ij} = A_{ij} + B_{ij}T + C_{ij}T^2$.

[b] σ_4=0.3 kJmol^{-1}, calculated assuming a 3% error in $\hat{\gamma}_C$(Ni).

[c] Assumed zero.

[d] σ_4=0.2 kJmol^{-1}, calculated assuming a 2.5% error in $\hat{\gamma}_C$(Fe).

Table 10.2. Some Relative Lattice Stabilities[a] for Elements of Interest.

Element	Transformation[b]	$\overline{H}_i^{b-a}$/kJ·mol^{-1}[c]	$\overline{S}_i^{b-a}$/J·mol^{-1}K^{-1}[c]
C	Graphitic FCC	138	15
Ti	BCC FCC	-1.0	3.8
Cr	BCC FCC	10.5	0.63
Fe	FCC FCC	0	0
Ni	FCC FCC	0	0
Mo	BCC FCC	10.5	0.63

[a] From Kaufman and Nesor (1973, 1975), Uncertainties not stated.

[b] FCC=Face Centered Cubic, BCC=Body Centered Cubic.

[c] $\overline{H}_i^{b-a} = (\overline{H}_i^b - \overline{H}_i^a)$, $\overline{S}_i^{b-a} = (\overline{S}_i^b - \overline{S}_i^a)$ and $\overline{G}_i^{b-a} = \overline{H}_i^{b-a} - T\overline{S}_i^{b-a}$.

To solve for ψ_{CNi} and ψ_{CFe}, Equations (10.1) are evaluated at other values of x_C. In the case of the nickel-carbon system, $\hat{\gamma}_C$ is a constant to the saturation limit, and to insure that the interaction energies reflects this we evaluate ψ_{CNi} at $(x_C)_{sat}$.

For the iron-carbon system the results of Smith (1946) in the form of Eq. (3.6) were used to determine the values of ψ_{CFe} and ψ_{FeC} from Eqs. (10.1) and (10.2).

Experimental values for $\hat{\gamma}_C$ and $(x_C)_{sat}$ from Chapter VI were used together with $\overline{G}_C^{FCC-gr}$ estimates of Kaufman and Nesor (1975) to obtain ψ_{NiC} and ψ_{CNi} at 900°C, 1100°C, and 1215°C. Data for nickel were fit with an equation of the type

$$\psi_{ij} = A_{ij} + B_{ij}T + C_{ij}T^2 \qquad (10.3)$$

B. Analysis of the Nickel-Iron-Carbon System

Smith (1960) and Wada et al. (1971) studied the nickel-iron-carbon system from $x_{Fe} = 0$ to 1.00. Tables 10.3 and 10.4 contain the results of these two investigations. The appropriate Kohler-Kaufman equation for $\overline{G}_C^E$ at $x_C = 0$ is

$$\overline{G}_C^E = RT \ln \hat{\gamma}_C = \overline{G}_C^{FCC-gr} + x_{Ni}\psi_{NiC} + x_{Fe}\psi_{FeC} \qquad (10.4)$$

$$- x_{Ni}^2 x_{Fe}\psi_{NiFe} - x_{Fe}^2 x_{Ni}\psi_{FeNi}$$

Table 10.3. The Reanalyzed Results of Smith (1960) for the Activity Coefficient of Carbon[a] in Nickel-Iron-Carbon Alloys.

Mole Fraction Nickel x_{Ni}	Activity Coefficient of Carbon $\hat{\gamma}_C^{\infty}$	rms Residual σ
0.0	8.45	0.2
0.0379	10.5	1
0.0775	13.2	1
0.148	17.3	1
0.258	29	3
0.395	54	6
0.599	119	9
0.787	148	7
0.994	87.6	4.5

[a]Table contains values of $\hat{\gamma}_C^{\infty}$ calculated for $x_C < 0.02$. When $x_C < 0.02$ $\hat{\gamma}_C = \hat{\gamma}_C^{\infty}$ = a constant. (See Figure 6.4). Equation (3.6) was used to recalculate the activity of carbon in iron, which was used as a secondary standard in all runs.

Table 10.4. The Reanalyzed Results of Wada et al. (1971) for the Activity Coefficient of Carbon[a] in Nickel-Iron-Carbon Alloys.

Mole Fraction Nickel x_{Ni}	Activity Coefficient of Carbon $\hat{\gamma}_C^{\infty}$	rms Residual σ
0.207	23	2
0.401	57	6
0.506	85	9
0.598	130	18
0.655	139	23
0.792	159	16
0.892	115	13

[a]This table contains values of $\hat{\gamma}_C$ calculated for $x_C<0.02$. When $x_C<0.02$ $\hat{\gamma}_C = \hat{\gamma}_C$ = a constant (see Figure 6.4). Equation (3.6) was used to recalculate the activity of carbon in iron, which was used as a secondary standard in all runs.

To use Equation (10.4) values of ψ_{NiFe} and ψ_{FeNi} were taken from Kaufman and Nesor (1975) Table (10.1)). Figure 10.1a compares the values of $\ell n\hat{\gamma}_C^{\infty}$ calculated using Equation (10.4) and the values of the interaction energies listed in Tables 10.1 and Table 10.5 with the experimental results of Smith (1960) and Wada et al. (1971). In Figure 10.1a the x's are experimental points and the zeros, 0, are points calculated from Equation (10.4) with only the nickel-carbon and the iron-carbon binary interaction energies of Table 10.1. The difference between calculated and experimental points is very large, and at the nickel-rich end the binary Kohler-Kaufman equation predicts that the activity coefficient of carbon will decrease upon the addition of iron. Experimentally, however, the activity coefficient increases until $x_{Fe} \sim 0.25$ and then decreases as more iron is added. Obviously the Kohler-Kaufman equation with only binary interaction energies is unable to predict the form of $\ell n\ \hat{\gamma}_C^{\infty}$ in the ternary mixture.

Figure 10.1b is an attempt to fit all of the ternary data in Tables 10.3 and 10.4 with Equation (10.4). Again only binary terms are considered. The difference between Figures 10.1a and 10.1b is that the values of ψ_{FeC} and ψ_{NiC} were determined as a best fit to all of the ternary data. The fit is very poor. The calculated values are high for the iron rich alloys and low for the nickel rich alloys.

The values of ψ_{NiFe} and ψ_{FeNi} were taken from Kaufman and Nesor (1975), (Table 10.5). The experimental results for $\hat{\gamma}_C^{\infty}$ in the nickel-iron-carbon system can be fit with only binary terms if ψ_{NiFe} and ψ_{FeNi} are allowed to increase by a factor of five. The resulting parameters, however, would not correctly describe the thermodynamics of the binary iron-nickel system. Kubaschewski et al (1977) have reviewed the iron-nickel system and their results agree with those of Kaufman and Nesor (1975). In no case then were the values of ψ_{NiFe} and ψ_{FeNi} allowed to vary.

Figure 10.2 is the result of fitting the data of Smith (1960) and Wada et al (1971) to the Kohler-Kaufman equation where ternary terms have been added to Eq. (10.4).

$$\overline{G}_C^E = RT \ln \hat{\gamma}_C^{\infty} = \overline{G}_C^{FCC\text{-}gr} + x_{Ni}\psi_{NiC} + x_{Fe}\psi_{FeC}$$

$$- x_{Ni}^2 x_{Fe}\psi_{NiFe} - x_{Fe}^2 x_{Ni}\psi_{FeNi} + x_{Ni}^2 x_{Fe}\psi_{NiFeC} + x_{Fe}^2 x_{Ni}\psi_{FeNiC}. \qquad (10.5)$$

The equal signs in this figure indicated that the experimental and calculated points agree within 2%. The root mean square residual of the fit to the Kohler-Kaufman equation was 5.6%. The values of the ternary parameters are $\psi_{NiFeC} = 61.9$ kJ mol^{-1}, $\sigma = 1.8$ kJ mol^{-1} and $\psi_{FeNiC} = 20.7$

Figure 10.1. Comparison of calculated, O, and experimental, X, values of $\ell n\ \hat{\gamma}_C^{\infty}$ as a function of X_{Ni} in the Ni-Fe-C system. The experimental results are those of Smith (1960) and Wada et al. (1971) (see Tables 10.3 and 10.4). (a) Calculated points determined from Equation (10.4) with the values ψ_{NiC} and ψ_{FeC} taken from the binary results (Table 10.1). (b) Calculated points determined as a "best fit" of Equation (10.4); the experimental values were the independent variable and ψ_{NiC} and ψ_{FeC} the dependent variables. ψ_{NiFe} and ψ_{FeNi} were taken from Kaufman and Nesor (1975), Table 10.5.

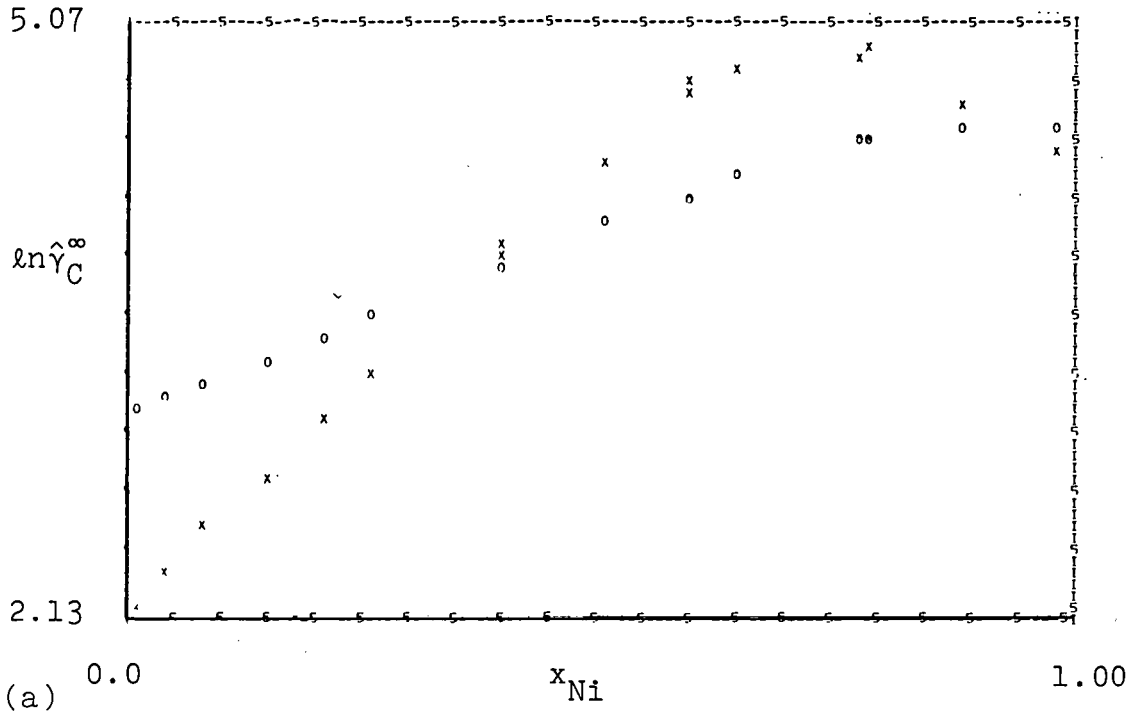
5.07
$\ell n\hat{\gamma}_C^{\infty}$
2.13
0.0
x_{Ni}
1.00

(a)

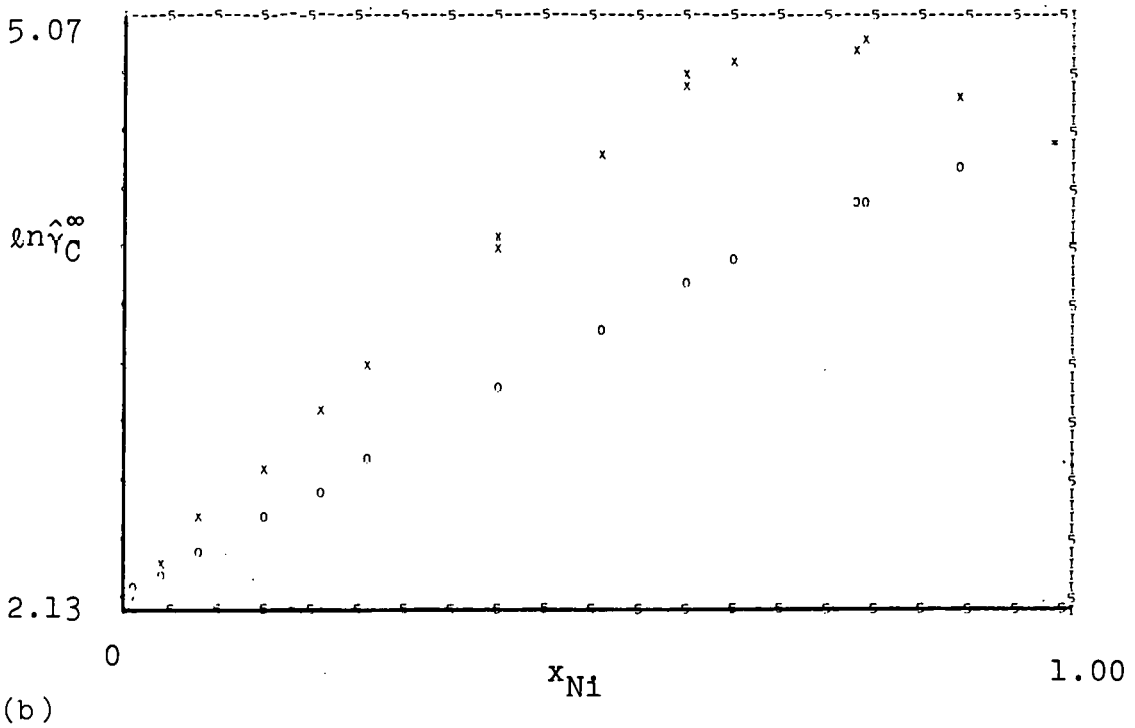
5.07
$\ell n\hat{\gamma}_C^{\infty}$
2.13
0
x_{Ni}
1.00

(b)

THIS PAGE

WAS INTENTIONALLY

LEFT BLANK

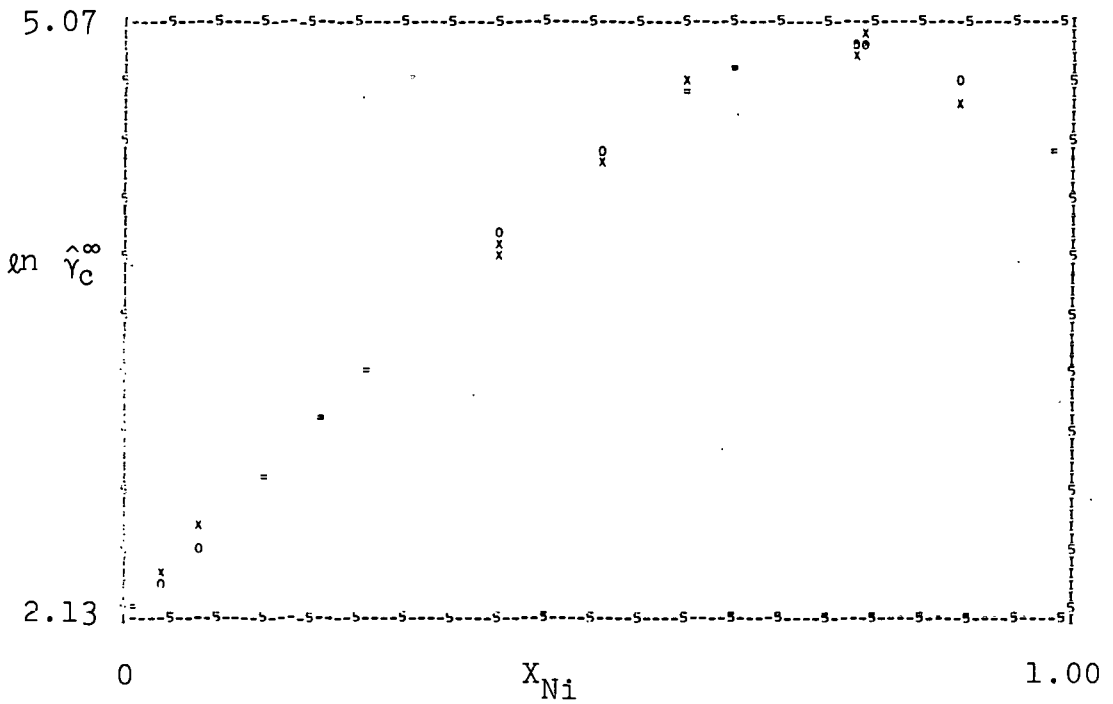

Figure 10.2. Comparison of calculated, 0, and experimental, X, values of ℓn $\hat{\gamma}_C^{\infty}$ as a function of x_{Ni} in the Ni-Fe-C system. An equal sign, =, indicates that the experimental and calculated values differ by less than 2%. The calculated points were determined as a best fit of Equation (10.5) to experimental results of Smith (1960) and Wada et al (1971) (see Tables 10.3 and 10.4). Values of ψ_{FeNi} and ψ_{NiFe} were taken from Kaufman and Nesor (1975), Table 10.5.

kJ mol^{-1}, σ = 5.3 kJ mol^{-1}. The dramatic improvement in the fit of the data to the equation clearly indicates that ternary coefficients must be included.

C. Calculation of Interaction Energies in the Nickel-Titanium-Carbon System

As mentioned in the Introduction, one of the goals of this research was to test the validity of using only binary parameters to describe the thermodynamics of multicomponent solutions. Therefore, in this section and the next ternary terms in the Kohler-Kaufman equation are initially ignored.

The equations for $\overline{G}^E_{Ti}$ and $\overline{G}^E_C$ in the ternary alloy are obtained from Equation (2.30). For $\overline{G}^E_{Ti}$

$$\overline{G}^E_{Ti} = \overline{G}^{FCC-BCC}_{Ti} + \psi_{TiNi}\left[\frac{x_{Ti}x_{Ni}^2}{(x_{Ti}+x_{Ni})^2} + \frac{x_{Ti}x_{Ni}}{(x_{Ti}+x_{Ni})}(1-x_{Ti})\right]$$

$$+ \psi_{TiC}\left[\frac{x_{Ti}x_C^2}{(x_{Ti}+x_C)^2} + \frac{x_{Ti}x_C}{(x_{Ti}+x_C)}(1-x_{Ti})\right]$$

$$+ \psi_{NiTi}\left[\frac{x_{Ni}^2}{(x_{Ti}+x_{Ni})}\left(\frac{x_{Ni}}{(x_{Ti}+x_{Ni})} - x_{Ti}\right)\right]$$

$$+ \psi_{CTi}\left[\frac{x_C^2}{(x_C+x_{Ti}}\left(\frac{x_c}{x_C+x_{Ti}} - x_{Ti}\right)\right]$$

$$- \psi_{CNi}\left(\frac{x_C^2 x_{Ni}}{x_C+x_{Ni}}\right) - \psi_{NiC}\left(\frac{x_{Ni}^2 x_C}{x_C+x_{Ni}}\right), \qquad (10.6)$$

where ternary interaction energies are excluded. At x_C = 0, Equation (2.30) yields for $\bar{G}_C^E$,

$$\bar{G}_C^E = RT \ln \hat{\gamma}_C = \bar{G}_C^{FCC\text{-}gr} + x_{Ni}\psi_{NiC} + x_{Ti}\psi_{TiC} + - x_{Ni}^2 x_{Ti}\psi_{NiTi} - x_{Ti}^2 x_{Ni}\psi_{TiNi}, \quad (10.7)$$

where ternary interaction energies are excluded.

Following Kaufman and Nesor (1975) we assume $\psi_{TiC} = \psi_{CTi}$ and $\psi_{NiTi} = \psi_{TiNi}$. In both cases this is justified because of narrow range of experimental data. These assumptions result in a symmetric excess Gibbs free energy as a function of composition in the binaries. While Eqs. (10.6) and (10.7) could in principle be solved simultaneously they are easily solved by iteration. The estimate of ψ_{TiC} (= ψ_{CTi}) proposed by Kaufman and Nesor (1975) was used in Eq. (10.4) to solve for ψ_{TiNi} (= ψ_{NiTi}). Then a value for ψ_{TiC} was calculated from the results in Chapter 8 and Eq. (10.7). This value for ψ_{TiC} was then used to recalculate by Eq. (10.6) the value of ψ_{NiTi}. Kaufman and Nesor's (1975) estimate was close to our calculated value and only one iteration was necessary. The use of the value of ψ_{TiC} obtained Eq. (10.7) to recalculate ψ_{NiTi} changed the value of ψ_{NiTi} by approximately 0.4 KJ·mol^{-1}. Recalculation of ψ_{TiC} produced no significant change. The values for ψ_{NiTi} at several temperatures were

fit by least squares to Eq. (10.3) ψ_{TiC} was found to be constant within experimental error and no ternary term is needed.

D. Calculation of the Molybdenum-Carbon and Chromium-Carbon Interaction Energies

The values of ψ_{MoC} and ψ_{CrC} were calculated at $x_C = 0$ from the results in Table 9.1 for alloys 7262 and 7264, 7263 and 7265, and the following equations which are derived from Eq. (2.30).

$$\overline{G}_C^E = \overline{G}_C^{FCC\text{-}gr} + x_{Ni}\psi_{NiC} + x_{Ti}\psi_{TiC} + x_{Mo}\psi_{MoC}$$

$$- x_{Ni}^2 x_{Ti}\psi_{NiTi} - x_{Ti}^2 x_{Ni}\psi_{TiNi} - x_{Ni}^2 x_{Mo}\psi_{NiMo} - x_{Mo}^2 x_{Ni}\psi_{MoNi}$$

$$- x_{Ti}^2 x_{Mo}\psi_{TiMo} - x_{Mo}^2 x_{Ti}\psi_{MoTi}, \qquad (10.8)$$

$$\overline{G}_C^E = \overline{G}_C^{FCC\text{-}gr} + X_{Ni}\psi_{NiC} + x_{Ti}\psi_{TiC} + x_{Cr}\psi_{CrC}$$

$$- x_{Ni}^2 x_{Ti}\psi_{NiTi} - x_{Ti}^2 x_{Ni}\psi_{TiNi} - x_{Ni}^2 x_{Cr}\psi_{NiCr} - x_{Cr}^2 x_{Ni}\psi_{CrNi}$$

$$- x_{Ti}^2 x_{Cr}\psi_{TiCr} - x_{Cr}^2 x_{Ti}\psi_{CrTi}; \qquad (10.9)$$

where ternary interaction energies are excluded. The previously calculated ψ_{ij} were employed and the values of ψ_{NiCr}, ψ_{CrNi}, ψ_{NiMo}, ψ_{MoNi}, ψ_{CrTi}, ψ_{TiCr}, ψ_{MoTi}, ψ_{TiMo} and

$\bar{G}_C^{FCC-gr}$ were taken from Kaufman and Nesor (1973, 1975) (see Tables 10.2 and 10.5).

The values of the interaction energies calculated assuming only binary terms were important are listed in Table 10.6. It is clear from the results in Tably 10.6 that in the cases of ψ_{MoC} and ψ_{CrC} that the calculated values are all composition dependent. Further, all of the binary interaction energies become more negative as the mole fraction of the total solute is increased. This means that the activity coefficient is smaller in the more concentrated solutions than would be expected from extrapolation of the dilute results. The trend is to lower than expected activity coefficients continued to an even larger extent in alloys 7267 and 7268 as discussed in Chapter IX. It thus appears that, as in the Fe-Ni-C system, the binary interaction energies are not sufficient to describe the systems in question.

At $x_C = 0$ the appropriate ternary terms from Eq. (2.30) are

$$\bar{G}_C^E \text{ (ternary)} = \sum_{\substack{i=1 \\ i\neq j}}^{n-1} \sum_{j=1}^{n-2} \psi_{ijn} \left(\frac{x_i^2 x_j}{x_i + x_j}\right)$$

$$+ \sum_{\substack{i=1 \\ k\neq i\neq j \\ j<k}}^{n-1} \sum_{j=1}^{n-2} \sum_{k=1}^{n-1} - \frac{2x_i^2 x_j x_k}{(x_i + x_j + x_k)} \psi_{ijk} \qquad (10.10)$$

Table 10.5. Interaction Energies ψ_{ij}^{FCC} for the Kohler-Kaufman Formalism,[a] $\psi_{ij}^{FCC} = A_{ij} + B_{ij}T + C_{ij}T^2 + D_{ij}T^3$.

j/i	Ti	Cr	Fe	Ni	Mo
			$A_{ij}/kJ \cdot mol^{-1}$		
Ti		52.0	-33.5	-100	15.4
Cr	39.4	----	7.41	-25.1	21.3
Fe	-10.5	7.41	----	-34.8	25.3
Ni	-100	-8.37	2.1	------	13.6
Mo	15.4	34.3	24.8	-13.6	----
			$B_{ij}/J \cdot mol^{-1}K^{-1}$		
Ti	----	0	0	-95.8	0
Cr	0	----	-6.3	0	-5.9
Fe	0	-6.3	-----	0	0
Ni	-95.8	0	0	----	13.8
Mo	0	-11.3	-8.4	13.8	----
			$C_{ij}/10^{-3}J \cdot mol^{-1}K^{-1}$		
Ti	----	0	0	47.2	0
Cr	0	----	0	9.47	0
Fe	0	0	----	24.4	0
Ni	47.2	4.69	-3.83	----	0
Mo	0	0	0	0	0

Table 10.5. Continued.

j/i	Ti	Cr	Fe	Ni	Mo
			$D_{ij}/10^{-6}$ J·mol^{-1}K^{-3}		
Ti	----	0	0	0	0
Cr	0	----	0	-2.61	0
Fe	0	0	----	-10.4	0
Ni	0	-7.85	1.63	----	0
Mo	0	0	0	0	----

[a]All values are from Kaufman and Nesor (1973, 1975) except $\psi_{NiTi} = \psi_{TiNi}$ which were calculated from the results of Chapter VIII.

Table 10.6. Incorrect Values for the Binary Interaction Parameters, ψ_{iC}^{FCC} Calculated with Only Binary Terms.

i (Element)	ψ_{iC}^{FCC}/kJ·mol^{-1}		
	Temperature (°C)		
	900	1100	1215
Ni[a]	-73.41	-70.86	-70.46
Ti			
7261, x_{Ti} = 0.0244	-254.8	-234.7[b]	-238.9
7068, x_{Ti} = 0.0361	-258.2	-263.6[b]	-243.5
Cr			
7265, x_{Cr} = 0.0457	-76.8	-78.2	-75.9
7263, x_{Cr} = 0.0801	-81.6	-95.1	-90.7
Mo			
7264, x_{Mo} = 0.0417	-10.9	-5.7	-6.5
7262, x_{Mo} = 0.0820	-29.9	--27.9	-27.3

[a] ψ_{NiC} was fit to a quadratic equation in temperature.

[b] The 1100°C results appear to be in error. The 7261 result being too large and the 7068 result being too small. If the concentrations of carbon in 7261 and 7068 at 1100°C are compared directly to the nickel carbon concentrations the values of ψ_{TiC} become -250.3 and -258.9 kJ·mol^{-1}, respectively.

From the array of alloys that have been studied here we cannot discriminate between the possible ternary terms in Eq. 10.10. It seems logical, however, to fit the results with those terms having the largest concentration factors. The terms with largest factors are ψ_{NiCrC}, ψ_{NiMoC} and ψ_{NiTiC}.

The difference in ψ_{TiC} for alloys 7261 and 7068 is not large enough ($\sim$3%) to justify calculating a nickel-titanium-carbon interaction. However, values for ψ_{NiCrC} and ψ_{NiMoC} have been calculated from the results because of the higher concentrations of Mo and Cr.

A ternary term, ψ_{NiMC} $(x_{Ni}^2 x_M)$, where M is either molybdenum or chromium, was added to Equation (10.6) and (10.7). Results for alloy pair 7262 and 7264 and pair 7263 and 7265 were used to solve for ψ_{MC} and ψ_{NiMC} simultaneously. The resulting values can be found in Table 10.7. The fact that binary and ternary terms are approximately the same magnitude agrees with the results of Section 10B where it was calculated that $\psi_{NiC} = -71.8$ kJ mol^{-1} and $\psi_{NiFeC} = 61.9$ kJ mol^{-1} at 1000°C. The absolute uncertainty in ψ_{MC} and ψ_{NiMC} is difficult to ascertain. The uncertainty in the sum of ψ_{MC} and ψ_{NiMC} however is approximately 2 kJ. The precision in the values of the binary and ternary interaction energies can be improved if more ternary alloys, such as Ni-Cr-C and Ni-Mo-C, are investigated. The larger the addition of the metal used the more precise

Table 10.7. Interaction Energies in $kJ \cdot mol^{-1}$ Calculated from the Kohler-Kaufman Equation[a] Including Ternary Terms.

Interaction Energy	$kJ\ mol^{-1}$
ψ^{FCC}_{TiC}	-248.5
ψ^{FCC}_{MoC}	-247.5
ψ^{FCC}_{CrC}	-290.8
ψ^{FCC}_{NiMoC}	268.0
ψ^{FCC}_{NiCrC}	241.3

[a]Equations (10.6), (10.7), (10.8), (10.9) and (10.10) or (2.30).

the values of the interaction energies will be.

Table 10.8 contains the values of the activity coefficient of carbon calculated using previously presented interaction energies including both binary and ternary terms from Tables 10.1, 10.4 and 10.6. Note that the experimental values for alloys 7267 and 7268 agree within 10% with the calculated values. When the ternary terms are not included the calculated results for 7267 and 7268 differ from the experimental by 20 to 30%. Furthermore, the binary equations predict that the addition of molybdenum always result in an increase in the activity coefficient of carbon, which is not observed.

E. Prediction of Carbon Solubilities

Another of the goals of this work was the prediction of carbon solubility in multicomponent solutions. The data of Kaufman and Nesor (1975, 1973) and Stover and Wulff (1959) (see Section 8B) have been used to calculate the activity of all the metallic solutes except carbon in the various alloys studied in this work. Table 10.9 contains the values of the activity of the solutes at 900, 1100 and 1215°C. The activities were calculated using a pure component reference state and a body centered cubic crystal structure, the normal structure for these solutes at the temperatures investigated. The activities in Table

Table 10.8. Comparison of the Value of the Activity Coefficient of Carbon Calculated Using the Kohler-Kaufman Equation and the Value Determined Experimentally.

Alloy[a]	Activity Coefficient ($\hat{\gamma}_C$)					
	Temperature (°C)					
	900		1100		1215	
	Calc	Expt[b]	Calc	Expt[b]	Calc	Expt[b]
7261 Ni + 2.4 Ti	130	128	59.2	61.0	40.3	41.1
7262 Ni + 2.5 Ti + 8.2 Mo	174	172	75.6	75.8	47.8	48.1
7263 Ni + 2.4 Ti + 8.0 Cr	116	127	52.9	53.3	35.3	35.8
7264 Ni + 2.4 Ti + 4.2 Mo	162	160	72.3	72.8	45.6	46.3
7265 Ni + 2.5 Ti + 4.6 Cr	130	130	59.8	59.5	38.7	38.9
7266 Ni + 2.4 Ti + 8.3 Cr + 8.1 Mo						
7267 Ni + 2.5 Ti + 4.4 Cr + 8.2 Mo			63.0	62.0	40.3	37.5
7268 Ni + 2.5 Ti + 4.1 Mo + 8.4 Cr			53.4	51.4	34.6	33.3
7068 Ni + 3.6 Ti	124	120	56.6	54.0	38.3	39.3

[a]Compositions are given in atom percent.

[b]Values were taken from Tables 8.2 and 9.1. Estimates of uncertainties are contained in Tables 8.2 and 9.1.

Table 10.9. Activities of the Alloying Elements Calculated Using the Kohler-Kaufman Equation (Eq. 2.30).

Temperature (°C) / Activity[a]	900			1100			1215		
	A_{Ti}	A_{Cr}	A_{Mo}	A_{Ti}	A_{Cr}	A_{Mo}	A_{Ti}	A_{Cr}	A_{Mo}
Alloy									
7261 Ni + 2.4 Ti	1.9×10^{-8}			2.4×10^{-7}			8.5×10^{-7}		
7262 Ni + 2.4 Ti + 8.2 Mo	7.4×10^{-8}		0.47	7.2×10^{-7}		0.44	2.3×10^{-6}		0.43
7263 Ni + 2.4 Ti + 8.0 Cr	1.0×10^{-7}	0.10		9.5×10^{-7}	0.11		3.0×10^{-6}	0.11	
7264 Ni + 2.4 Ti + 4.2 Mo	3.7×10^{-8}		0.25	4.1×10^{-7}		0.24	1.4×10^{-6}		0.23
7265 Ni + 2.5 Ti + 4.6 Cr	5.1×10^{-8}	0.054		5.2×10^{-7}	0.059		1.8×10^{-6}	0.061	
7266 Ni + 2.4 Ti + 3.3 Cr + 8.1 Mo	3.8×10^{-7}	0.13	0.55	2.8×10^{-6}	0.13	0.49	7.8×10^{-6}	0.12	0.46
7267 Ni + 2.5 Ti + 4.4 Cr + 8.2 Mo	1.8×10^{-7}	0.065	0.52	1.5×10^{-6}	0.067	0.47	4.5×10^{-6}	0.067	0.44
7268 Ni + 2.5 Ti + 8.4 Cr + 4.1 Mo	2.2×10^{-7}	0.12	0.30	1.8×10^{-6}	0.12	0.27	5.1×10^{-6}	0.12	0.25
A Ni + 2.6 Ti + 8.7 Mo	8.4×10^{-8}		0.48	8.1×10^{-7}		0.46	2.5×10^{-6}		0.44
B Ni + 2.1 Ti	1.5×10^{-8}			1.9×10^{-7}			6.8×10^{-7}		
C Ni + 2.4 Ti + 8.2 Cr	1.0×10^{-7}	0.11		1.0×10^{-6}	0.11		3.0×10^{-6}	0.11	
449 Ni + 2.5 Ti + 8.8 Cr + 7.2 Mo	3.9×10^{-7}	0.14	0.50	2.9×10^{-6}	0.14	0.45	8.0×10^{-6}	0.13	0.42
7068 Ni + 3.6 Ti	4.0×10^{-8}			4.7×10^{-7}			1.6×10^{-6}		

[a] Activities calculated using the pure component reference state at 1 atmosphere pressure. The parameters used in the calculations can be found in Tables 10.2 and 10.4.

10.9 have been used to calculate the solubility limit of carbon in the various alloys in equilibrium with pure titanium carbide according to

$$A_c = (A_{Ti} K_{f,TiC})^{-1}$$

where $K_{f,TiC}$ is the equilibrium constant for Ti (solv) + C (soln) = TiC (solid). Values of $K_{f,TiC}$ are listed in Table 8.4.

Table 10.10 contains values of the activity of carbon at the titanium carbide solubility limit obtained from the results presented in Chapters VIII and IX and the values calculated with the Kohler-Kaufman equation. In this work the highest carbon activities investigated were 0.76 at 1215°C, 0.72 at 1100°C, and 0.59 at 900°C. Titanium carbide did not form, at any activity, in alloys 7261, 7265, and 7068. The lack of a two phase region, in these alloys, at the experimental activities is in agreement with the calculated solubility limit, in Table 10.10. In alloy 7263, which contains no molybdenum, the precipitate can be assumed to have an activity of one, based on arguments presented in Chapter VII. Experimentally, it is found that precipitation of titanium carbide does not commence, in alloy 7263, until an activity 50% higher at 900 and 25% at 1100 and 1215°C than the calculated value. This discrepancy could be due to experimental error. The data obtained from

Table 10.10. Comparison of Calculated[a] and Experimental Value of the Carbon Activity Where Precipitation of Titanium Carbide Should Start.

Alloy	Temperature/°C 900 A_C (Calc)	900 A_c (Exp)	1100 A_C (Calc)	1100 A_C (Exp)	1215 A_C (Calc)	1215 A_C (Exp)
7261 Ni + 2.4 Ti	1.3		1.7		1.7	
7262 Ni + 2.4 Ti +8.2 Mo	0.33	0.17	0.56	0.18	0.63	0.18
7263 Ni + 2.4 Ti[b] + 8.0 Cr	0.25	0.50	0.43	0.54	0.48	0.63
7264 Ni + 2.4 Ti + 4.2 Mo	0.66	0.36	0.99	0.38	1.04	0.32
7265 Ni + 2.5 Ti + 4.6 Cr	0.48		0.75		0.81	
7266 Ni + 2.4 Ti + 8.3 Cr + 8.1 Mo	0.064		0.14	0.046	0.19	0.067
7267 Ni + 2.5 Ti + 4.4 Cr + 8.2 Mo	0.14		0.27	0.19	0.32	0.095
7268 Ni + 2.5 Ti + 8.4 Cr + 4.1 Mo	0.11		0.23	0.11	0.28	0.13
7068 Ni + 3.6 Ti	0.61		0.86		0.91	

[a] Activities calculated using results in Table 10.9

[b] Experimental values are approximate. They were obtained by interpolating between the solid solution data and one point in the two phase region.

Stover and Wulff (1959), although the best available, could be in error by 25% in the solubility product for titanium carbide. They relied on Curie point measurements, whose precision was not stated, to determine the phase boundary. Another possibility is that the model was not adequate. The assumption that titanium and nickel form a temperature dependent regular solution in the nickel-rich corner of the phase diagram may be incorrect. Unfortunately, the true nature of $\overline{G}^{E}_{Ti}$ as a function of x_{Ti} in nickel will have to await further data. Stover and Wulff's (1959) data do not cover a broad enough range of composition to yield more than one point on the $\overline{G}^{E}_{Ti}$ curve.

TiC formed at all three temperatures in alloys 7262, 7264, 7266, 7267 and 7268. The solubility in these alloys determined experimentally is 1/3 to 1/2 the calculated solubility (Table 10.10). If the arguments in the preceding paragraph are correct the agreement between predicted and experimental solubilities are even worse. If one assumes that the molybdenum carbide forms an ideal solid solution with titanium carbide, the activity of the titanium, based on the compositions discussed in Chapter IX, would be 0.7 in alloy 7264 and 7268 and 0.58 in alloys 7262, 7266 and 7267. While lowering the activity of the carbide is a move in the right direction, the change is not sufficient to bring the calculated and observed values together. The most plausible explanation for the remaining discrepancy is that,

rather than forming an ideal solution, the carbides mix with a negative heat of mixing. If a value of approximately -6.7 ± 2 kJ·mol^{-1} is assumed for the heat of mixing and if the entropy of mixing is assumed to be ideal, the calculated and experimental values of the solubility agree to ±15 percent. A slightly more negative value for the heats of mixing is needed if the calculated values of A_C are shown to be too low. Clearly, more precise thermodynamic data are required for the nickel-titanium system in order to resolve the discrepancies.

CHAPTER XI

THERMOMIGRATION

A. Introduction

Until recently, thermomigration, the mass flux induced by a temperature gradient, was studied exclusively in liquids and gases. Experimental difficulties associated with establishing and maintaining a large, well-defined temperature gradient in a solid dissuaded researchers from investigating thermomigration in solids. Modern work in the field started with Shewmon (1958) and Darken and Oriani (1954) who investigated several metal-metal and metal-metalloid systems. Oriani (1969) reviewed the 1960's experiments on metal-metalloid binary systems, which yielded little quantitative data. Poor temperature control and poor chemical analyses plagued most investigators.

Thermomigration in solids is an important phenomenon in, for example, nuclear reactors and in welding. In nuclear reactors, large temperature gradients are the norm rather than the exception. Thermomigration of hydrogen in the Zircalloy fuel cladding and in the oxide fuel are of great technical importance. In welding the tremendous temperature gradients at the liquid-solid interface cause a mass flux which may be responsible for cracks that form in many

welds after cooling.

Thermomigration experiments have as their immediate goal the measurement of the "thermal diffusion factor", α_1. For a binary system with a linear temperature gradient in the Z direction, α_1 can be determined from [Horne and Anderson (1970)]

$$w_1 = \alpha_1 w_1^o w_2^o [1 + \frac{d}{4Z} \exp(-t/\theta)] \sin(\frac{2Z}{d}) \qquad (11.1)$$

w_1 = weight fraction of component i

w_i^o = initial weight fraction of component i

Z = coordinate in the direction of the temperature gradient. At the center of the specimen Z = 0.

t = time

d = the diffusion pathlength

$\theta = d^2/\pi^2 D$ relaxation time

D = binary diffusion coefficient

Equation (11.1) indicates that the composition of the specimen as a function of position will continue to change until $t \approx 4\theta$, after which time a steady state will persist as long as the temperature gradient is maintained. Measurements made after $t = 4\theta$ will not provide any information on D but do provide data for calculation of α_1. To date the few thermomigration experiments in solids have all been done at the steady state ($t > 4\theta$). In this work the

measurements were to be time dependent so that α_1 and D could be determined in the same experiment.

B. Experiments

Specimens were annealed in a temperature gradient of approximately 1000°C/cm in a Gleeble. A Gleeble is an instrument designed to simulate the large temperature fluctuations produced in metal alloys during welding. A cylindrical sample is clamped at both ends in water cooled copper jaws, and a large alternating current is then passed through the sample. The sample is brought from 20 to 1300° C in less than 10 sec. The temperature of the sample is controlled via a feedback loop containing a thermocouple attached to the center of the sample. Solution of the heat conduction equation for this experimental arrangement as well as actual experimental measurements show that the temperature distribution in the sample is parabolic with a maximum in the center. For sample B-6-B the temperature was found to obey

$$T_c^\circ = -2371d^2 + 82.06d + 1350,$$

with the root mean square residual σ = 10°C. The temperature of the sample was measured at three sites on the specimen with platinum-platinum 10% rhodium thermocouples

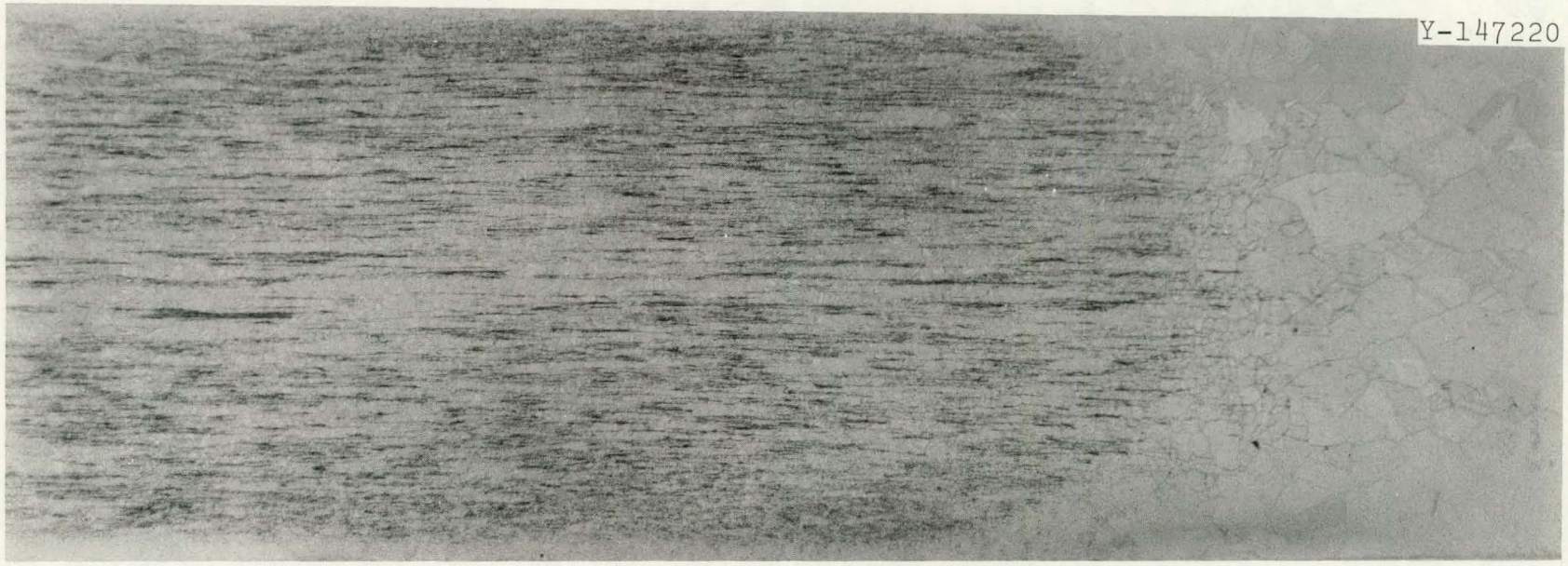

Figure 11.1. Sample B-6-B at 25x annealed two hours in the Gleeble. The right hand side of photo is the hot end approximately 1300°C. Note decarburization in hot zone.

and recorded as voltage on a three pen pentiometric strip-chart recorder. The end temperatures were also known. The atmosphere around the samples was supposed to be controlled by flowing pure argon at approximately 100 liters per hour through a pyrex cover box surrounding the sample.

C. Results

Several specimens were annealed in the Gleeble for times varying from five minutes to two hours. The results were of two kinds: either a gradient of carbon concentration was not observed or the sample was partially decarburized. Figure 11-1 shows half of a sample annealed two hours in the Gleeble and then annealed 100 hours at 760°C to precipitate the carbon from solution. The carbon distribution in the sample approaches the shape of an hour glass. This distribution would be expected in a sample with a sink at the surface and a maximum in temperature at the center. From these results it is apparent that better control over the atmosphere surrounding the sample is necessary if quantitative results are to be obtained. Cost, time consideration, and the requirements of other users mitigated against modification of the Gleeble for further study of thermomigration.

There is still a need for thermomigration experiments in interstitial metal alloys, and a suitably modified

Gleeble would offer many advantages, such as rapid heat-up and cool-down. The modification most needed is a high quality vacuum system in order to control the chemical environment surrounding the specimen.

CHAPTER XII

SUGGESTIONS FOR FURTHER WORK

A. Analytical Chemistry

While a great deal of effort has been expended in improving techniques for analysis, further improvements are still desirable. The carbon analyses are in need of accurate standards; as discussed in Chapter III, the standards currently available have an accuracy of about ±5%. The carbon analyses could also be improved if a more selective detector were used. Our apparatus used a conductometric detector. Newer instruments use infra-red detectors, which are not as sensitive to impurities such as SO_2 and do not require CO_2 traps and chromatographic columns.

In the area of metal analysis more study is needed on "matrix" effects in the acidic solutions. These effects require the use of standards of similar composition to the samples. In some cases this is not convenient or possible. For analysis of small quantities of solid material the development of x-ray fluorescence capability would be desirable. The electron microprobe technique, while useful, is limited in that only relative concentrations are readily obtainable.

B. Experiments

Six different series of alloys need to be studied in order to understand better the ternary interactions that this research has revealed. The six systems are Ni-Mo-C, Fe-Mo-C, Ni-Cr-C, Ni-Mo-Cr-C and Fe-Mo-Cr-C. Experiments should be carried out with as high a concentration of Mo and/or Cr as possible without leaving the face-centered cubic solid solution phase field. The goal of these experiments would be to determine quantitatively the values of the ternary interaction energies. The question of whether there is any solvent dependence in the binary interaction energy could also be resolved by these experiments. If the binary interaction energies determined in nickel and iron solutions do not agree once ternary terms are taken into account, still higher order terms will have to be introduced into Kohler-Kaufman formalism.

In solutions with low carbon solubility the carburization technique needs to be refined to facilitate experiments at carbon activities of less than 0.05. This would involve using gas mixtures of lower CH_4/H_2^2 ratios and possibly lowering P_{O_2} in the furnace. The result would be a better understanding of the titanium-molybdenum-carbon precipitation process and the molybdenum-chromium-carbon solid solution interaction.

More controlled experiments are necessary on the

precipitation of carbon upon quenching. Resistance heating and a helium quench offer the most convenient methods of controlling the quench rate. Annealing samples at temperatures of around 500°C for short periods of times and observing changes in the weight percent of the precipitate and in the x-ray diffraction patterns would provide insight into the precipitation process. It is also hoped that short anneals at low temperatures would allow the precipitates to grow large enough to be viewed in the electron microscope.

APPENDIX A

The compositions of the uncarburized alloys are given in Table A-1. Tables A-2 through A-33 contain all of the gas phase carburization data generated in this investigation. The data in each table constitute one data set. That is, all of the specimens in the set were carburized at the same time in the same furnace run. Thus, the temperature and the equilibrating gas are identical for all the specimens described in a given table. For these two reasons all are listed together.

Unfortunately, the analytical standards used for carbon analysis of the specimens, even in a specific table, are not all the same. This arose because the supply of National Bureau of Standards Standard Reference Material (NBS SRM) 19E was exhausted. Thus, when rechecking specimens in some tables, a different NBS SRM was used. (In some tables, of course, only one NBS SRM was used.) As discussed in Chapter III, it is important when using the carbon data to relate all of the concentrations to the same NBS SRM. In all of the calculations in this work the carbon concentrations are relative to NBS SRM 19E. Extensive comparison of SRM 19E and 121B (the only other standard used in the carbon analyses) showed that a concentration relative to 121B must be multiplied by 0.966 to obtain the concentration relative to 19E. Analytical carbon data were rechecked frequently, as is

partially apparent from examination of the variation of NBS SRM's in the tables. Shortly after the gas phase carburization studies began it was apparent that problems existed in our ability to analyze for carbon. Comparison of weight change and the carbon analysis did not always agree. Inconsistencies between data sets and the size of the aliquot used in the analysis affected the results. Once it was realized that analytical difficulties existed, the stringent controls on the combustion procedure detailed in Chapter IV were developed. Unfortunately, before all of the analytical problems were solved, the supplies of four sets of specimens, A-7603-118, A-7603-121, A-7783-20, and A-7783-21, had been exhausted. When these specimens were analyzed the instrument was giving consistently low values for the carbon concentration when small aliquots were used. In the four sets of specimens mentioned above all of the one phase specimens, except the iron standards, contained less than 0.05 wt. % carbon. Analysis of data from these specimens showed that they had uniformly low activity coefficients relative to samples analyzed after the instrument problems had been corrected. In the final analysis of the data, therefore, the activity coefficient of the nickel alloys in the aforementioned data sets was obtained from the activity coefficient of carbon in nickel determined in the data sets listed in Table 5.1. The carbon analyses of specimens Ni-A7783-16 and 7068-A7603-106 were disregarded

in the analysis of the results. In both specimens the calculated activity coefficients were more than 3 standard deviations from the mean value and were not consistent with the other data sets with respect to equilibrium concentrations of carbon. That is, in data set A-7783-16 the nickel specimen analyzed to be lower in carbon than Ni + 4 at. % Mo (7264) and in A-7603-106 alloy 7068 analyzed to be lower in carbon than nickel. These are contrary to the results of all the other data sets. Data set A-7783-36 has not been considered in the analysis of the data. Repeated analyses of the specimen from this set gave non-reproducible results even when the carbon analyzer appeared to be functioning properly.

The abbreviation T.P. in the tables indicates that the specimen was assumed to be two phase, although the material was not extracted. The specimens were judged two phase on the basis of their activity coefficients. A decrease in the carbon activity coefficient at high carbon activity indicates that precipitation has occurred.

Table A.1. Composition[a] of Alloys Used for Calculations.

Alloy Melt No.	Element/wt %				
	Ti	Cr	Mo	C	Ni
7261	2.0			0.015	98.0
7262	1.95		12.81	0.014	85.3
7263	2.02	7.78		0.014	90.2
7264	1.95		6.68	0.015	91.4
7265	2.06	4.09		0.016	93.8
7266	1.91	7.08	12.76	0.021	78.2
7267	1.95	3.77	12.93	0.016	81.4
7268	2.00	7.33	6.66	0.015	84.0
7071	2.8	8.08		0.135	89.0
7095	3.06		13.9	0.380	82.7
A	2.0		13.0	0.094	84.9
B	1.73			0.086	98.2
C	2.0	7.40		0.109	90.5
719	1.95	7.36	11.4	0.035	79.0

[a]These values were picked from those in Table 5.1.

Table A.2. Data From Carburization Experiment A-7603-97.

Date: 4/28/76; Temperature: 1215°C; Duration: 40 hours
$H_2O(g)$ Concentration: 1.5 ppm; Quench: Water.

Alloy	Weight Change (%)	Final [C] (wt %) by Analysis	Cal. Std. For Carbon	Precip. (wt. %)	Microprobe Intensity Ratio $(\frac{Mo}{Ti})$	Lattice Parameter a_o/nm
7261	0.124	0.135	19E	0.24		
7262	0.325	0.321	121B	1.57	1.50±0.03	0.4315[a]
7263	0.132	0.160	121B	0.25		
7266	0.832	0.852	19E	6.05	3.00 0.08	
Ni	0.128	0.131	19E	0.22		

[a] σ_{a_o} =0.0001 nm.

Table A.3. Data From Carburization Experiment A-7603-105

Date: 5/4/76; Temperature: 1215°C; Duration: 36 hours;
$H_2O(g)$ Concentration: 1 ppm; Quench: Cold Zone.

Alloy	Weight Change (%)	Final [C] (wt %) by Analysis	Cal. Std. For Carbon	Precip. (wt. %)	Microprobe Intensity Ratio $(\frac{Mo}{Ti})$	Lattice Parameter a_o/nm
7264	0.125	0.138	19E	0.147		
7265	0.147	0.162	19E			
7267	0.687	0.708	121B	TP		
7268	0.487	0.523	121B	TP		
Ni-270	0.146	0.150	121B			

Table A.4. Data From Carburization Experiment A-7603-106.

Date: 5/6/76; Temperature: 1215°C; Duration: 36 hours; $H_2O(g)$ Concentration: 1 ppm; Quench: Cold Zone.

Alloy	Weight Change (%)	Final [C] (wt %) by Analysis	Cal. Std. For Carbon	Precip. (wt. %)	Microprobe Intensity Ratio $(\frac{Mo}{Ti})$	Lattice Parameter a_o/nm
7068	0.0663	0.140	19E			
7071	0.0802	0.217	19E			
7095	0.477	0.870	19E	6.19	1.75±0.02	
Ni-270	0.140	0.150	19E	0.24		
Ni-270	0.110	0.147	19E			
Fe'E'	0.941	0.981	19E			

Table A.5. Data From Carburization Experiment A-7603-118.

Date: 5/17/76; Temperature: 1215°C; Duration: 22 hours; $H_2O(g)$ Concentration: 1 ppm; Quench: Cold Zone.

Alloy	Weight Change (%)	Final [C] (wt %) by Analysis	Cal. Std. For Carbon	Precip. (wt. %)	Microprobe Intensity Ratio $(\frac{Mo}{Ti})$	Lattice Parameter a_o/nm
7261	0.020	0.0337	19E			
7262	0.053	0.0274	19E			
7263	0.038	0.0410	19E			
7264	0.086	0.0285	19E			
7265	0.040	0.0359	19E			
7266	0.059	0.0557	19E	TP		
7267	0.047	0.0358	19E			
7268	0.103	0.0414	19E			
7068	0.188	0.0355	19E			
Ni-270	0.023	0.0330	19E			
Fe'E'[a]		0.261	121B			
		0.256	19E			

[a] initial wt not recorded.

Table A.6. Data From Carburization Experiment A-7603-121.

Date: 5/18/76; Temperature: 1215°C; Duration: 46 hours; $H_2O(g)$ Concentration: 1 ppm; Quench: Cold Zone.

Alloy	Weight Change (%)	Final [C] (wt %) by Analysis	Cal. Std. For Carbon	Precip. (wt. %)	Microprobe Intensity Ratio $(\frac{Mo}{Ti})$	Lattice Parameter a_o/nm
7261	0.035	0.0442	19E			
7262	0.020	0.0337	19E			
7263	0.019	0.0482	19E			
7264	0.013	0.0364	19E			
7265	0.018	0.0447	19E			
7266	0.124	0.142	19E	0.639		0.4311[a]
7267	0.044	0.0461	19E			
7268	0.019	0.0535	19E			
7068	-0.044	0.0444	19E			
7095	-0.301	0.0795	19E			
7071	-0.067	0.0568	19E			
Ni-270	0.041	0.0433	19E			
Fe'E'	0.291	0.325	19E			
		0.330	121B			

[a] σ_{a_o} =0.0001 nm.

Table A.7. Data From Carburization Experiment A-7603-123.

Date: 5/20/76; Temperature: 215°C; Duration: 64 hours; $H_2O(g)$ Concentration: 1 ppm; Quench: Cold Zone

Alloy	Weight Change (%)	Final [C] (wt %) by Analysis	Cal. Std. For Carbon	Precip. (wt. %)	Microprobe Intensity Ratio ($\frac{Mo}{Ti}$)	Lattice Parameter a_o/nm
7261	0.367	0.398	121B			
7263	1.91	0.535	121B	0.963		
7264	0.683	0.675	121B	2.55	1.15±0.03	.4326[a]
7265	0.441	0.447	121B			
7268	1.058	1.085	19E	TP		
7068	0.377	0.449	121B			
7071	0.657	0.832	121B			
Ni-270	0.355	0.37	19E			

[a] σ_{a_o} =0.0001 nm.

Table A.8. Data From Carburization Experiment A-7783-4.

Date: 6/16/76; Temperature: 1100°C; Duration: 48 hours; $H_2O(g)$ Concentration: 1 ppm; Quench: Cold Zone.

Alloy	Weight Change (%)	Final [C] (wt %) by Analysis	Cal. Std. For Carbon	Precip. (wt %)	Microprobe Intensity Ratio ($\frac{Mo}{Ti}$)	Lattice Parameter a_o/nm
7261	0.024	0.0407	19E			
7262	0.027	0.0323	121B			
7263	0.043	0.0450	121B			
7266	0.185	0.190	121B	1.36	1.24±0.02	.4311[a]
Ni-270	0.029	0.0376	121B			
F'E'	0.324	0.355	121B			

[a] σ_{a_o} =0.0001 nm.

Table A.9. Data From Carburization Experiment A-7783-14

Date: 7/1/76; Temperature: 1100°C; Duration: 48 hours; $H_2O(g)$ Concentration: 2.5 ppm; Quench: Cold Zone.

Alloy	Weight Change (%)	Final [C] (wt %) Analysis	Cal. Std. For Carbon	Precip. (wt. %)	Microprobe Intensity Ratio $(\frac{Mo}{Ti})$	Lattice Parameter a_o/nm
7264	0.017	0.0363	19E			
7265	0.019	0.0452	19E			
7267	0.071	0.0852	19E	0.385	1.17±001	
7268	0.048	0.0577	121B	TP		
Ni-270	0.032	0.0381	19E			
Fe'E'	0.350	0.401	121B			

Table A.10. Data From Carburization Experiment A-7783-15.

Date: 7/3/76; Temperature: 1100°C; Duration: 72 hours; $H_2O(g)$ Concentration: 1 ppm; Quench: Cold Zone.

Alloy	Weight Change (%)	Final [C] (wt %) by Analysis	Cal. Std. For Carbon	Precip. (wt. %)	Microprobe Intensity Ratio $(\frac{Mo}{Ti})$	Lattice Parameter a_o/nm
7262	0.330	0.346	121B	2.14	1.29±0.02	
7266	0.758	0.835	121B	6.53	2.44±0.06	
7267	0.561	0.610	121B	3.99	1.44±0.01	
7268	0.424	0.467	121B	2.39	0.82±0.02	
Ni-270	0.090	0.0951	121B			
Fe'E'	0.733	0.796	121B			

Table A.11. Data From Carburization Experiment A-7783-16

Date: 7/6/76; Temperature: 1100°C; Duration: 48 hours; $H_2O(g)$ Concentration: 1 ppm; Quench: Cold Zone.

Alloy	Weight Change (%)	Final [C] (wt %) by Analysis	Cal. Std. For Carbon	Precip. (wt. %)	Microprobe Intensity Ratio $(\frac{Mo}{Ti})$	Lattice Parameter a_o/nm
7261	0.081	0.0959	121B			
7263	0.118	0.116	121B			
7264	0.065	0.082	121B	TP		
7265	0.090	0.106	121B			
Ni-270	0.077	0.0793	121B			
Fe'E	0.784	0.811	121B			

Table A.12. Date From Carburization Experiment A-7783-17

Date: 7/8/76; Temperature: 1100°C; Duration: 46 hours; $H_2O(g)$ Concentration: 1 ppm; Quench: Cold Zone.

Alloy	Weight Change (%)	Final [C] (wt %) by Analysis	Cal. Std. For Carbon	Precip. (wt. %)	Microprobe Intensity Ratio $(\frac{Mo}{Ti})$	Lattice Parameter a_o/nm
7261	0.210	0.244	121B			
7263	0.345	0.383	121B	0.99		0.4324[a]
7264	0.456	0.506	121B	2.14	0.91±0.03	0.4321[a]
7265	0.228	0.252	121B			
Ni-270	0.208	0.225	121B			
Fe'E'	1.424	1.49	19E			

[a] σ_{a_o} =0.00001 nm.

Table A.13. Data From Carburization Experiment A-7783-18.

Date: 7/10/76; Temperature: 1100°C; Duration: 48 hours; $H_2O(g)$ Concentration: 1 ppm; Quench: Cold Zone.

Alloy	Weight Change (%)	Final [C] (wt %) by Analysis	Cal. Std. For Carbon	Precip. (wt. %)	Microprobe Intensity Ratio $(\frac{Mo}{Ti})$	Lattice Parameter a_o/nm
7261	0.164	0.202	121B			
7263	0.227	0.235	19E			
7264	0.184	0.325	19E	TP		
7265	0.314	0.196	19E			
7068	0.147	0.222	121B			
Ni-270	0.161	0.179	19E			
Fe"E'	1.20	1.28	121B			

Table A.14. Data from Carburization Experiment A-7783-19.

Date: 7/13/76; Temperature: 1100°C; Duration: 48 hours; $H_2O(g)$ Concentration: 2 ppm; Quench: Cold Zone.

Alloy	Weight Change (%)	Final [C] (wt %) by Analysis	Cal. Std. For Carbon	Precip. (wt. %)	Microprobe Intensity Ratio $(\frac{Mo}{Ti})$	Lattice Parameter a_o/nm
7262	0.160	0.174	121B	0.945	1.27±0.02	0.4318[a]
7266	0.556	0.624	121B	3.84	1.48±0.04	
7267	0.431	0.460	19E	2.95	1.33±0.02	0.4314[a]
7268	0.283	0.310	121B	1.52	0.85±0.03	0.4319[a]
7068	0.00	0.0873	121B			
Ni-270	0.067	0.0726	19E			
Fe'E'	0.577	0.616	121B			

[a] σ_{a_o} =0.0001 nm.

Table A.15. Data From Carburization Experiment A-7783-20.

Date: 7/16/76; Temperature: 1100°C; Duration: 60 hours; $H_2O(g)$ Concentration: 2 ppm; Quench: Cold Zone.

Alloy	Weight Change (%)	Final [C] (wt %) by Analysis	Cal. Std. For Carbon	Precip. (wt. %)	Microprobe Intensity Ratio $(\frac{Mo}{Ti})$	Lattice Parameter a_o/nm
7262	0.014	0.0182	121B			
7266	0.064	0.0633	19E			
7267	0.033	0.0228	19E			
7268	0.033	0.0285	19E			
7068	-0.063	0.0253	19E			
Ni-270	0.0128	0.0222	19E			
Fe'E'	0.179	0.205	121B			

Table A.16. Data From Carburization Experiment A-7783-21

Date: 7/16/76; Temperature: 1100°C; Duration: 60 hours; $H_2O(g)$ Concentration: 2.5 ppm; Quench: Cold Zone.

Alloy	Weight Change (%)	Final [C] (wt %) by Analysis	Cal. Std. For Carbon	Precip. (wt. %)	Microprobe Intensity Ratio $(\frac{Mo}{Ti})$	Lattice Parameter a_o/nm
7262	0.00	0.0106	19E			
7266	0.02	0.0192	19E			
7267	0.01	0.0133	19E			
7268	0.00	0.0164	19E			
Ni-270	0.00	0.0140	19E			
Fe'E'	0.084	0.111	19E			

Table A.17. Data From Carburization Experiment A-7783-32.

Date: 7/22/76; Temperature: 1100°C; Duration: 85 hours
$H_2O(g)$ Concentration: 1 ppm; Quench: Cold Zone.

Alloy	Weight Change (%)	Final [C] (wt %) by Analysis	Cal. Std. For Carbon	Precip. (wt. %)	Microprobe Intensity Ratio ($\frac{Mo}{Ti}$)	Lattice Parameter a_o/nm
Ni-270[a]	-0.177	0.169	19E			
Ni-270	0.154	0.174	121B			
Fe'E'[a]	-0.271	1.206	19E			
Fe'E	1.157	1.191	19E			
7068	0.116	0.204	121B			

[a]Equilibrium approached by decarburization.

Table A.18. Data from Carburization Experiment A-7783-33.

Date: 7/24/76; Temperature: 1100°C; Duration: 60 hours;
$H_2O(g)$ Concentration: 1 ppm; Quench: Cold Zone.

Alloy	Weight Change (%)	Final [C] (wt %) by Analysis	Cal. Std. For Carbon	Precip. (wt. %)	Microprobe Intensity Ratio ($\frac{Mo}{Ti}$)	Lattice Parameter a_o/nm
Ni-270	0.138	0.157	121B			
Fe'E'	1.076	1.114	19E			

Table A.19. Data From Carburization Experiment A-7783-35.

Date: 7/29/76; Temperature: 1100°C; Duration: 90 hours; $H_2O(g)$ Concentration: 1 ppm; Quench: Cold Zone.

Alloy	Weight Change (%)	Final [C] (wt %) by Analysis	Cal. Std. For Carbon	Precip. (wt. %)	Microprobe Intensity Ratio ($\frac{Mo}{Ti}$)	Lattice Parameter a_o/nm
7068	0.102	0.174	121B			
7264	0.170	0.177	19E	0.475	0.84±0.04	0.4324[a]
Ni-270	0.125	0.136	19E			
Fe'E'	1.008	1.032	19E			

[a] σ_{a_o} =0.0001 nm.

Table A.20. Data From Carburization Experiment A-7783-36.

Date: 8/2/76; Temperature: 1215°C; Duration: 96 hours; $H_2O(g)$ Concentration: 1 ppm; Quench: Cold Zone.

Alloy	Weight Change (%)	Final [C] (wt %) by Analysis	Cal. Std. For Carbon	Precip. (wt. %)	Microprobe Intensity Ratio ($\frac{Mo}{Ti}$)	Lattice Parameter a_o/nm
7261	0.152	0.183	121B			
7263	0.191	0.250	121B			
7264	0.146	0.181	121B	TP		
7265	0.172	0.212	121B			
7068	0.116	0.217	121B			
Ni-270	0.150	0.174	121B			
Fe'E'	1.01	1.18	121B			

Table A.21. Data From Carburization Experiment A-7783-37.

Date: 9/8/76; Temperature: 1215°C; Duration: 108 hours; $H_2O(g)$ Concentration: 1 ppm; Quench: Cold Zone.

Alloy	Weight Change (%)	Final [C] (wt %) by Analysis	Cal. Std. For Carbon	Precip. (wt. %)	Microprobe Intensity Ratio ($\frac{Mo}{Ti}$)	Lattice Parameter a_o/nm
7262	0.415	0.462	121B	2.17	1.55±0.04	0.4313[a]
7266	0.865	0.985	121B	7.20	3.19±0.04	0.4299[a]
7267	0.670	0.677	19E	4.42	1.90±0.05	0.4303[a]
7268	0.448	0.512	121B	2.11	0.92±0.03	0.4316[a]
Ni-270	0.107	0.157	121B			
Fe'E'	0.961	1.03	121B			

[a] σ_{a_o} =0.0001 nm.

Table A.22. Data From Carburization Experiment A-7783-38.

Date: 9/14/76; Temperature: 1215°C; Duration: 60 hours; $H_2O(g)$ Concentration: 1 ppm; Quench: Cold Zone.

Alloy	Weight Change (%)	Final [C] (wt %) by Analysis	Cal. Std. For Carbon	Precip. (wt. %)	Microprobe Intensity Ratio ($\frac{Mo}{Ti}$)	Lattice Parameter a_o/nm
7262	0.088	0.0971	121B		TP	
7266	0.526	0.626	121B	3.62	1.91±0.06	0.4300[a]
7267	0.323	0.384	121B	1.05	1.50±0.02	0.4310[a]
7268	0.146	0.202	121B	0.394	0.75±0.02	0.431[b]
Ni-270	0.084	0.0932	121B			
Fe'E'	0.624	0.750	121B			

[a] σ_{a_o} =0.0003 nm.

[b] σ_{a_o} =0.0001 nm.

Table A.23. Data From Carburization Experiment A-7783-44.

Date: 10/9/76; Temperature: 900°C; Duration: 108 hours; $H_2O(g)$ Concentration: 1 ppm; Quench: Cold Zone.

Alloy	Weight Change (%)	Final [C] (wt %) by Analysis	Cal. Std. For Carbon	Precip. (wt. %)	Microprobe Intensity Ratio $(\frac{Mo}{Ti})$	Lattice Parameter a_o/nm
7261	0.075	0.100	121B			
7263	0.195	0.218	121B	0.885		0.4320[a]
7264	0.206	0.235	121B	1.342	0.90 0.02	0.4326[a]
7265	0.086	0.0987	121B			
7068	0.031	0.107	121B			
Ni-270	0.074	0.0953	121B			
Fe'E'	0.781	0.832	121B			

[a] σ_{a_o} =0.00001 nm.

Table A.24. Data From Carburization Experiment A-7783-45

Date: 10/16/76; Temperature: 900°C; Duration: 132 hours; $H_2O(g)$ Concentration: 0.5 ppm; Quench: Cold Zone

Alloy	Weight Change (%)	Final [C] (wt %) by Analysis	Cal. Std. For Carbon	Precip. (wt. %)	Microprobe Intensity Ratio $(\frac{Mo}{Ti})$	Lattice Parameter a_o/nm
7261	0.035	0.0603	121B			
7263	0.038	0.0634	121B			
7264	0.011	0.0580	121B			
7265	0.037	0.0624	121B			
7068[a]	-0.031	0.0620	121B			
Ni-270	0.049	0.0544	121B			
Ni-270[a]	-0.058	0.0538	121B			
Fe'E'	0.501	0.544	121B			

[a] Equilibrium approached by decarburization.

Table A.25. Data From Carburization Experiment A-7783-47.

Date: 10/23/76; Temperature: 900°C; Duration: 120 hours; $H_2O(g)$ Concentration: 0.5 ppm; Quench: Cold Zone.

Alloy	Weight Change (%)	Final [C] (wt %) by Analysis	Cal. Std. For Carbon	Precip. (wt. %)	Microprobe Intensity Ratio $(\frac{Mo}{Ti})$	Lattice Parameter a_o/nm
7261	0.024	0.0457	121B			
7263	0.032	0.0445	121B			
7264	0.026	0.0360	121B			
7265	0.019	0.0436	121B			
7068	-0.036	0.0505	121B			
Ni-270	0.033	0.0425	121B			
Fe'E'	0.407	0.444	121B			

Table A.26. Data From Carburization Experiment A-7783-48.

Date: 10/28/76; Temperature: 900°C; Duration: 120 hours; $H_2O(g)$ Concentration: 0.5 ppm; Quench: Cold Zone.

Alloy	Weight Change (%)	Final [C] (wt %) by Analysis	Cal. Std. For Carbon	Precip. (wt. %)	Microprobe Intensity Ratio $(\frac{Mo}{Ti})$	Lattice Parameter a_o/nm
7262	0.083	0.102	121B			
7266	0.083	0.081	121B	1.22	1.64±0.02	
7267	0.202	0.243	121B	0.582	1.25±0.02	0.4318[a]
7268	0.176	0.191	121B	1.56	0.94±0.02	0.4320[a]
Ni-270	0.027	0.0423	121B			
Fe'E'	0.380	0.411	121B			

[a] σ_{a_o} =0.0001 nm.

Table A.27. Data From Carburization Experiment A-7783-49.

Date: 11/3/76; Temperature: 900°C; Duration: 120 hours; $H_2O(g)$ Concentration: 0.5 ppm; Quench: Cold Zone.

Alloy	Weight Change (%)	Final [C] (wt %) by Analysis	Cal. Std. For Carbon	Precip. (wt. %)	Microprobe Intensity Ratio $(\frac{Mo}{Ti})$	Lattice Parameter a_o/nm
7262	0.007	0.0125	121B			
7266	0.007	0.0218	121B			
7267	0.040	0.0458	121B	0.411	1.21±0.003	0.4313[a]
7268	0.021	0.0349	121B	0.042		
Ni-270	0.0141	0.0166	121B			
Fe'E'	0.168	0.191	121B			

[a] σ_{a_o} =0.0001 nm.

Table A.28. Data From Carburization Experiment A-7783-57.

Date: 11/9/76; Temperature: 900°C; Duration: 144 hours; $H_2O(g)$ Concentration: 0.5 ppm; Quench: Cold Zone.

Alloy	Weight Change (%)	Final [C] (wt %) by Analysis	Cal. Std. For Carbon	Precip. (wt. %)	Microprobe Intensity Ratio $(\frac{Mo}{Ti})$	Lattice Parameter a_o/nm
7262	0.0226	0.0326	121B			
7266	0.0186	0.0362	121B			
7267	0.0598	0.0465	121B			
7268	0.0973	0.112	121B			
Ni-270	0.0189	0.0299	121B			
Fe'E'	0.287	0.312	121B			

Table A.29. Data From Carburization Experiment A-7783-116.

Date: 1/22/77; Temperature: 1215°C; Duration: 48 hours; $H_2O(g)$ Concentration: 0.5 ppm; Quench: Cold Zone

Alloy	Weight Change (%)	Final [C] (wt %) by Analysis	Cal. Std. For Carbon	Precip. (wt. %)	Microprobe Intensity Ratio $(\frac{Mo}{Ti})$	Lattice Parameter a_o/nm
7261	0.064	0.0747	121B			
7262	0.079	0.0628	121B			
7263	0.065	0.0862	121B			
7264	0.062	0.0640	121B			
7265	0.057	0.0810	121B			
7266	0.413	0.475	121B			
7267	0.198	0.221	121B	TP		
7268	0.072	0.109	121B	TP		
7068	0.002	0.0783	121B			
Ni-270	0.068	0.0704	121B			
Fe'E'	0.489	0.554	121B			

Table A.30. Data From Carburization Experiment A-7783-120.

Date: 1/25/77; Temperature: 1215°C; Duration: 60 hours; $H_2O(g)$ Concentration; Quench: Cold Zone.

Alloy	Weight Change (%)	Final [C] (wt %) by Analysis	Cal. Std. For Carbon	Precip. (wt. %)	Microprobe Intensity Ratio $(\frac{Mo}{Ti})$	Lattice Parameter a_o/nm
7261	0.132	0.147	121B			
7262	0.352	0.361	121B	TP		
7263	0.142	0.173	121B			
7264	0.127	0.124	121B			
7265	0.146	0.153	121B			
7266	0.781	0.867	121B			
7267	0.598	0.652	121B	TP		
7268	0.423	0.451	121B	TP		
7068	0.084	0.152	121B			
Ni-270	0.150	0.144	121B			
Fe'E'	0.911	1.01	121B			

Table A.31. Data From Carburization Experiment A-7783-123[a]

Date: 2/8/77; Temperature: 1215°C; Duration: 72 hours; $H_2O(g)$ Concentration: 0.5 ppm; Quench: Cold Zone.

Alloy	Weight Change (%)	Initial [C] (wt %)	Final [C] (wt %) by Analysis	Cal. Std. For Carbon	Precip. (wt. %)
7261	+0.020	0.147	0.137	121B	
7262	+0.001	0.361	0.346	121B	TP
7263	-0.027	0.173	0.163	121B	
7264	+0.003	0.124	0.125	121B	
7265	-0.085	0.153	0.143	121B	
7266	-0.034	0.867	0.859	121B	TP
7267	-0.017	0.652	0.634	121B	TP
7268	-0.055	0.451	0.423	121B	TP
7068	-0.005	0.152	0.143	121B	
Ni-270	+0.008	0.144	0.131	121B	
Fe'E'	-0.106	1.01	0.959	121B	

[a]Equilibrium approached by decarburization.

Table A.32. Data From Carburization Experiment A-7783-125.[a]

Date: 2/11/77; Temperature: 1100°C; Duration: 96 hours; $H_2O(g)$ Concentration: 0.5 ppm; Quench: Cold Zone.

Alloy	Weight Change (%)	Initial [C] (wt. %)	Final [C] (wt %) by Analysis	Cal. Std. For Carbon	Precip. (wt. %)
7261	-0.071	0.147	0.0691	121B	
7262	-0.126	0.361	0.218	121B	TP
7263	-0.074	0.173	0.0745	121B	
7264	-0.069	0.124	0.0570	121B	
7265	-0.058	0.153	0.0714	121B	
7266	-0.096	0.867	0.763	121B	TP
7267	-0.110	0.652	0.515	121B	TP
7268	-0.135	0.451	0.316	121B	TP
7068	-0.065	0.152	0.0743	121B	
Ni-270	-0.076	0.144	0.0643	121B	
Fe'E'	-0.352	1.01	0.565	121B	

[a]Equilibrium approached by decarburization.

Table A.33. Data From Carburization Experiment A-7783-136.[a]

Date: 2/17/77; Temperature: 990°C; Duration: 192 hours; $H_2O(g)$ Concentration: 0.5 ppm; Quench: Cold Zone.

Alloy	Weight Change (%)	Initial [C] (wt. %)	Final [C] (wt %) by Analysis	Cal. Std. For Carbon	Precip. (wt. %)
7261	-0.016	0.075	0.049	121B	
7262[b]	-0.002	0.218			
7263	-0.006	0.087	0.0847	121B	
7264	-0.011	0.064	0.0537	121B	
7265	-0.030	0.081	0.0472	121B	
7266[b]	+0.004	0.763			
7267[b]	+0.009	0.515			
7268[b]	+0.003	0.316			
7068[b]	-0.015	0.078	0.0578	121B	
Ni-270	-0.030	0.070	0.0447	121B	
Fe'E'	-0.113	0.553	0.462	121B	

[a]Equilibrium approached by decarburization.

[b]Equilibrium was not achieved in these alloys.

BIBLIOGRAPHY

A. M. Abdel-Gawad, The American Mineralogist, 51, 464 (1966).

K. W. Andrews and H. Hughes, Am. Soc. Testing Mats., ASTM, STP 393, 3 (1966).

I. Ansara, Metallurgical Chemistry Symposium, O, Kubaschewski editor, National Physical Society, 403 (1971).

S. Ban-Ya, J. F. Elliott, and J. Chipman, Met. Trans., 1, 1313 (1970).

S. Ban-Ya, J. F. Elliott, and J. Chipman, TMS-AIME, 245, 1199 (1969).

G. Beck and R. Bigot, Rev. Met. (Paris) 62, 681 (1965).

J. Belzer, L. G. Savedoff, and H. L. Johnston, Ohio State U. Research Foundation TR316-6 (1953).

M. Benz and J. F. Elliott, TMS-AIME, 215, 954 (1959).

M. J. Bradley, M. O. Pattengill, and L. M. Ferris, Inorganic Chemistry, 4, 1080 (1965).

D. N. Braski and J. M. Leitnaker, Production of Homogeneous Titanium-Hastelloy N Alloys, ORNL/TM-5697 (Feb. 1977).

K. Bungardt, H. Preizendanz, and G. Lehnert, Arch Eisenhuett., 35, 999 (1964).

R. A. Buckley and W. Hume-Rothery, J. Iron Steel Inst., 201, 227 (1963).

J. Chipman, Met. Trans., 3, 55 (1972).

J. Chipman, TMS-AIME, 239, 1332 (1967).

J. Chipman, TMS-AIME, 239, 2 (1967).

J. Chipman, J. Iron and Steel Institute, London, 180, 97 (1955).

J. Chipman and E. F. Brushy, TMS-AIME, 242, 35 (1968).

J. O. Clayton and W. F. Giaugue, J.A.C.S., 54, 2610 (1932).

L. S. Darken, JACS, 68, 1163, Appendix (1946).

L. S. Darken, TMS-AIME, 180, 430 (1949).

L. S. Darken, TMS-AIME, 239, 80 (1967).

L. S. Darken and R. A. Oriana, Acta Met. 2, 841 (1954).

M. J. Donachie, Jr. and O. H. Kriege, Journal of Materials, 7, 269 (1972)

C. K. H. DuBose and J. O. Stiegler, Rev. Sci. Inst., 38, 694 (1967).

W. W. Dunn, R. B. McLellan, and W. A. Oates, TMS-AIME, 242, 2129 (1968).

H. Dunwald and C. Wagner, Z. Anorg. Allgem. Chem., 199, 321 (1931).

J. F. Elliott and M. Gleiser, Thermochemistry for Steelmaking, Addison-Wesley Publishing Co., Cambridge, Mass. (1960).

T. Ellis, I. M. Davidson and C. Bodsworth, Journal of the Iron and Steel Institute, 201, 582 (1963).

Leslie M. Ferris and Mildred J. Bradley, JACS, 87, 1710 (1965).

S. A. Golovenenko, I. A. Tomilin, I. Yu. Konnova, IZU Akad Nauk SSR Met (Russian Metallurgy), 2, 72 (1973).

S. R. de Groot, Thermodynamics of Irreversible Processes, North Holland Publishing Co. (1951).

R. Haase, Thermodynamics of Irreversible Processes, Addison-Wesley, Reading MA (1969).

M. Hansen and K. Anderko, Constitution of Binary Alloys, McGraw-Hill, New York (1958).

G. Herzberg, Molecular Spectra and Molecular Structure I Diatomic Molecules, Prentice Hall, Inc., New York (1939), p. 198f.

G. Herzberg and K. N. Rao, J. Chem. Phys. 17, 1099 (1949).

K. F. Herzfeld and W. Heitler, Z. Electrochemie, 31, 536 (1925).

J. H. Hildebrand, JACS 51, 66 (1929).

J. H. Hildebrand, Proc. Nat. Acad. Sci. 13, 267 (1927).

J. H. Hildebrand, Proc. Nat. Acad. Sci. 13, 167 (1927).

F. H. Horne and T. G. Anderson, J. Chem. Phys. 53, 2321 (1970).

W. Hume-Rothery, H. M. Irving, and J. R. P. Williams, Proc. Roy. Soc. A208, 431 (1951).

JANAF Thermochemical Tables, Dow Chemical Company, Midland, MI (1971).

L. Kaufman, Acta Met., 7, 575 (1959).

L. Kaufman, Prog. Mat. Sci., 14, 2 (1969).

L. Kaufman, Phase Stability in Metals and Alloys, (P. S. Rudman, J. Stringer, and R. I. Jaffer, eds.), McGraw Hill, NY, 1967, p. 125f.

L. Kaufman and H. Nesor, Ann. Rev. of Material Sci. (R. Huggin, ed.), Vol. 3, Annual Reviews, Palo Alto, CA (1973).

L. Kaufman and H. Nesor, Treatise on Solid State Chemistry, N. B. Hannay, editor, Plenum Press, New York (1975), 5, 179-232.

L. Kaufman and H. Nesor, Computer Calculation of Phase Diagrams, Academic Press, New York (1970).

E. Kenik and R. Carpenter, private communication, ORNL (1977).

J. M. Leitnaker, G. A. Potter, D. J. Bradley, J. C. Franklin and W. R. Laing, Met. Trans., In Press.

J. M. Leitnaker, unpublished results, ORNL (1977).

F. Kohler, Monat. Fur Chemie, 91, 738 (1960).

G. N. Lewis and M. Randall, Thermodynamics, 2nd Ed., Revised by K. Pitzer and L. Brewer, McGraw Hill, New York, 1961.

O. Kubaschewski, K. Geiger and K. Hack, Z. Metallkde., 68, 337 (1977).

C. H. P. Lupis and J. F. Elliott, Acta Met., 47, 529 (1966).

M. L. McGlasken, JPAL, 21, 1 (1970).

F. Newmaun, H. Schenck, and W. Patterson, Giesserei., Tech.-Wiss. Beih. Giessereiw. Metallk. 23, 1217. 1959.

R. A. Oriani, J. Phys. Chem. Solids 30, 339 (1969).

E. K. Plyer, L. R. Blaine, and W. S. Connor, J. Optical Society of America, 45, 102 (1955).

D. H. Rank, D. P. Eastman, B. S. Rao, and T. A. Wiggins, J. of the Optical Society of America, 51, 929 (1961).

F. D. Richardson, J. Iron and Steel Inst. 175, 33 (1953).

G. Scatchard, Chemical Reviews, 44, 7 (1949).

G. Scatchard, Chemical Reviews, 8, 321 (1931).

E. Scheil, T. Schmidt, and J. Wunning, Arch. Eisenhiitt, 32, 251 (1961).

H. Schneck, M. Frohberg, and E. Jaspert, Arch. Eisenh., 36, 683 (1965).

E. Schurmann, T. Schmidt, and H. Wagener, Giesserei.-Forsch, 16, 91 (1964).

P. Shewmon, Acta Met. 8, 605 (1960).

P. Shewmon, J. Chem. Phys. 29, 1032 (1958).

P. Shewmon, TMS-AIME, 212, 642 (1958).

B. L. Shriver, M. Wuttig, Acta Met. 20, 1 (1972).

G. K. Sigworth and J. E. Elliott, Canadian Met. Quart. 13, 455 (1974).

G. K. Sigworth and J. E. Elliott, Canadian Met. Quart. 15, 123 (1976).

J. C. Slater, J. Chem. Phys. 41, 3199 (1964).

R. P. Smith, TMS-AIME, 236, 1224 (1966).

R. P. Smith, TMS-AIME, 218, 62 (1960).

R. P. Smith, JACS, 70, 2724 (1948).

R. P. Smith, JACS, 68, 1163 (1946).

W. H. Smith, TMS-AIME, 209, 47 (1952).

C. P. Snow and E. K. Rideal, Pro. Royal Soc., London, A125, 462 (1929).

K. E. Spear and J. M. Leitnaker, J. Am. Ceram. Soc., 52, 257 (1969).

E. R. Stover and J. Wulff, TMS-AIME, 215, 127 (1959).

M. G. Ulitchny and R. Gibala, Met. Trans., 4, 497 (1973).

U. S. National Bureau of Standards, Selected Values of Chemical Thermodynamic Properties TN270-3, 1968.

T. Wada, H. Wada, J. F. Elliott and J. Chipman, Met. Trans. 3, 2865 (1972).

T. Wada, H. Wada, J. Elliott, and J. Chipman, Met. Trans., 2, 2199 (1971).

C. Wagner, Thermodynamics of Alloys, Addison-Wesley Press Inc. Cambridge, Mass (1952).

E. W. White, P. J. Oenny, and S. M. Irving, The Electron Microprobe, (T. D. McKinley, K. F. J. Heinrich, and D. B. Wittry, editors); J. Wiley and Sons, New York (1966).

C. E. Wick and F. E. Block, Thermodynamic Properties of 65 Elements Their Oxides, Halides, Carbides, and Nitrides, Bureau of Mines Bulletin 605, 1963.

THIS PAGE

WAS INTENTIONALLY

LEFT BLANK

ORNL/TM-6282

INTERNAL DISTRIBUTION

1–2. Central Research Library
3. Document Reference Section
4–7. Laboratory Records Department
8. Laboratory Records, ORNL RC
9. ORNL Patent Office
10. P. Angelini
11. J. Bentley
12. D. N. Braski
13. J. Brynestad
14. P. T. Carlson
15. J. V. Cathcart
16. G. W. Clark
17. G. L. Copeland
18. D. A. Costanzo
19. J. H. DeVan
20. J. R. DiStefano
21. L. M. Ferris
22. C. B. Finch
23. G. R. Gessel
24. T. G. Godfrey
25. M. L. Grossbeck
26. J. A. Horak
27. H. Inouye
28. J. R. Keiser
29. E. A. Kenik
30. J. F. King
31. W. R. Laing
32. J. M. Leitnaker
33. J. S. Lin
34. C. T. Liu
35. K. C. Liu
36. H. E. McCoy, Jr.
37. C. J. McHargue
38. P. J. Maziasz
39. C. S. Morgan
40. R. E. Pawel
41. H. Postma
42. A. F. Rowcliffe
43. A. C. Schaffhauser
44. P. S. Sklad
45. J. O. Stiegler
46. C. L. White
47. R. O. Williams

EXTERNAL DISTRIBUTION

48. Dr. M. G. Bowman, CMB Division, Los Alamos Scientific Laboratory, Los Alamos, NM 87545

49–58. Dr. D. J. Bradley, Chemistry Department, University of California at Berkeley, Berkeley, CA 94720

59. Prof. Leo Brewer, Chemistry Department, University of California at Berkeley, Berkeley, CA 94720

60. Prof. Harry A. Black, Chemistry Department, Michigan State University, East Lansing, MI 48824

61. Prof. John Elliott, Materials Science Department, Massachusetts Institute of Technology, Cambridge, MA 02139

62. Prof. R. Gibala, Chemistry Department, Case Western Reserve University, Cleveland, OH 44106

63. Prof. Paul W. Gilles, Department of Chemistry, University of Kansas, Lawrence, KS 66044

64. Prof. F. H. Horne, Chemistry Department, Michigan State University, East Lansing, MI 48824

65. Dr. Larry Kaufman, 21 Erie Street, Cambridge, MA 02139

66. Dr. Robert Mulford, CMB-5, Los Alamos Scientific Laboratory, Los Alamos, NM 87545

67. Dr. Paul Potter, Chemistry Department, UKAEA, Harwell, Didcot, Berkshire, England

68. Dr. Malcolm Rand, Chemistry Department, UKAEA, Harwell, Didcot, Berkshire, England

69. Prof. Gerd Rosenblatt, Chemistry Department, Pennsylvania State University, State College, PA 16802

70. Prof. K. E. Spear, Materials Science Department, Pennsylvania State University, State College, PA 16802

71. Dr. R. J. Thorn, Chemistry Department, Argonne National Laboratory, 9700 South Cass Avenue, Argonne, IL 60439

72. Prof. E. A. Westrum, Chemistry Department, University of Michigan, Ann Arbor, MI 48104

73. Mr. W. G. Witteman, CMB-3, Los Alamos Scientific Los Alamos, NM, 87545

74. Director, Research and Technical Support Division, DOE-ORO

75-101. DOE TECHNICAL INFORMATION CENTER, Office of Information Services, P.O. Box 62, Oak Ridge, TN 37830

☆ U.S. GOVERNMENT PRINTING OFFICE: 1978-748-189/454